

**2019 Fall**

**“Advanced Physical Metallurgy”  
- Non-equilibrium Solidification -**

**10.22.2019**

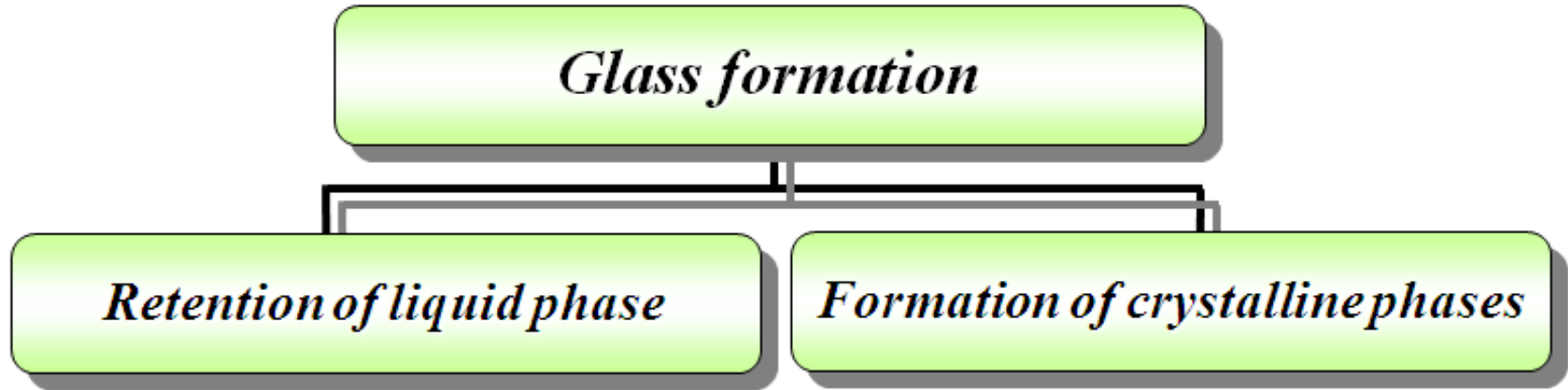
**Eun Soo Park**

**Office: 33-313**

**Telephone: 880-7221**

**Email: [espark@snu.ac.kr](mailto:espark@snu.ac.kr)**

**Office hours: by appointment**



**Glass Formation** results when

Liquids are cooled to below  $T_m$  ( $T_L$ ) sufficiently fast to avoid crystallization.

- ┌ **Nucleation** of crystalline seeds are avoided
- └ **Growth** of Nuclei into crystallites (crystals) is avoided

Liquid is “**frustrated**” by internal structure that hinders both events

➔ **“Glass Formation”**

## 2.5.2 Kinetics of Glass Formation

### A. Homogeneous Nucleation rate, $I$ (by David Turnbull)

$$I = \frac{k_n}{\eta(T)} \exp \left[ -\frac{b\alpha^3\beta}{T_r (\Delta T_r)^2} \right] \quad (2.4)$$

where

$b$  is a shape factor ( $= 16\pi/3$  for a spherical nucleus)

$k_n$  is a kinetic constant

$\eta(T)$  is the shear viscosity of the liquid at temperature  $T$

$T_r$  is the reduced temperature ( $T_r = T/T_l$ )

$\Delta T_r$  is the reduced supercooling ( $\Delta T_r = 1 - T_r$ )

$\alpha$  and  $\beta$  are dimensionless parameters related, respectively, to the liquid/solid interfacial energy ( $\sigma$ ) and to the molar entropy of fusion,  $\Delta S_f$

Thus,

$$\alpha = \frac{\left(N_A \bar{V}^2\right)^{1/3} \sigma}{\Delta H_f}$$

$$\beta = \frac{\Delta S_f}{R}$$

where

$N_A$  is Avogadro's number

$\bar{V}$  is the molar volume of the crystal

$R$  is the universal gas constant

## A. Homogeneous Nucleation rate, $I$ (by David Turnbull)

$$I = \frac{k_n}{\eta(T)} \exp\left[-\frac{b\alpha^3\beta}{T_r(\Delta T_r)^2}\right]$$

$$\alpha = \frac{\left(N_A \bar{V}^2\right)^{1/3} \sigma}{\Delta H_f}$$

$$\beta = \frac{\Delta S_f}{R}$$

1)  $\eta \uparrow$  (dense random packed structure)  $\rightarrow I \downarrow$

2) For given  $T$  and  $\eta$ ,  $\alpha^3\beta \uparrow$  ( $\sigma$  solid interfacial E &  $\Delta S_f \uparrow / \Delta H_f \downarrow$ )  $\rightarrow I \downarrow$

3)  $\eta \sim T_{rg}$  ( $=T_g/T_l$ ) &  $\alpha^3\beta \sim$  thermal stability of supercooled liquid

\* For metallic melt :  $\alpha\beta^{1/3} \sim 0.5$

\* if  $\alpha\beta^{1/3} > 0.9$ , impossible to crystallization by homogeneous nucleation  
under any cooling condition

\* if  $\alpha\beta^{1/3} \leq 0.25$ , difficult to prevent crystallization

## B. Growth rate of a crystal from an undercooled liquid, $U$

$$U = \frac{10^2 f}{\eta} \left[ 1 - \exp\left(-\frac{\Delta T_r \Delta H_f}{RT}\right) \right] \quad (2.7)$$

where  $f$  represents the fraction of sites at the crystal surfaces where atomic attachment can occur (=1 for close-packed crystals and  $0.2 \Delta T_r$  for faceted crystals). Here also we can see that  $U$  decreases as  $\eta$  increases, and will thus contribute to increased glass formability.

- 1)  $\eta \uparrow$  (dense random packed structure)  $\rightarrow U \downarrow$
  - 2) For given  $T, I$  &  $U \sim \eta \rightarrow T_{rg}$  or  $\alpha, \beta \uparrow \rightarrow \text{GFA} \uparrow$
  - 3)  $f \downarrow$  through atomic rearrangement like local ordering or segregation  $\rightarrow U \downarrow$
- \* metallic melt:  $\alpha\beta^{1/3} \sim 0.5 / T_{rg} > 2/3 \sim \text{high GFA}$
  - \* Pure metal:  $R_c \sim 10^{10-12}$  K/s, but if  $T_{rg} = 0.5$ ,  $R_c \sim 10^6$  K/s

Based on the treatment of Uhlmann [25], Davies [26] combined the values of  $I$  and  $U$  (calculated using Equations 2.4 and 2.7, respectively) with the Johnson–Mehl–Avrami treatment of transformation kinetics, and calculated the fraction of transformed phase  $x$  in time  $t$ , for small  $x$ , as

$$C. \quad x = \frac{1}{3} \pi I U^3 t^4 \quad (2.8)$$

Substituting the values of  $I$  and  $U$  in Equation 2.8, the time needed to achieve a small fraction of crystals from the melt was calculated as

$$t \approx \frac{9.3 \eta a_o^2 x}{k T f^3 \bar{N}_v} \left[ \frac{\exp\left(\frac{1.07}{\Delta T_r^2 T_r^3}\right)}{\left\{1 - \exp\left(-\frac{\Delta H_f \Delta T_r}{RT}\right)\right\}^3} \right]^{1/4} \quad (2.9)$$

where

$a_o$  is the mean atomic diameter

$\bar{N}_v$  is the average volume concentration of atoms, and all the other parameters have the same meaning, as described earlier

A time–temperature–transformation ( $T$ – $T$ – $T$ ) curve was then computed by calculating the time,  $t$ , as a function of  $T_v$  to transform to a barely detectable fraction of crystal, which was arbitrarily taken to be  $x = 10^{-6}$ .

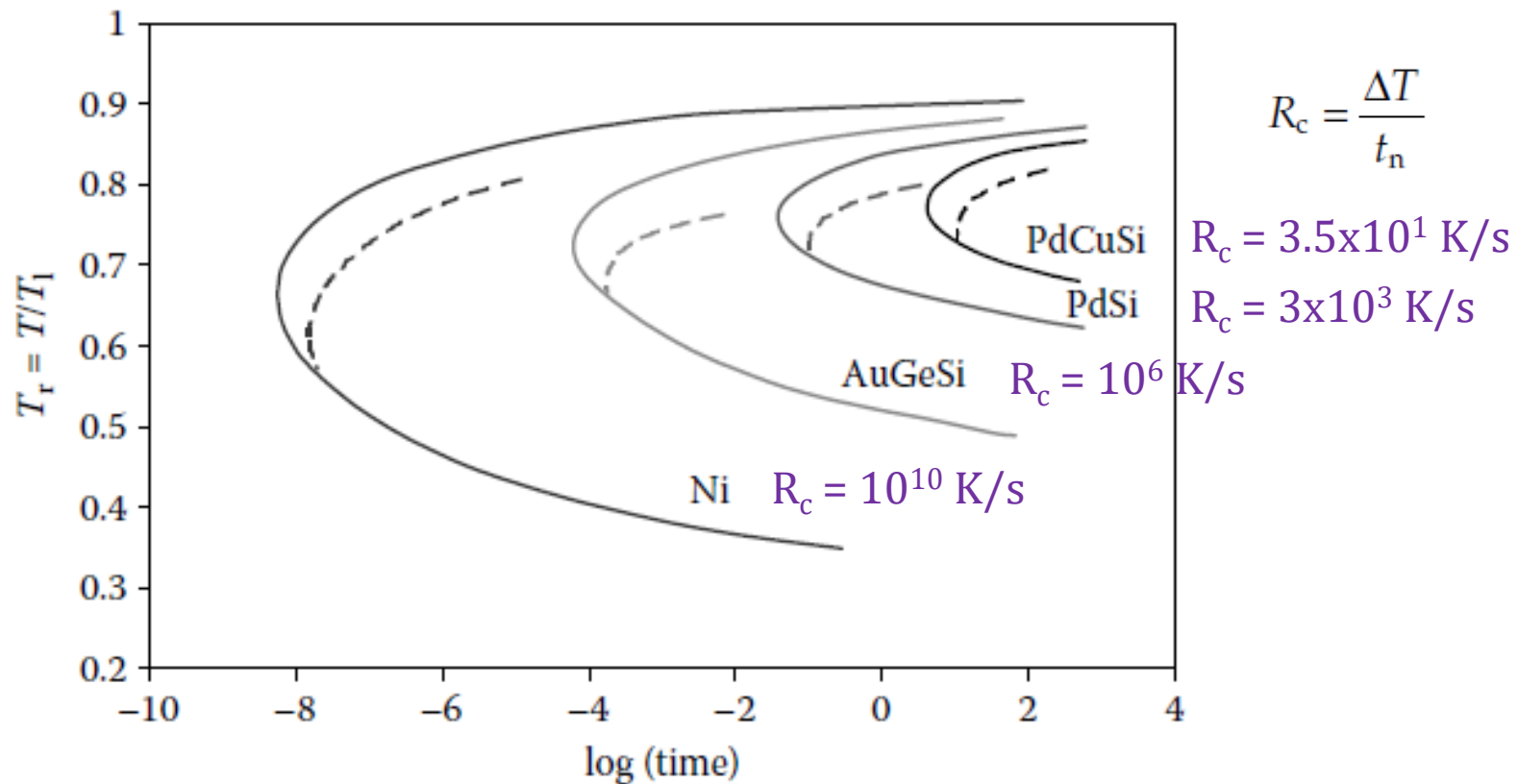


**FIGURE 2.3**

Time-temperature-transformation ( $T$ - $T$ - $T$ ) curves (solid lines) and the corresponding continuous cooling transformation curves (dashed lines) for the formation of a small volume fraction for pure metal Ni, and  $\text{Au}_{78}\text{Ge}_{14}\text{Si}_8$ ,  $\text{Pd}_{82}\text{Si}_{18}$ , and  $\text{Pd}_{78}\text{Cu}_6\text{Si}_{16}$  alloys.

$T_{rg}$

1/4

1/2

2/3

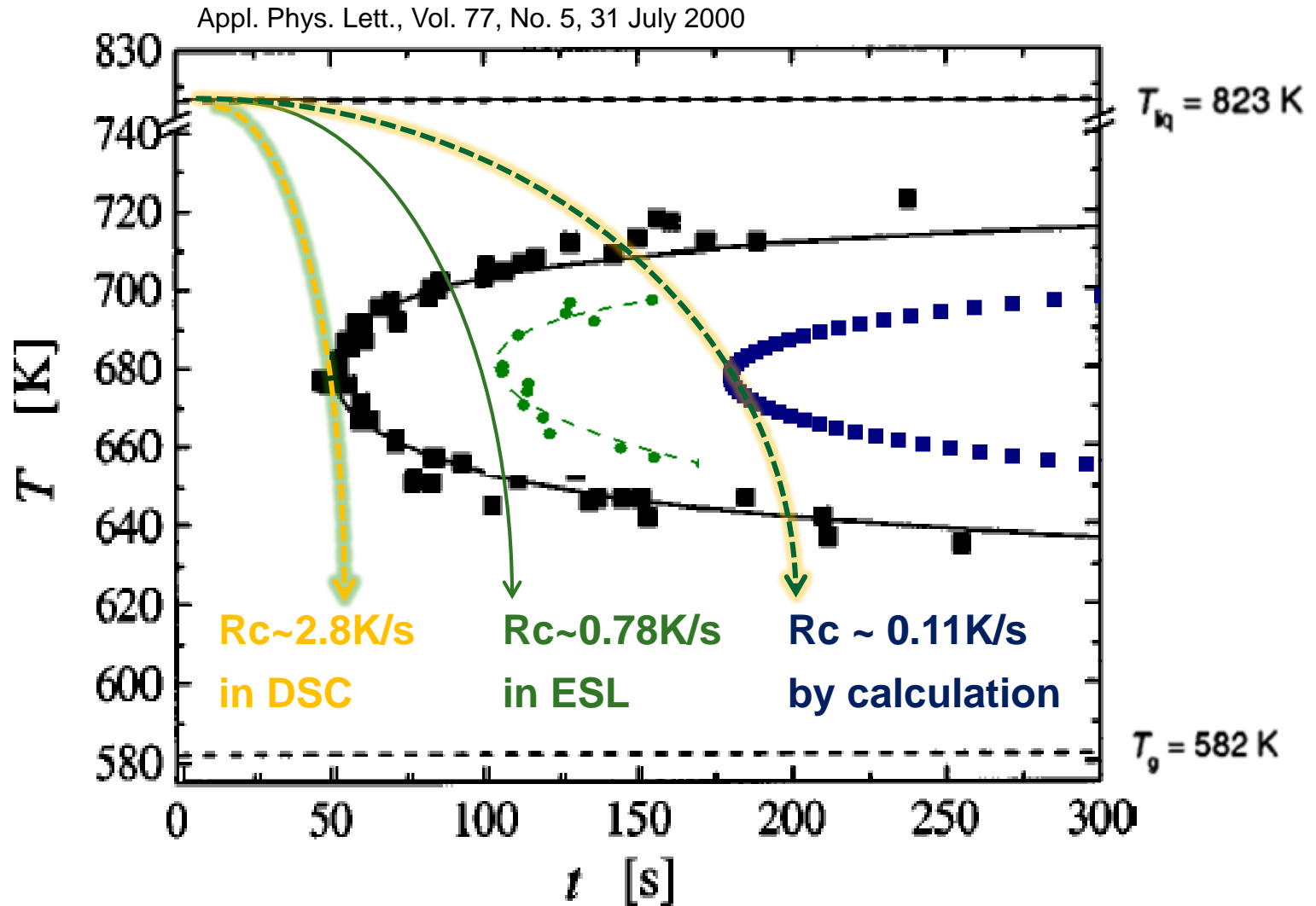
# Critical Cooling Rates for Various Liquids

**Table 3-5.** Examples of Critical Cooling Rates ( $^{\circ}\text{C}/\text{s}$ ) for Glass Formation

Material	Homogeneous nucleation	Heterogeneous nucleation contact angle (deg)		
		100	60	40
SiO <sub>2</sub> glass <sup>a</sup>	$9 \times 10^{-6}$	$10^{-5}$	$8 \times 10^{-3}$	$2 \times 10^{-1}$
GeO <sub>2</sub> glass <sup>a</sup>	$3 \times 10^{-3}$	$3 \times 10^3$	1	20
Na <sub>2</sub> O·2SiO <sub>2</sub> glass <sup>a</sup>	$6 \times 10^{-3}$	$8 \times 10^{-3}$	10	$3 \times 10^{+2}$
Salol	10			
Water	$10^7$			
Ag	$10^{10}$			
Typical metal <sup>a</sup>	$9 \times 10^8$	$9 \times 10^9$	$10^{10}$	$5 \times 10^{10}$

<sup>a</sup> After P. I. K. Onorato and D. R. Uhlmann, *J. Non-Cryst. Sol.*, 22(2), 367–378 (1976).

# TTT Diagram of Pd<sub>40</sub>Cu<sub>30</sub>Ni<sub>10</sub>P<sub>20</sub>



## 2.6 Methods to Synthesize Metallic Glasses

### 2.6.1 Vapor-state Processes: expensive & slow, electronic & magnetic applications

#### Thermal Evaporation/ Sputtering/ Vapor Chemical Deposition



### 2.6.2 Liquid-state Processes : Rapid Solidification Process (RSP) $10^{5-6}$ K/s most ideal way to obtain metallic glasses, especially the bulk foam

#### Splat Quenching/ Melt-spinning/ Electro Deposition/ Gas Atomization

### 2.6.3 Solid-state Processes\_Solid state diffusional amorphization

#### Mechanical Alloying & Milling/Hydrogen-induced Amorphization/ Multilayer Amorphization/ Pressure-induced Amorphization/ Amorphization by Irradiation/ Severe Plastic Deformation\_Intense deformation at low temperatures /Accumulative Roll Bonding (ARB process)

## 2.7 Bulk Metallic Glasses (BMGs)

- More commonly, metallic glasses with at least a diameter or section thickness of 1 mm are considered “bulk.” (Nowadays researchers tend to consider 10mm as the minimum diameter or section thickness at which a glass is designated bulk.)

### 2.7.1 Characteristics of Bulk Metallic Glasses

- The alloy systems have a minimum of three components; more commonly the number is much larger and that is why they are frequently referred to as multicomponent alloy systems.
- They can be produced at slow solidification rates, typically  $10^3 \text{ K s}^{-1}$  or less. The lowest solidification rate at which BMGs have been obtained was reported as  $0.067 \text{ K s}^{-1}$ , that is,  $4 \text{ K min}^{-1}$  [61]; a really slow solidification rate indeed!
- BMGs exhibit large section thicknesses or diameters, a minimum of about 1 mm. The largest diameter of a bulk metallic glass rod produced till date is 72 mm in a  $\text{Pd}_{40}\text{Cu}_{30}\text{Ni}_{10}\text{P}_{20}$  alloy [62].
- They exhibit a large supercooled liquid region. The difference between the glass transition temperature,  $T_g$ , and the crystallization temperature,  $T_x$ , that is,  $\Delta T_x = T_x - T_g$ , is large, usually a few tens of degrees, and the highest reported value so far is 131 K in a  $\text{Pd}_{43}\text{Ni}_{10}\text{Cu}_{27}\text{P}_{20}$  alloy [17].

When the as-cast alloy is characterized by XRD techniques, the presence of a broad and diffuse peak is often taken to be evidence for the presence of a glassy phase. This is normally true. But, it should be realized that the technique of XRD is not very sensitive to the presence of a small volume fraction of a crystalline phase in a glassy phase, especially when the crystals are in nanocrystalline condition. Therefore, even if the XRD pattern shows a broad halo, the material may contain a small volume fraction of a crystalline phase dispersed in the glassy matrix. Further, a structure consisting of a glassy phase, or extremely fine grains, or a nanocrystalline material with a small grain size of about <10nm, will all produce a broad and diffuse halo. Therefore, it is always desirable to confirm the lack of crystallinity in the material by conducting (high-resolution) transmission electron microscopy investigations.

## 2.7.2 The Origins of BMGs

### \* History of Metallic Glasses

- First **amorphous metal** produced by evaporation in 1934.

*\* j. Kramer, Annalen der Phys. 1934; 19: 37.*

- First **amorphous alloy**(CoP or NiP alloy)  
produced by electro-deposition in 1950.

*\* A. Brenner, D.E. Couch, E.K. Williams, J. Res. Nat. Bur. Stand. 1950: 44; 109.*

- First **metallic glass** ( $\text{Au}_{80}\text{Si}_{20}$ )  
produced by splat quenching at Caltech by Pol Duwez in 1957.

*\* W. Klement, R.H. Willens, P. Duwez, Nature 1960; 187: 869.*

- First **bulk metallic glass** ( $\text{Pd}_{77.5}\text{Cu}_6\text{Si}_{16.5}$ )  
produced by droplet quenching at Harvard Univ.  
by **H.S. Chen and D. Turnbull** in 1969

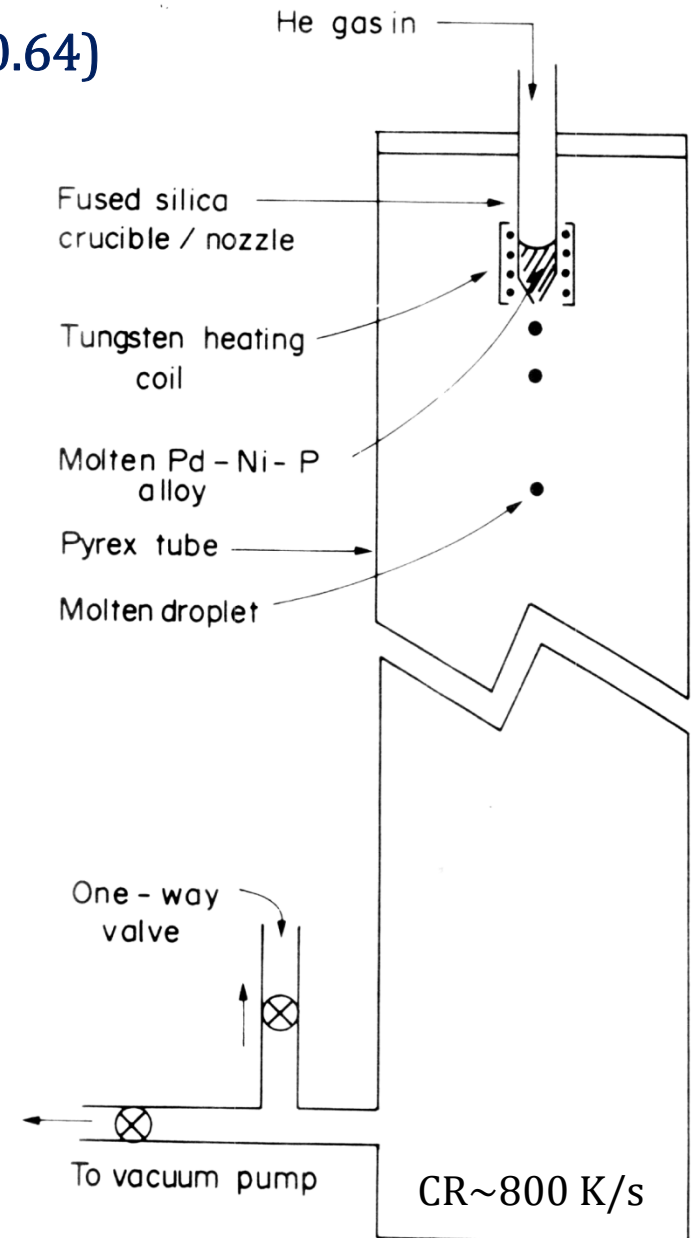
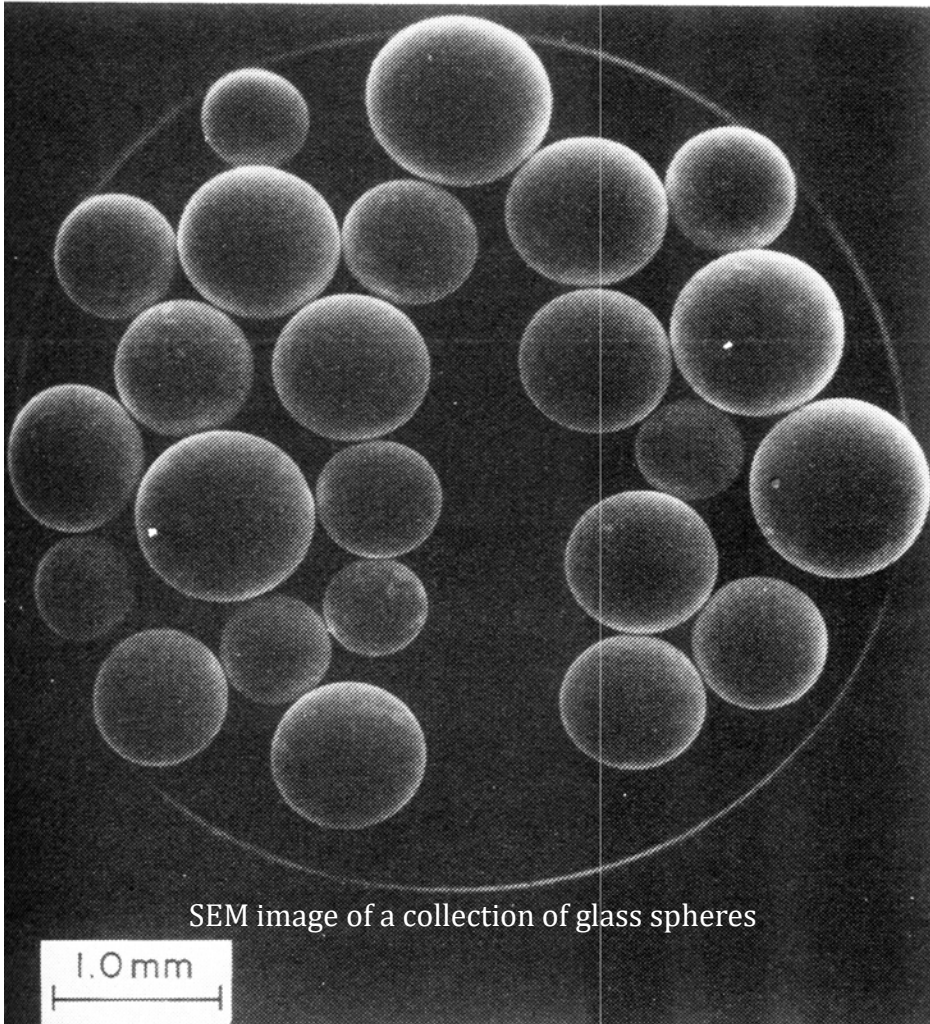
*\* H.S. Chen and D. Turnbull, Acta Metall. 1969; 17: 1021.*

produced by water quenching of PdTMSi, Pt-Ni-P and Pd-Ni-P system  
by **H.S. Chen** in 1974 ( long glassy rods, 1-3 mm in diameter and several centimeters in length)

*\* H.S. Chen, Acta Metall. 1974; 22: 1505*

► **First bulk metallic glass: Pd<sub>77.5</sub>Cu<sub>6</sub>Si<sub>16.5</sub> (T<sub>rg</sub>=0.64)**

By droplet quenching (CR~800 K/s)



\* H.S. Chen and D. Turnbull, *Acta Metall.* 1969; 17: 1021.

# Bulk formation of a metallic glass: Pd<sub>40</sub>Ni<sub>40</sub>P<sub>20</sub>

## Alloy Selection: Consideration of $T_{rg}$

\* Pd<sub>82</sub>Si<sub>18</sub> →  $T_{rg}=0.6$

- Homogeneous nucleation rate:  $>10^5/\text{cm}^3\text{s}$

- Critical cooling rate:  $> 800 \text{ K/s}$

\* Pd<sub>77.5</sub>Cu<sub>6</sub>Si<sub>16.5</sub> →  $T_{rg}=0.64$

\* Pd<sub>40</sub>Ni<sub>40</sub>P<sub>20</sub> →  $T_{rg}=0.67$

$T_g=590 \text{ K}$ ,  $T_e = 880 \text{ K}$ ,  $T_l = 985 \text{ K}$

## Suppression of Heterogeneous nucleation

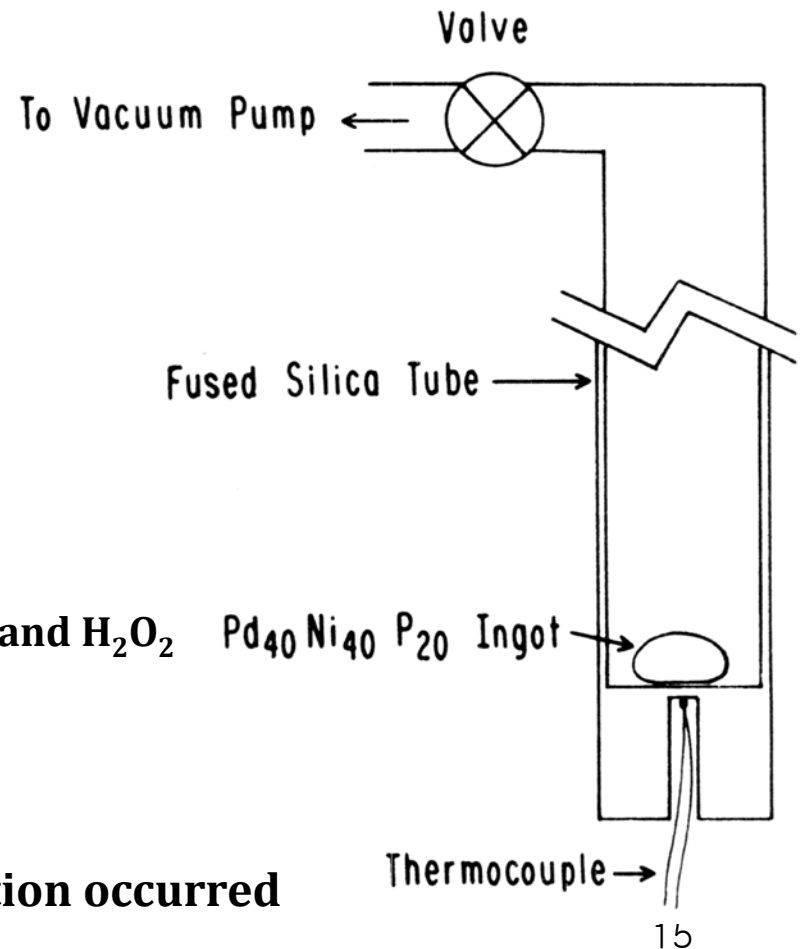
1. **Surface Etching of ingot** in a mixture of HCL and H<sub>2</sub>O<sub>2</sub>  
: elimination of surface heterogeneities

2. **Thermal cycling -5 cycles**

: dissolution of nucleating heterogeneities

→ reduce the temperature at which nucleation occurred

<Schematic diagram of apparatus>



# Bulk formation of a metallic glass: Pd<sub>40</sub>Ni<sub>40</sub>P<sub>20</sub>

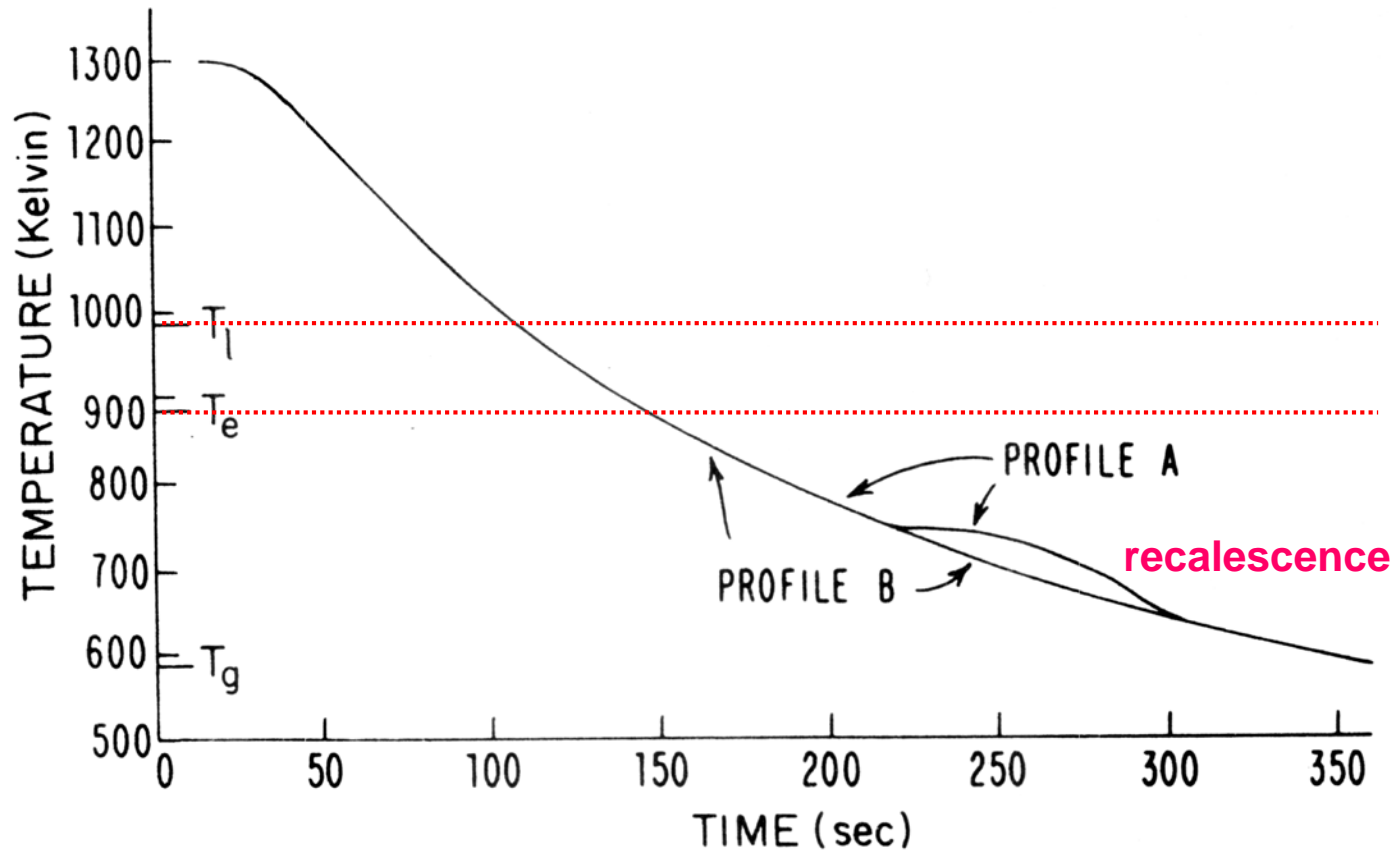


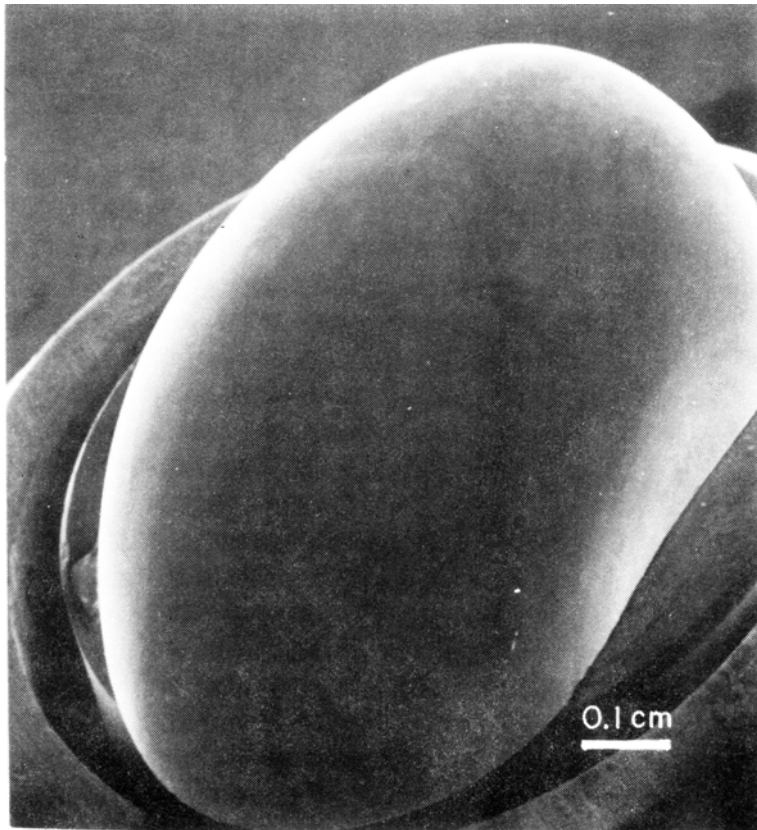
FIG. 2. Superposition of two cooling profiles: A—bulk crystallization which began at 740 K. B—formation of a glassy ingot.

*A.J. Drehman, A.L. Greer, D. Turnbull, Appl. Phys. Lett. 1982; 41: 716.*

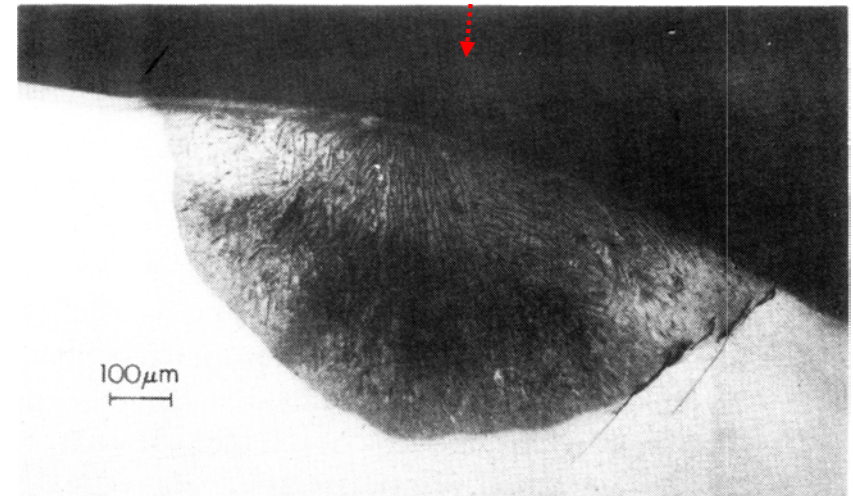
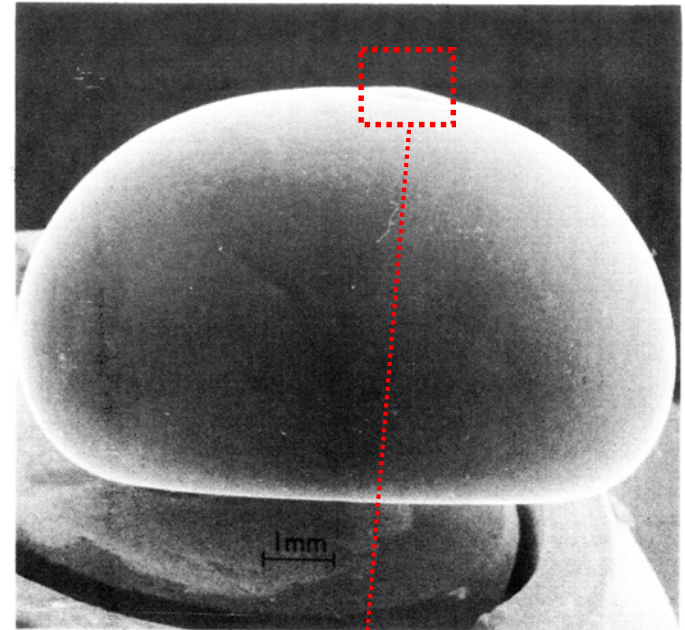
# Bulk formation of a metallic glass: Pd<sub>40</sub>Ni<sub>40</sub>P<sub>20</sub>

- Largest ingot

- minimum dimension 0.6 cm and mass of 2.3 g
- Critical cooling rate: ~ 1.4 K/sec.



*\*Appl. Phys. Lett. 1982; 41: 716.*



OM image of the cross section of a crystalline inclusion showing the eutectic structure

# Formation of bulk metallic glass by fluxing

## • Heterogeneous nucleation

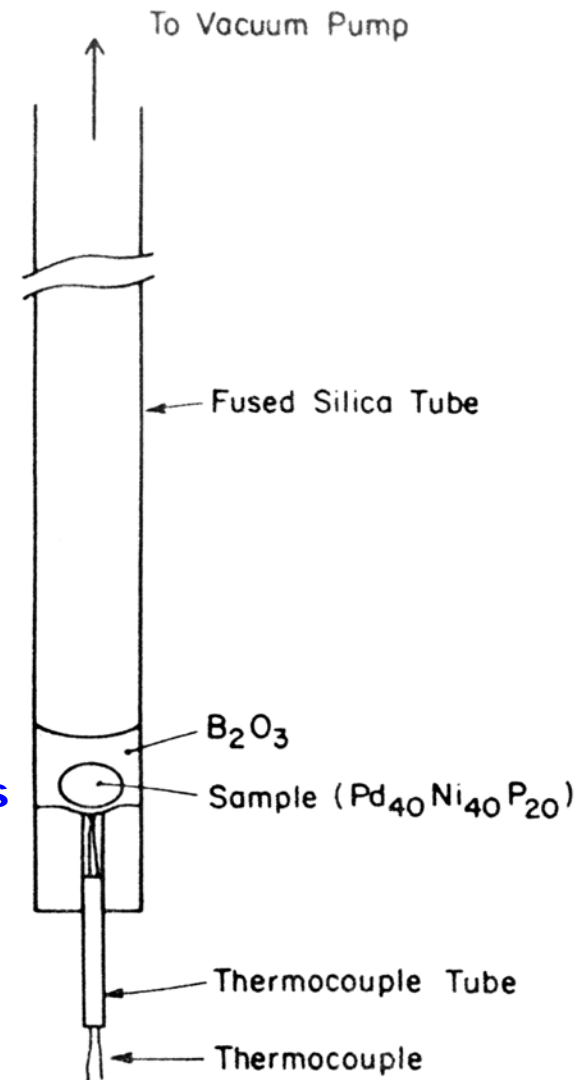
1. Surface oxide layer
2. Container walls
3. Motes in the liquid

## → Suppression

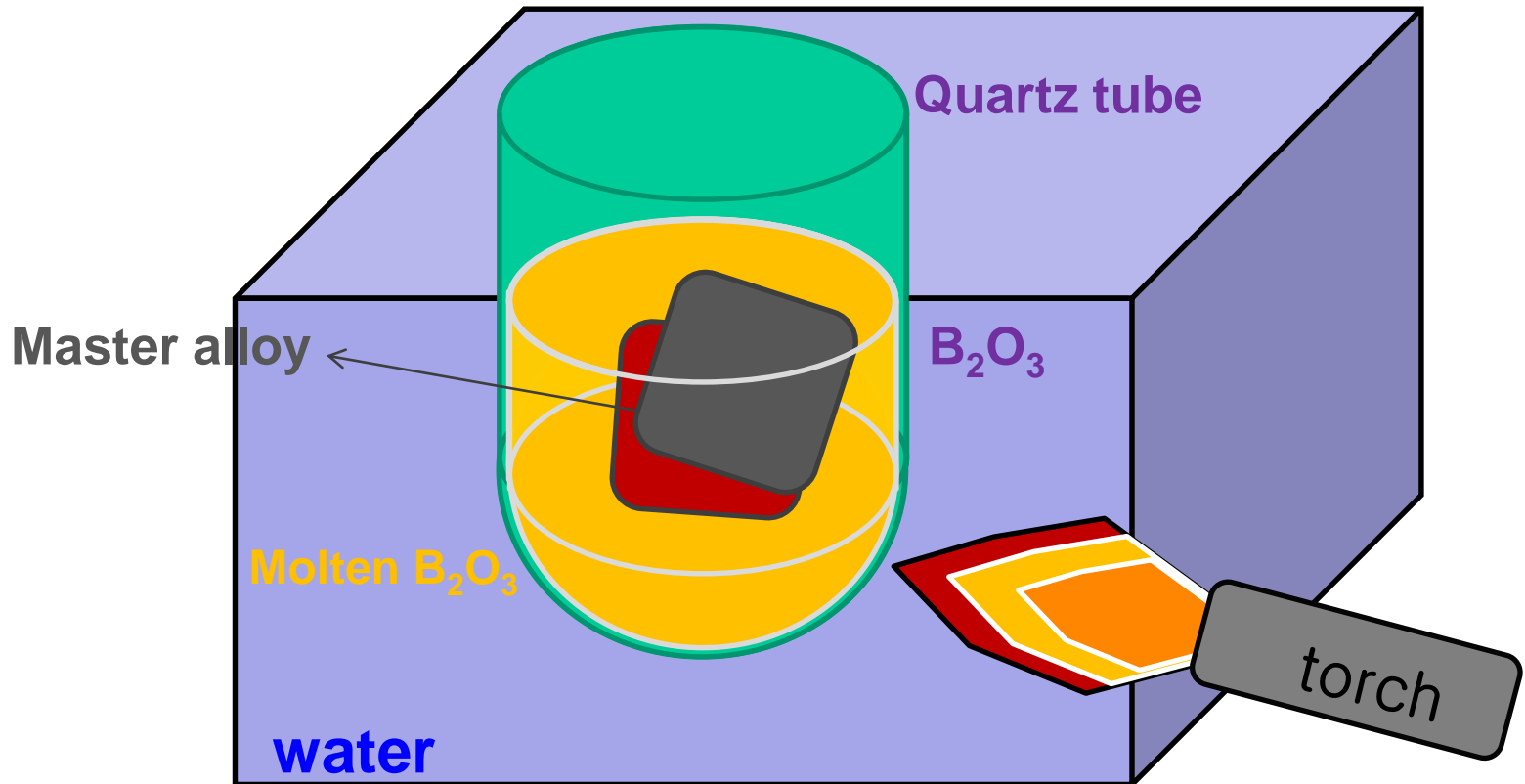
1. **Ingot = Chemical etching**  
by dilute aqua regia ( $\text{HNO}_3 + \text{HCl}$ )
2. **Interior of the vessel = Cleaning**  
by hydrofluoric acid
3. **Impurities = Successive heating-cooling cycles**  
in a molten oxide flux

$\text{B}_2\text{O}_3$  melting point 723 K, boiling point  $< 40,000$  K

After gravity segregation to the oxide-metal interface most heterophase impurities presumably are dissolved or deactivated (e.g., by being wet) by the molten oxide

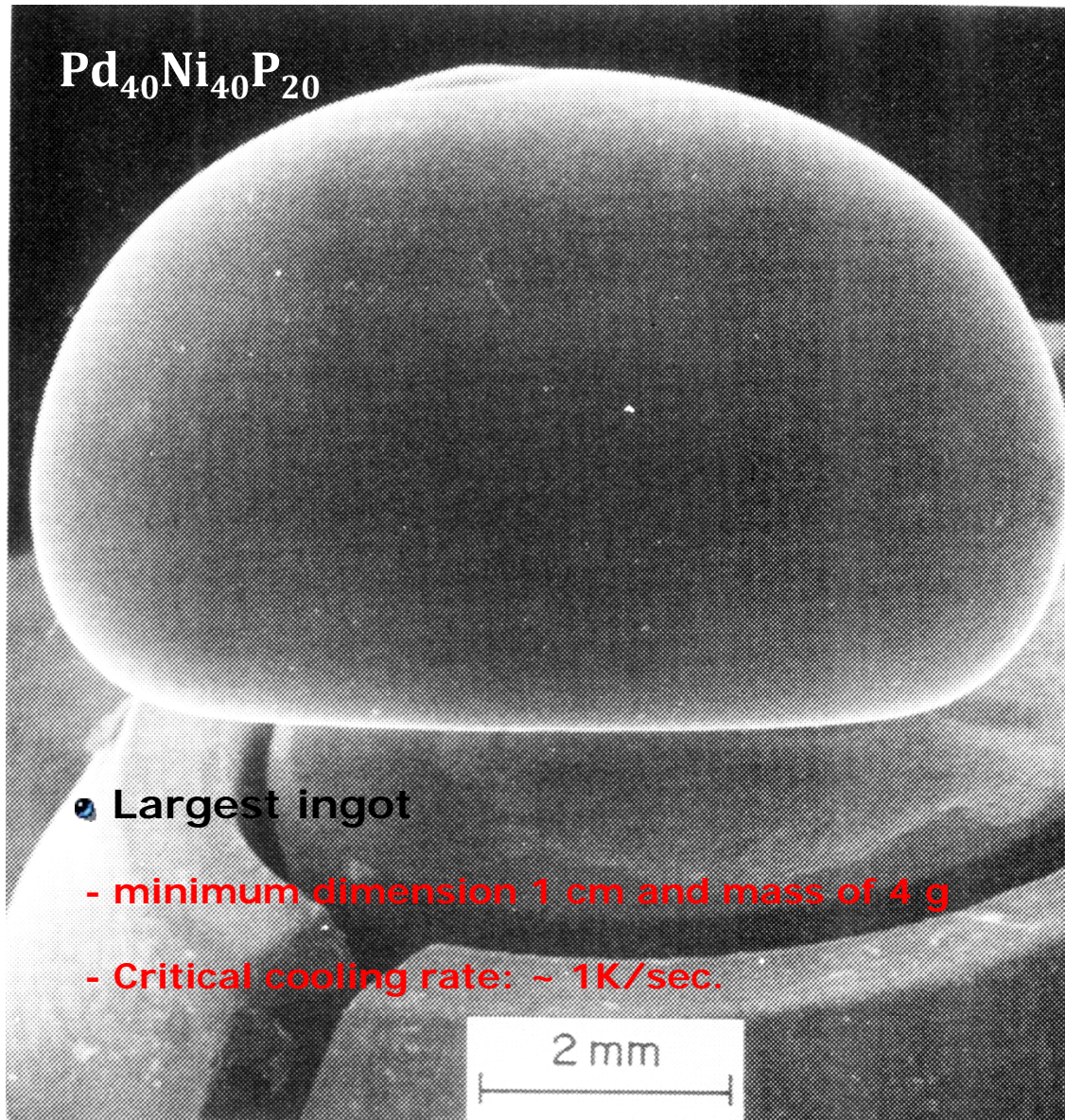


# Schematic process of fluxing



B<sub>2</sub>O<sub>3</sub> melting point 723 K, boiling point <40,000 K

# Formation of centimeter-sized BMG by fluxing



## *BMG formation*

### *Alloy design optimization*

1. Consideration of thermodynamic, kinetic and structural aspects for glass formation
2. Empirical rules by trial and error
3. Minor additions
4. Computer simulation

### *Process optimization*

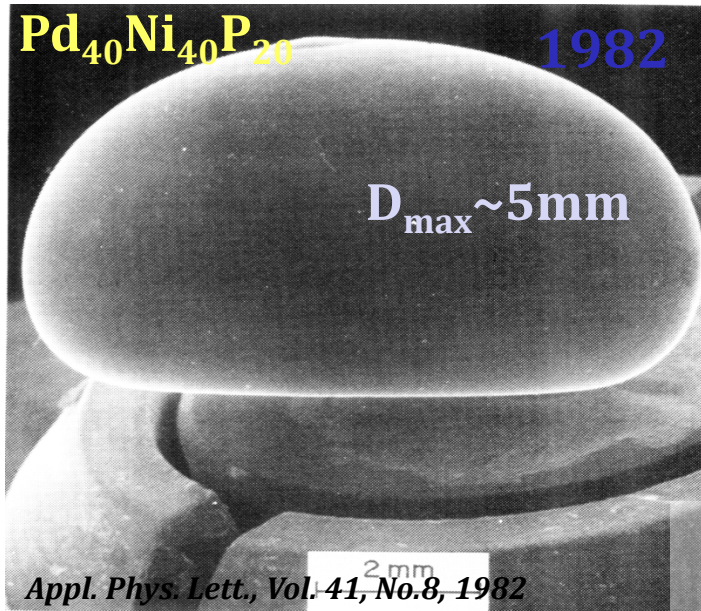
1. Chemical etching of ingot & vessel
2. Alloying at high temperature
3. Successive heating-cooling cycles in a molten oxide flux
4. Addition of oxygen scavenger
5. Process with high coolability

*Suppression of nucleation and growth of crystalline phase*

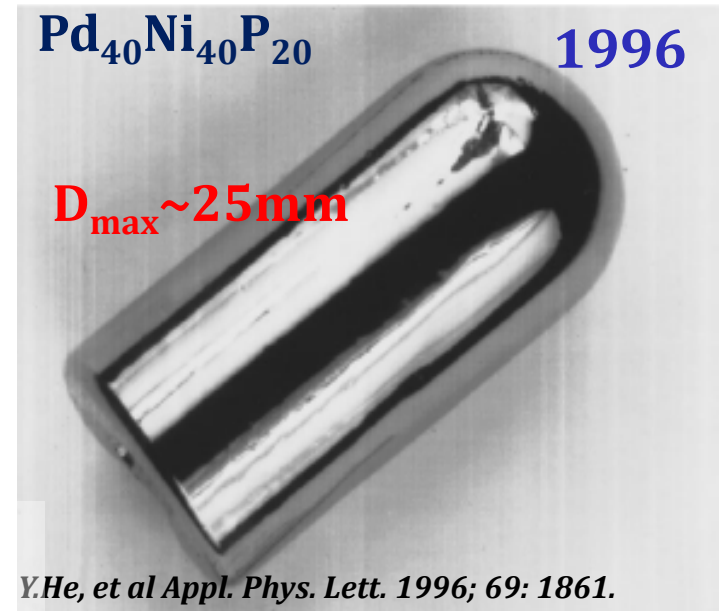


**High BMG Manufacturability**

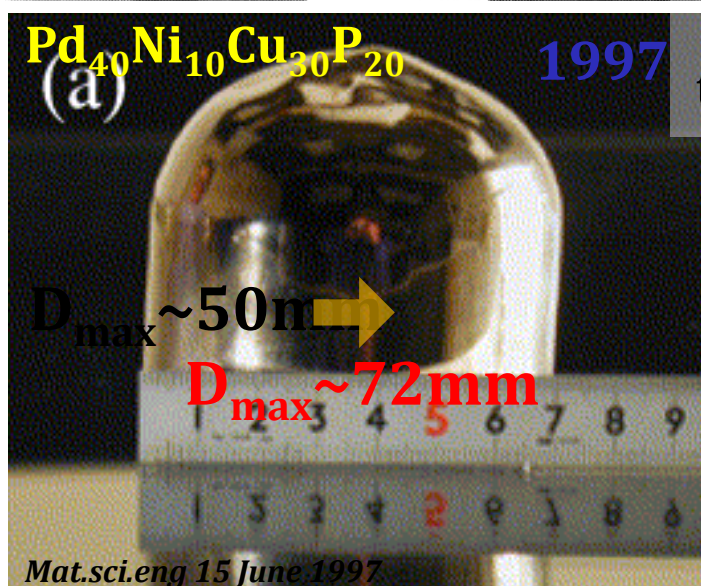
# Formation of centimeter-sized BMG by fluxing



1984  
→  
 $D_{\text{max}} \sim 10\text{mm}$



After  
fluxing  
treatment

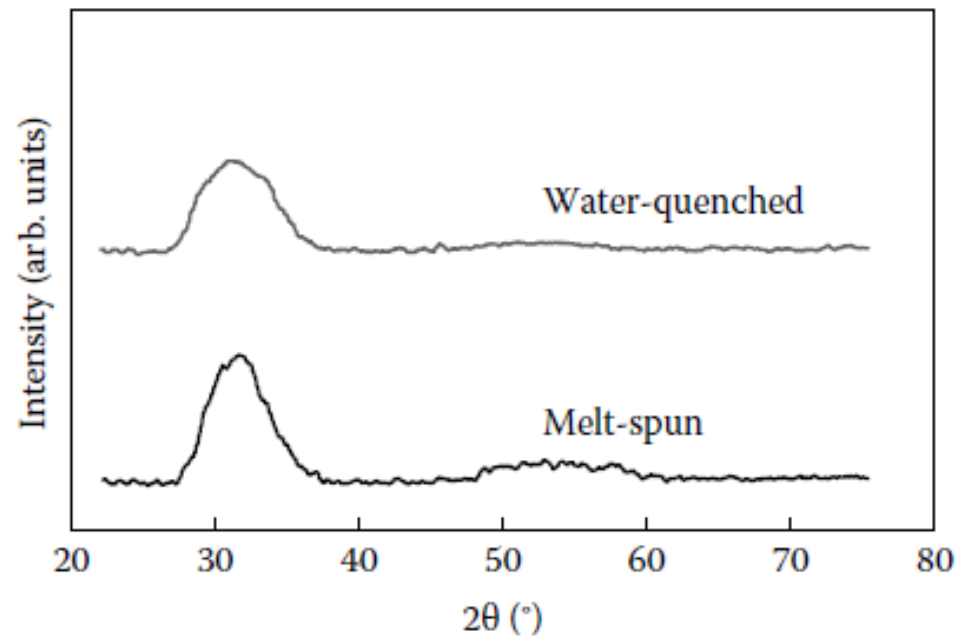


Starting in the late 1980s, the RSP group at Tohoku University in Sendai, Japan, has systematically investigated the glass-forming ability (GFA) of different alloy systems and was able to produce bulk glassy alloys in some of the systems at solidification rates of  $10^3 \text{ K s}^{-1}$  or lower. A brief account of the development of BMGs at Tohoku University is described below.

Al–La–Ni [67] and Mg–Ni–La [68] glassy alloys were produced in a wide composition range  $\longrightarrow$  The  $\Delta T_x$  values reported were 69 K for the  $\text{La}_{55}\text{Al}_{25}\text{Ni}_{20}$  glass and 58 K for the  $\text{Mg}_{50}\text{Ni}_{30}\text{La}_{20}$  glass. These  $\Delta T_x$  values are much larger than those reported for the noble-metal-based glasses, Pd–Ni–P and  $\text{Pt}_{60}\text{Ni}_{15}\text{P}_{25}$  (35–40 K) reported earlier.

## Figure 2.6

X-ray diffraction patterns of  $\text{La}_{55}\text{Al}_{25}\text{Ni}_{20}$  glassy samples in the water-quenched rod (0.8 mm dia.  $\rightarrow D_{\text{max}} = 1.2 \text{ mm}$ ) and melt-spun ribbon (20  $\mu\text{m}$ ) conditions. Note that in both the cases, the diffraction pattern shows only a broad peak and sharp peaks indicative of any crystalline phase are absent. Furthermore, the position of the broad peak is the same in both the samples, suggesting that the glassy phase produced in same in both the cases.



\* Inoue A, et al., *Mater. Trans. JIM*, 30, 722, 1989.

These observations have subsequently been confirmed in a number of other alloy systems and by several researchers. Subsequent to this initial discovery, Peker and Johnson [70] produced a 14 mm diameter fully glassy rod in the composition Zr<sub>41.2</sub>Ti<sub>13.8</sub>Cu<sub>12.5</sub>Ni<sub>10.0</sub>Be<sub>22.5</sub> (most commonly referred to as Vitreloy 1 or Vit 1, and now redesignated as liquid metal or LM-001), and since then there has been an explosion in the research activity in this area all over the world.

### **A highly processable metallic glass: Zr<sub>41.2</sub>Ti<sub>13.8</sub>Cu<sub>12.5</sub>Ni<sub>10.0</sub>Be<sub>22.5</sub>**

A. Peker and W. L. Johnson

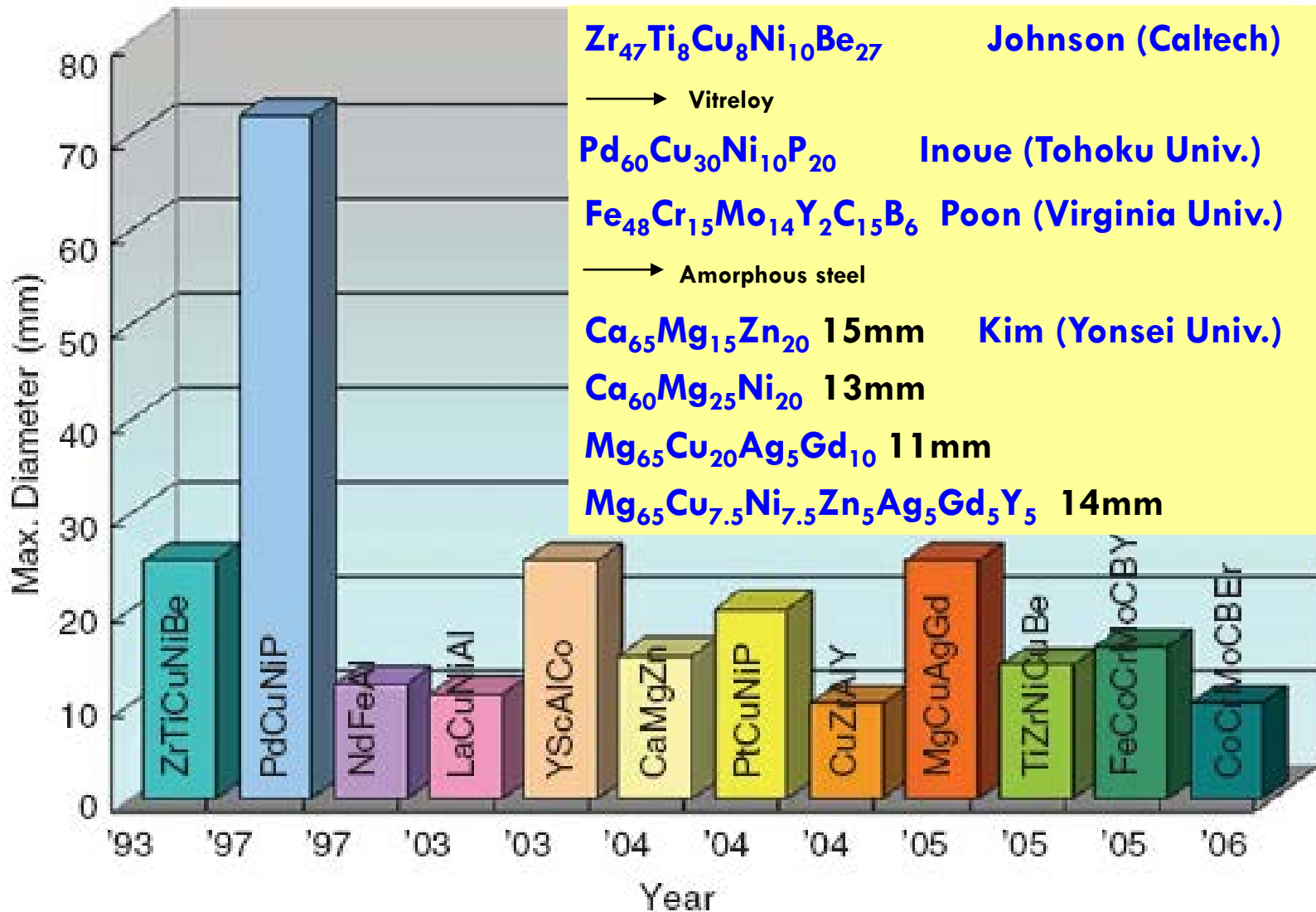
*W. M. Keck Laboratory of Engineering Materials, California Institute of Technology, Pasadena, California 91125*

We report on the properties of one example of a new family of metallic alloys which exhibit excellent glass forming ability. The critical cooling rate to retain the glassy phase is of the order of 10 K/s or less. Large samples in the form of rods ranging up to 14 mm in diameter have been prepared by casting in silica containers.

*\* [Appl. Phys. Lett. 63: 2342-2344.](#)*

Starting with the initial discovery of the formation of BMGs in the La–Al–Ni system, the Tohoku group has produced a very large number of BMGs in different alloy systems based on Mg, Zr, Ti, Pd, Fe, Co, Ni, and Cu. They have been able to produce several new alloys in the BMG state and also increase the critical (or maximum) diameter of the BMG alloy rods during the last nearly 20 years.

# Recent BMGs with critical size $\geq 10$ mm



# Bulk glass formation in the Pd-/Ni-/Cu-/Zr-element system

## Massy Ingot Shape

(a) Pd-Cu-Ni-P



72φx 75 mm 80φx 85 mm

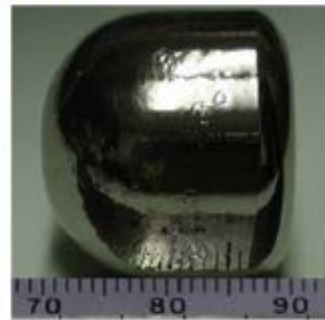
(b) Zr-Al-Ni-Cu



(c) Cu-Zr-Al-Ag



(d) Ni-Pd-P-B

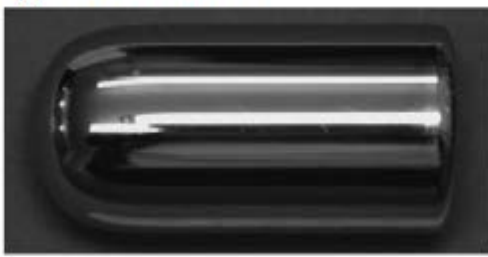


## Cylindrical Rods

(e) Pd-Cu-Ni-P



(f) Pt-Pd-Cu-P

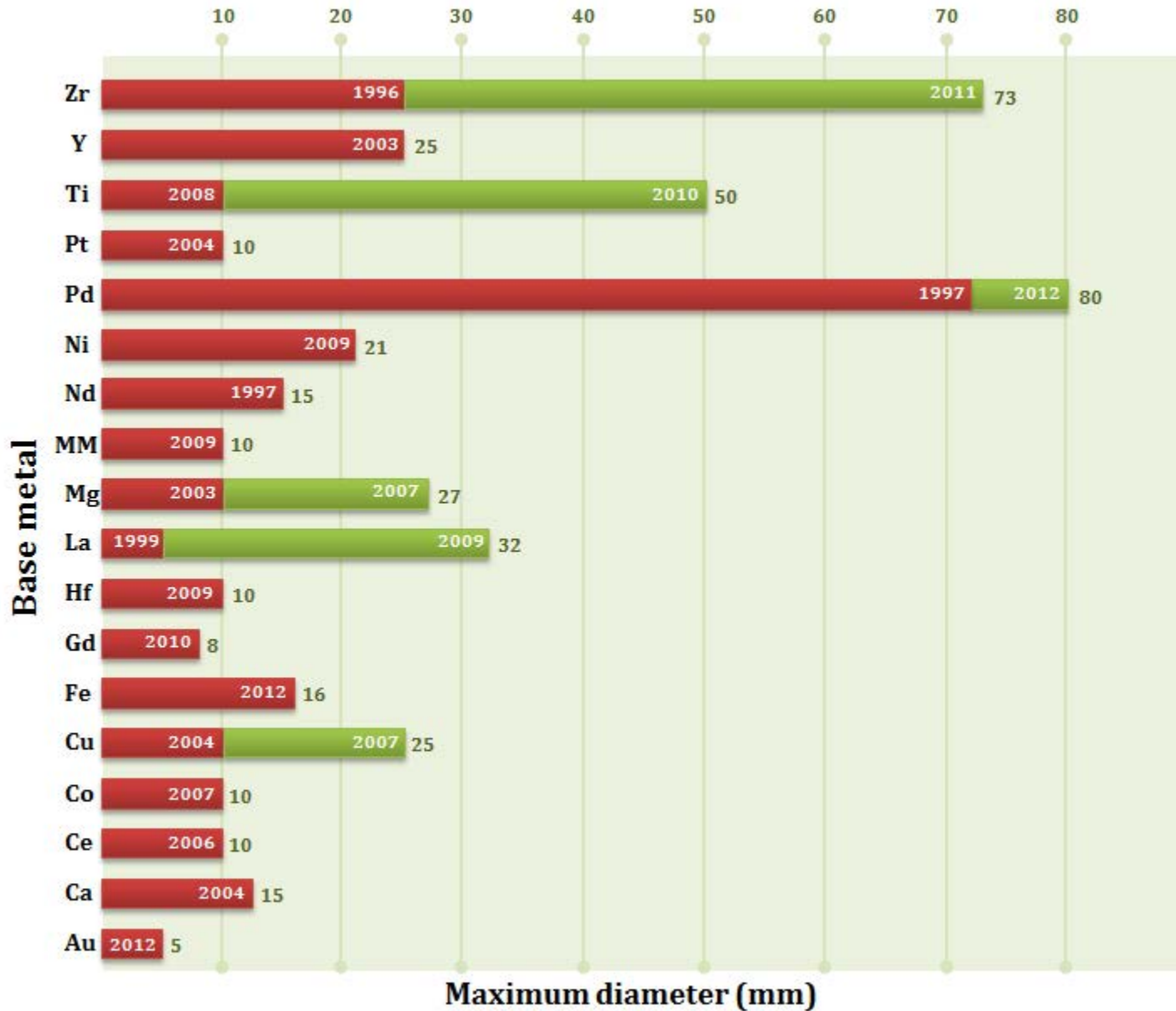


## Hollow Pipes

(g) Pd-Cu-Ni-P



# Recent BMGs with critical size $\geq 10$ mm



# *Glass formation*

*Retention of liquid phase*

*Formation of crystalline phases*

*Thermodynamical point*

Small change in free E. (liq. → cryst.)

*Kinetic point*

Low nucleation and growth rates

*Structural point*

Highly packed random structure

*Empirical rules*

- (1) multi-component alloy system
- (2) significant difference in atomic size ratios
- (3) negative heats of mixing
- (4) close to a eutectic composition
- (5) compositions far from a Laves phase region

- **Higher degree of dense random packed structure**
- *Suppression* of nucleation and growth of crystalline phase



*High glass-forming ability (GFA)*

# *Glass formation*

*Retention of liquid phase*

*Formation of crystalline phases*

*Thermodynamical point*

Small change in free E. (liq. → cryst.)

*Kinetic point*

Low nucleation and growth rates

*Structural point*

Highly packed random structure

## *Empirical rules*

- (1) multi-component alloy system
- (2) significant difference in atomic size ratios
- (3) negative heats of mixing
- (4) close to a eutectic composition
- (5) compositions far from a Laves phase region

- **Higher degree of dense random packed structure**
- *Suppression* of nucleation and growth of crystalline phase



**High glass-forming ability (GFA)**

### 3. Glass-Forming Ability of Alloys

- Many glasses were produced more or less by trial and error.  
→ The ability of a metallic alloy to transform into the glassy state is defined in this chapter as the glass-forming ability (GFA).

#### 3.2 Critical Cooling Rate

If an alloy melt is solidified from a temperature above the liquidus temperature,  $T_l$  to below the glass transition temperature,  $T_g$ , then the volume fraction of the solid crystalline phase,  $X$  formed under non-isothermal crystallization conditions can be given by the equation [8,9]

$$X(T) = \frac{4\pi}{3R^4} \int_{T_l}^{T_g} I(T') \left[ \int_{T''}^{T_g} U(T'') dT'' \right]^3 dT' \quad (3.1)$$

where  $I$  and  $U$  are the steady-state nucleation frequency and crystal growth rate,

$$\boxed{X = 10^{-6}} \rightarrow R_c^4 = \frac{4\pi}{3 \times 10^{-6}} \int_{T_l}^{T_g} I(T') \left[ \int_{T''}^{T_g} U(T'') dT'' \right]^3 dT' \quad (3.2)$$

Since the equations for  $I$  and  $U$  contain terms like viscosity of the supercooled liquid,  $\eta$ , entropy of fusion,  $\Delta S_f$ , etc., the critical cooling rate,  $R_c$  decreases with increasing  $\eta$ ,  $\Delta S_f$  and decreasing liquidus temperature,  $T_l$ . The best way to experimentally determine  $R_c$  is by constructing the time-temperature-transformation ( $T$ - $T$ - $T$ ) diagrams.

### 3.2.1 T-T-T Diagrams: isothermal processes

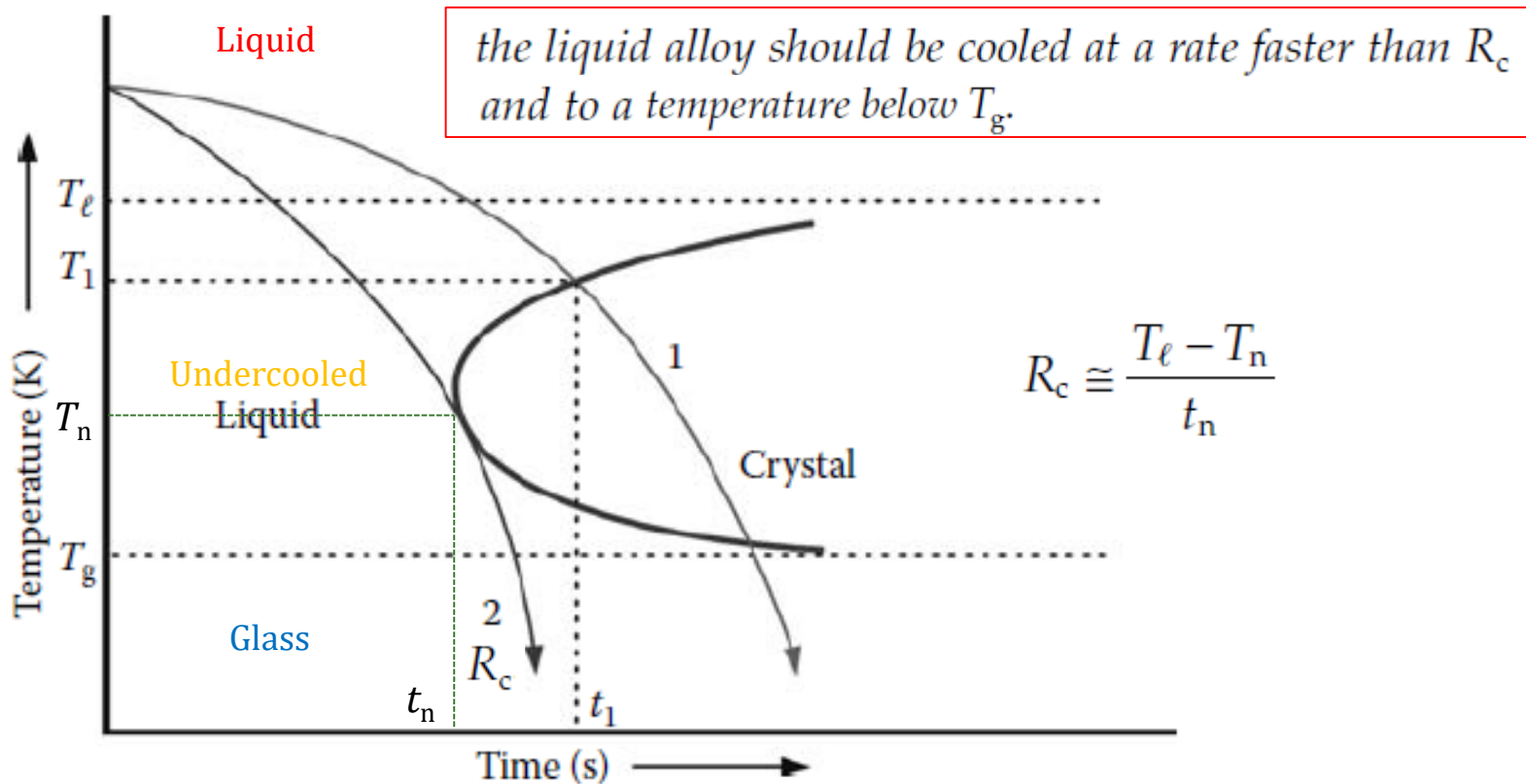


FIGURE 3.1

Schematic time-temperature-transformation ( $T$ - $T$ - $T$ ) diagram for a hypothetical alloy system. When the liquid alloy is cooled from above the liquidus temperature  $T_\ell$ , at a rate indicated by curve "1," solidification starts at a temperature  $T_1$  and time  $t_1$ . The resultant product is a crystalline solid. However, if the same liquid alloy is now cooled, again from  $T_\ell$ , at a rate faster than the rate indicated by curve "2," the liquid will continue to be in the undercooled state, and when cooled below the glass transition temperature  $T_g$ , the liquid is "frozen-in" and a glassy phase is formed. The cooling rate represented by curve "2" is referred to as the critical cooling rate,  $R_c$ .

# $R_c$ vs $D_{max}$ in Ti-Zr-Cu-Ni alloy system

J. Appl. Phys. 78, 1 December 1995

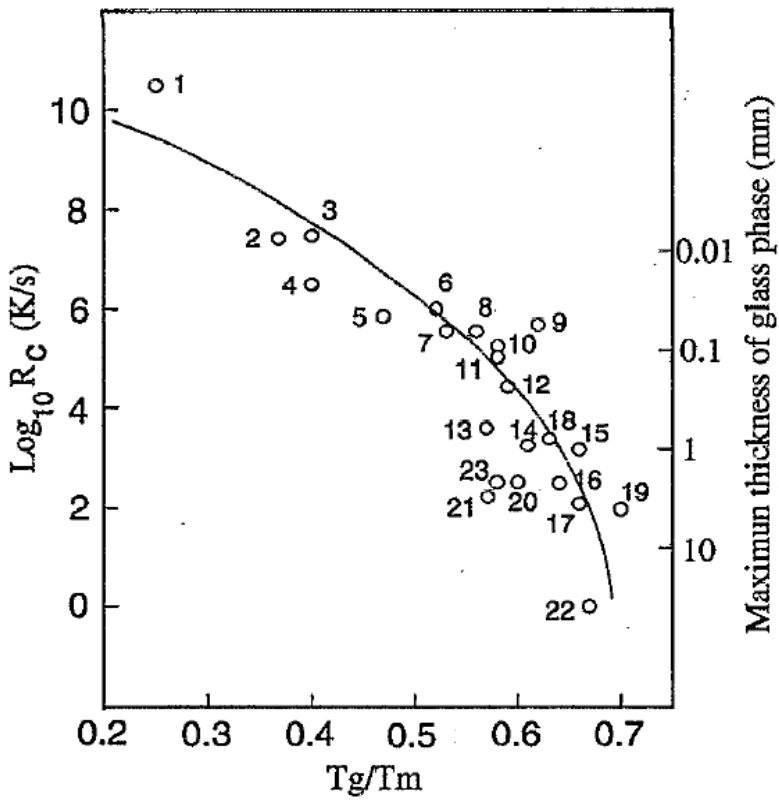


FIG. 1. Critical cooling rates for glass formation and corresponding maximum thickness of glass phase. Key to the alloys: (1) Ni; (2)  $Fe_{91}B_9$ ; (3)  $Fe_{89}B_{11}$ ; (4) Te; (5)  $Au_{77.8}Ge_{13.8}Si_{8.4}$ ; (6)  $Fe_{83}B_{17}$ ; (7)  $Fe_{41.5}Ni_{41.5}B_{17}$ ; (8)  $Co_{75}Si_{15}B_{10}$ ; (9) Ge; (10)  $Fe_{79}Si_{10}B_{11}$ ; (11)  $Ni_{75}Si_8B_{17}$ ; (12)  $Fe_{80}P_{13}C_7$ ; (13)  $Pt_{60}Ni_{15}P_{25}$ ; (14)  $Pd_{82}Si_{18}$ ; (15)  $Ni_{62.4}Nb_{37.6}$ ; (16)  $Pd_{77.5}Cu_6Si_{16.5}$ ; (17)  $Pd_{40}Ni_{40}P_{20}$  (above from Ref. 3); (18)  $Au_{53}Pb_{22.5}Sb_{22.5}$  (Ref. 6); (19)  $La_{55}Al_{25}Ni_{10}Cu_{10}$  (Ref. 7); (20)  $Mg_{65}Cu_{25}Y_{10}$  (Ref. 8); (21)  $Zr_{65}Cu_{17.5}Ni_{10}Al_{7.5}$  (Ref. 9); (22)  $Zr_{41.2}Ti_{13.8}Cu_{12.5}Ni_{10}Be_{22.5}$  (Refs. 4 and 5); (23)  $Ti_{34}Zr_{11}Cu_{47}Ni_8$ .

Total cooling time  $\tau \sim (R^2/\kappa)$

sample dimension (dia. or thickness) :  $R$

initial temperature:  $T_m$

thermal diffusivity :  $\kappa$

$$\kappa = K/C$$

thermal conductivity :  $K$

heat capacity per unit volume:  $C$

$$\dot{T} = \frac{dT}{dt} = \frac{(T_m - T_g)}{\tau} = \frac{K(T_m - T_g)}{CR^2}$$

For Ti-Zr-Cu-Ni system,

$$T_m - T_g \sim 400K \quad K \sim 0.1W/cm s^{-1}K^{-1} \quad C \sim 4J/cm^3K^{-1}$$

$$\dot{T}(K/s) = 10/R^2(cm)$$

### 3.2.2. Effect of Alloying Elements

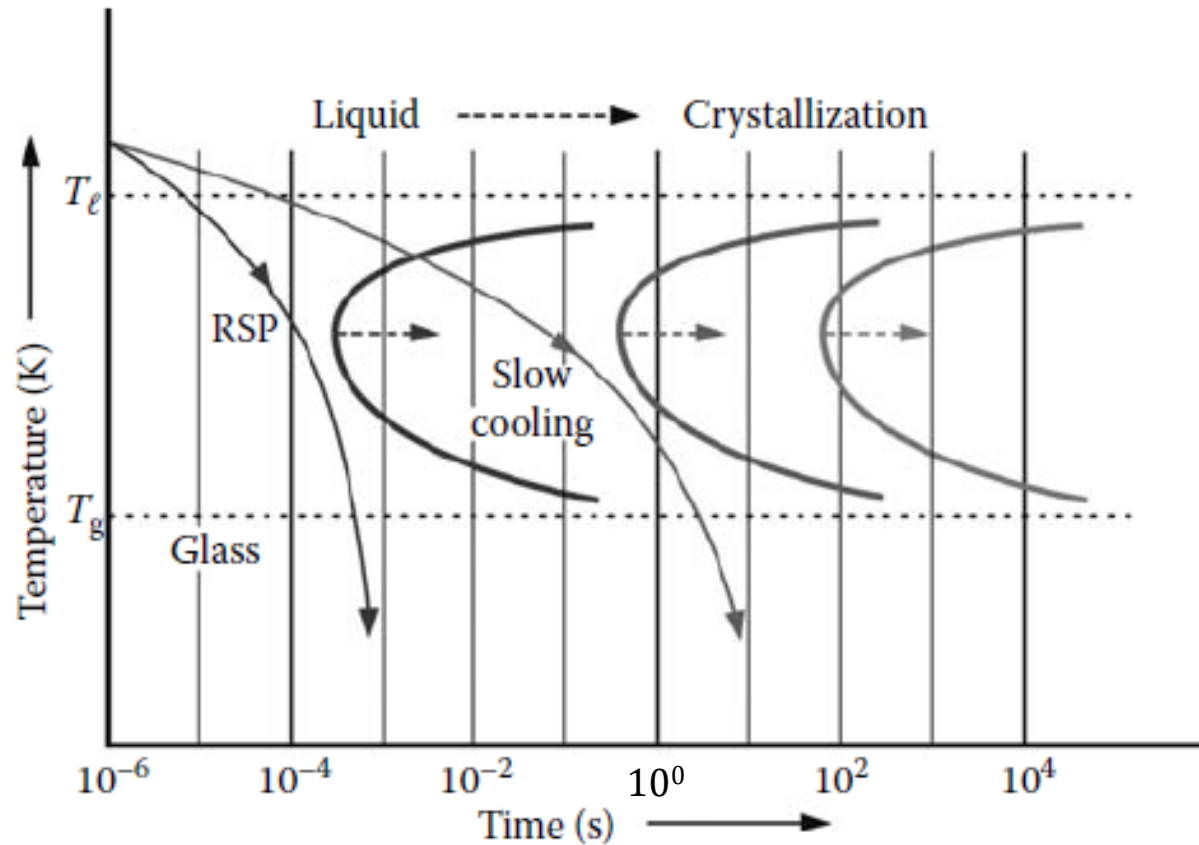


**FIGURE 3.2**

Position of the  $T$ - $T$ - $T$  curves with the addition of a large number of alloying elements. The  $C$ -curve shifts to the right with increasing number of alloying elements and consequently, the glassy phase can be synthesized at slow solidification rates. The left-most  $C$ -curve represents a typical situation of an alloy system where a glassy phase is obtained by rapid solidification processing (RSP) from the liquid state. The middle  $C$ -curve represents an alloy composition where a glassy phase can be obtained by slow cooling. The right-most  $C$ -curve represents a situation when an alloy can be very easily produced in a glassy state.

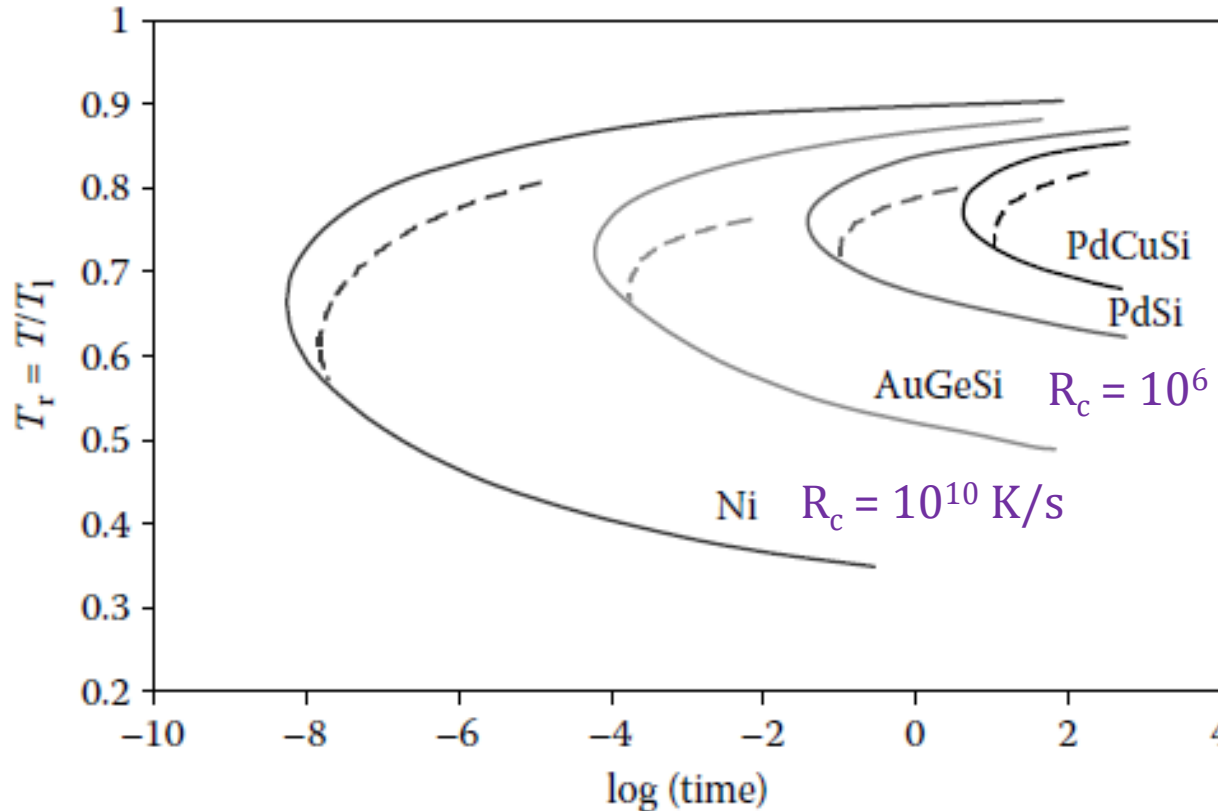
$R_c$  $> 10^{10-12}$  K/s $10^{4-6}$  K/s $10^2$  K/s $1.3 \times 10^{-2}$  or 0.067 K/s $10^{-5}$  to  $10^{-4}$  K/s

pure metals

binary metallic liquids, multicomponent

Pd<sub>37.5</sub>Cu<sub>32.5</sub>Ni<sub>10</sub>P<sub>20</sub>  
Pd<sub>30</sub>Pt<sub>17.5</sub>Cu<sub>32.5</sub>P<sub>20</sub>

Oxide glasses



$$R_c = \frac{\Delta T}{t_n}$$

 $R_c = 3.5 \times 10^1$  K/s $R_c = 3 \times 10^3$  K/s $R_c = 10^6$  K/s $R_c = 10^{10}$  K/s

FIGURE 2.3

Time-temperature-transformation ( $T$ - $T$ - $T$ ) curves (solid lines) and the corresponding continuous cooling transformation curves (dashed lines) for the formation of a small volume fraction for pure metal Ni, and Au<sub>78</sub>Ge<sub>14</sub>Si<sub>8</sub>, Pd<sub>82</sub>Si<sub>18</sub>, and Pd<sub>78</sub>Cu<sub>6</sub>Si<sub>16</sub> alloys.

 $T_{rg}$ 

1/4

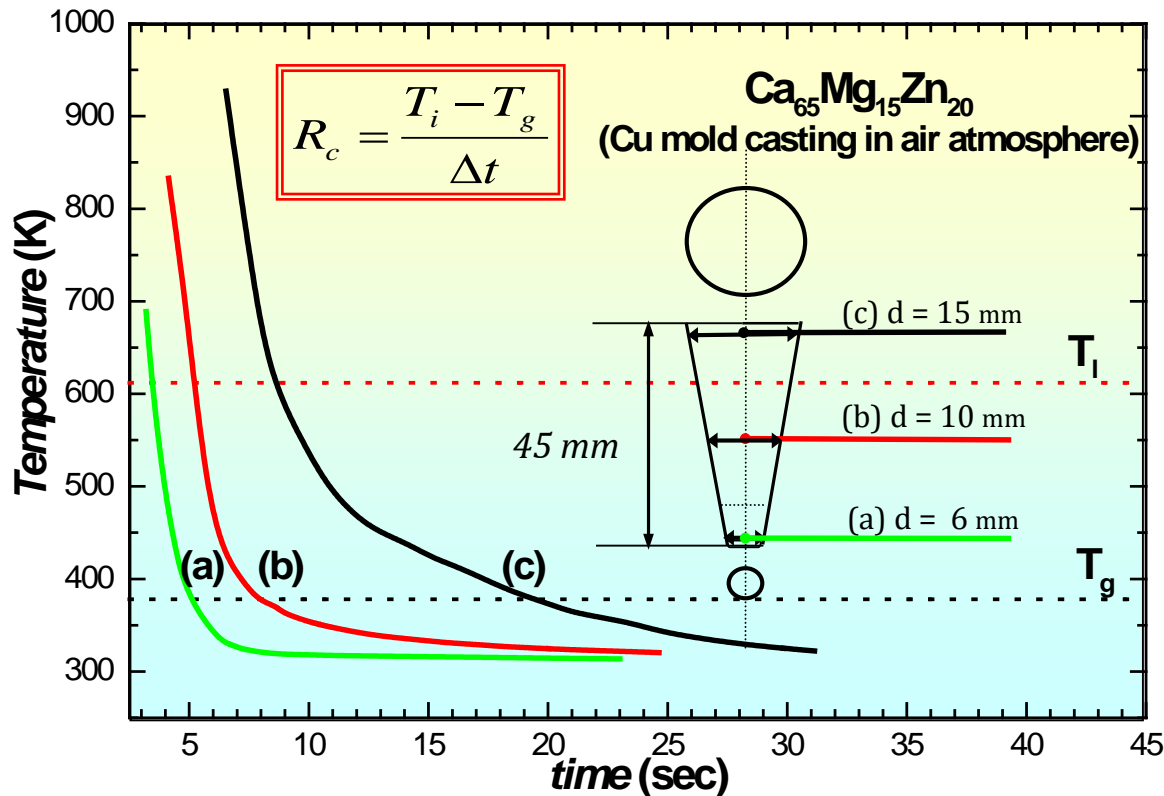
1/2

2/3

### 3.2.3 Measurement of $R_c$

The measurement of  $R_c$  is an involved and time-consuming process. One has to take a liquid alloy of a chosen composition and allow it to solidify at different cooling rates and determine the nature and amount of phases formed after solidification.

#### Measurement of $R_c$ in $\text{Ca}_{65}\text{Mg}_{15}\text{Zn}_{20}$ ( $D_{\text{max}} > 15 \text{ mm}$ )



top position : 20 K/s  
middle position : 93 K/s  
bottom position : 149 K/s

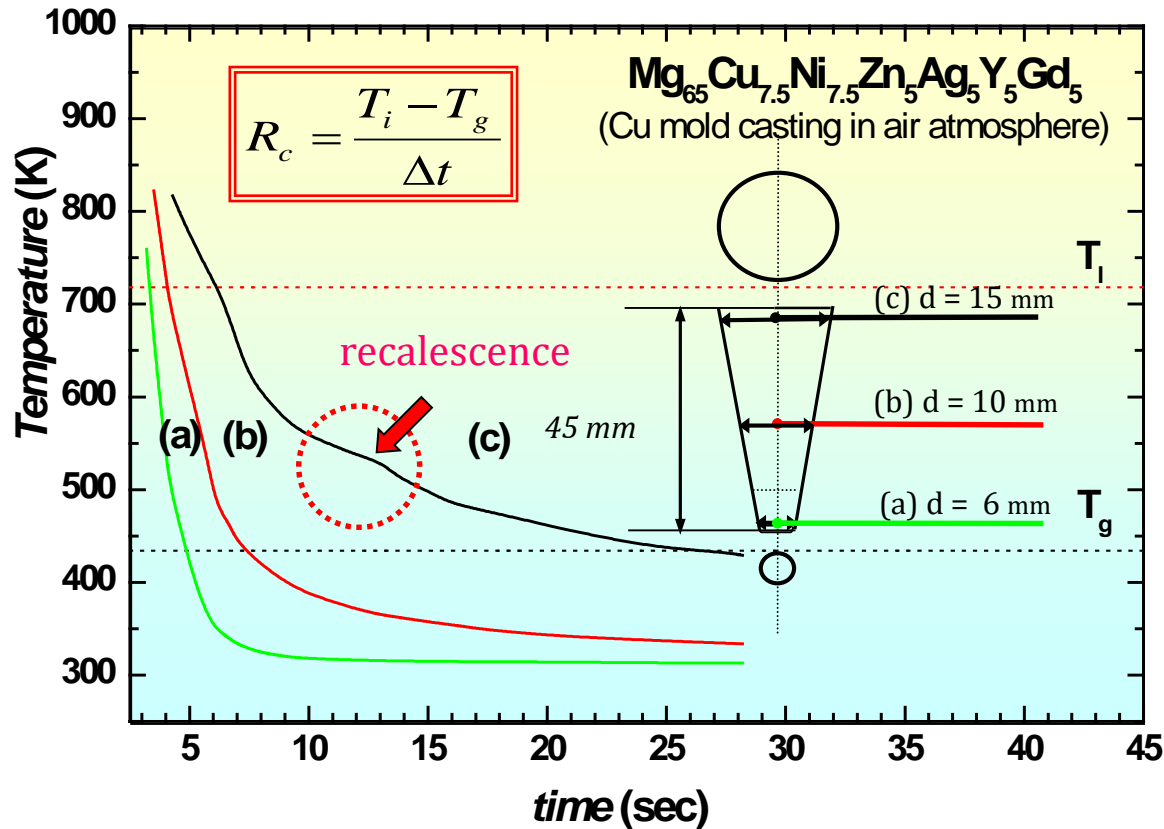
\* Cooling curves measured at the center of the three transverse cross sections

\* J. Mater. Res. 19, 685 (2004)

\* Mater. Sci. Forum 475-479, 3415 (2005)

### 3.2.3 Measurement of $R_c$

## Measurement of $R_c$ in Mg BMG ( $D_{\max}=14$ mm)



top position : recalcescence

middle position : 64K/s

bottom position : 137 K/s

\* Cooling curves measured at the center of the three transverse cross sections

**TABLE 3.1**

Some Representative Critical Cooling Rates ( $R_c$ ) for Formation of Glassy Phases in Different Alloy Systems

1) Effect of  $B_2O_3$  fluxing

$Pd_{40}Cu_{30}Ni_{10}P_{20}$   $1.58 K s^{-1}$  without fluxing [22]  
 $0.1 K s^{-1}$  with fluxing [18]

2) Effect of # of components

$Pd_{82}Si_{18}$   $1.8 \times 10^3 K s^{-1}$   $\longleftrightarrow$   $550 K s^{-1}$   $Pd_{78}Cu_6Si_{16}$   
 $Cu_{50}Zr_{50}$   $250 K s^{-1}$   $\longleftrightarrow$   $\leq 40 K s^{-1}$   $Cu_{48}Zr_{48}Al_4$

3) Nature of alloying addition

$Mg_{65}Cu_{25}Y_{10}$   $100 K s^{-1}$   $\longleftrightarrow$   $1 K s^{-1}$   $\longleftrightarrow$   $0.7 K s^{-1}$   
 $Mg_{65}Cu_{25}Gd_{10}$   $Mg_{65}Cu_{15}Ag_5Pd_5Gd_{10}$

Alloy Composition	$R_c$ (K s <sup>-1</sup> )	Reference
<del><math>Au_{77.8}Ge_{13.8}Si_{8.4}</math></del>	<del><math>3 \times 10^6</math></del>	<del>[24]</del>
$Ca_{60}Mg_{25}Ni_{15}$	24	[25]
$Ca_{65}Mg_{15}Zn_{20}$	<20	[26]
$Cu_{50}Zr_{50}$	250	[27]
$Cu_{48}Zr_{48}Al_4$	<40	[27]
$Cu_{42}Zr_{42}Ag_8Al_8$	4.4	[28]
$Fe_{43}Cr_{16}Mo_{16}C_{10}B_5P_{10}$	100	[29]
<del><math>Fe_{40}Ni_{40}P_{14}B_6</math> (Metglas 2826)</del>	<del><math>4.4 \times 10^7</math></del>	<del>[30]</del>
<del><math>Hf_{70}Pd_{20}Ni_{10}</math></del>	<del>124</del>	<del>[31]</del>
$La_{55}Al_{25}Cu_{20}$	58	[32]
$La_{55}Al_{25}Ni_{20}$	69	[32]
$Mg_{65}Cu_{25}Gd_{10}$	1	[16]
$Mg_{65}Cu_{25}Y_{10}$	100	[33]
$Mg_{65}Cu_{15}Ag_5Pd_5Gd_{10}$	0.7	[34]
$Mg_{65}Cu_{7.5}Ni_{7.5}Ag_5Zn_5Gd_5Y_5$	20	[35]
$Nd_{60}Co_{30}Al_{10}$	4	[36]
$Ni_{62}Nb_{38}$	57	[37]
$Ni_{65}Pd_{15}P_{20}$	$10^5$	[38]
$Pd_{78}Cu_6Si_{16}$	550	[39]
$Pd_{40}Ni_{40}P_{20}$	128	[22]
$Pd_{42.5}Cu_{30}Ni_{7.5}P_{20}$	0.067	[18]
$Pd_{40}Cu_{25}Ni_{15}P_{20}$	0.150	[18]
$Pd_{40}Cu_{30}Ni_{10}P_{20}$ (without fluxing)	1.58	[22]
$Pd_{40}Cu_{30}Ni_{10}P_{20}$ (with flux treatment)	0.1	[18]
$Pd_{30}Pt_{17.5}Cu_{32.5}P_{20}$	0.067	[19]
$Pd_{82}Si_{18}$	$1.8 \times 10^3$	[40]
$Pd_{81}Si_{19}$ (with flux treatment)	800	[41]
$Pd_{81}Si_{19}$ (with flux treatment)	6	[42]
$Zr_{65}Al_{7.5}Ni_{10}Cu_{17.5}$	1.5	[43]
$Zr_{41.2}Ti_{13.8}Cu_{12.5}Ni_{10.0}Be_{22.5}$	1.4	[44]
$Zr_{46.25}Ti_{8.25}Cu_{7.5}Ni_{10.0}Be_{27.5}$	28	[44]
$Zr_{57}Cu_{15.4}Ni_{12.6}Al_{10}Nb_5$	10	[45]

# *Glass formation*

*Retention of liquid phase*

*Formation of crystalline phases*

*Thermodynamical point*

Small change in free E. (liq. → cryst.)

*Kinetic point*

Low nucleation and growth rates

*Structural point*

Highly packed random structure

## *Empirical rules*

- (1) multi-component alloy system
- (2) significant difference in atomic size ratios
- (3) negative heats of mixing
- (4) close to a eutectic composition
- (5) compositions far from a Laves phase region

- **Higher degree of dense random packed structure**
- *Suppression* of nucleation and growth of crystalline phase

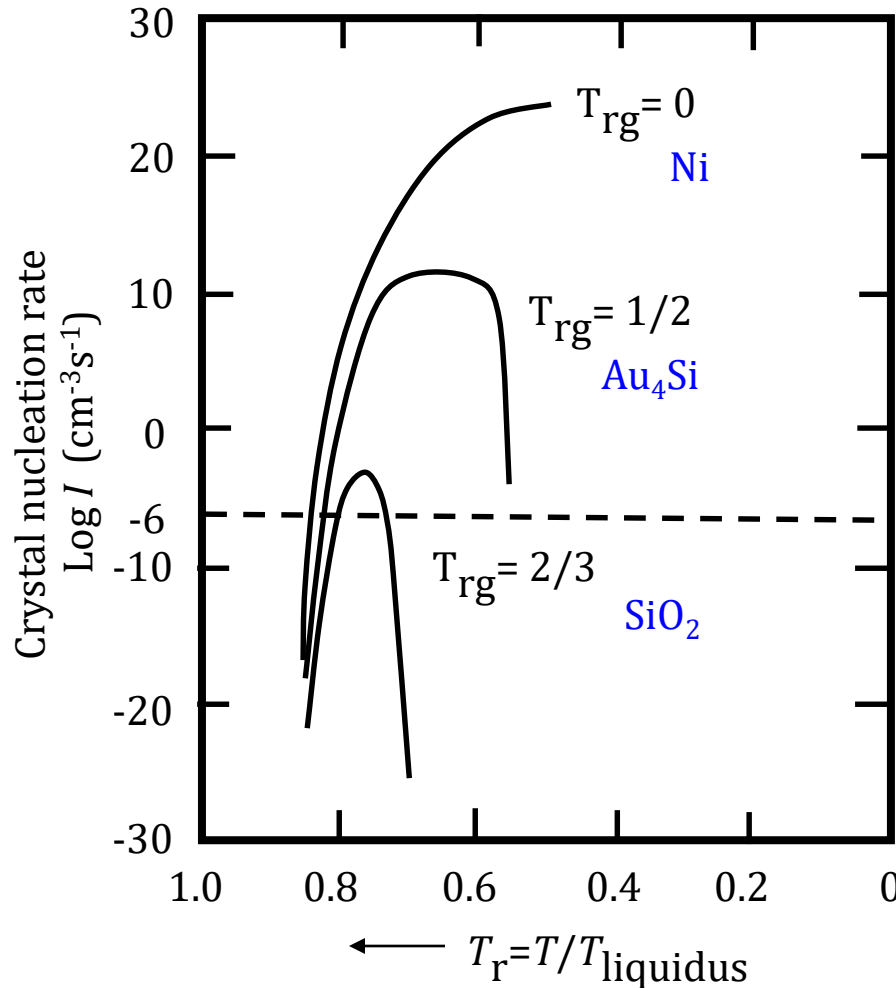


*High glass-forming ability (GFA)*

### 3.3 Reduced Class Transition Temperature (Kinetic aspect for glass formation)

$T_{rg}$  parameter =  $T_g/T_l \sim \eta$  : the higher  $T_{rg}$ , the higher  $\eta$ , the lower  $R_c$

: ability to avoid crystallization during cooling



$$T_{rgNi} < T_{rgAu4Si} < T_{rgSiO2}$$

$$R_{Ni} > R_{Au4Si} > R_{SiO2}$$

Turnbull, 1959 ff.

- Based on the nucleation theory, Turnbull suggested that at  $T_{rg} \geq 2/3$ , homogeneous nucleation of the crystalline phase is completely suppressed. Most typically, a minimum value of  $T_{rg} \sim 0.4$  has been found to be necessary for the glass to form.
- One should note the  $T_l$ , liquidus temperature as the point at the end of the liquid formation, and not at the beginning of melting.

**TABLE 3.2**  
 Reduced Glass Transition Temperatures ( $T_{rg}$ )  
 for Different Glass-Forming Alloys

Alloy Composition	$T_{rg}$	References
$Ca_{65}Al_{35}$	0.69	[47]
$Ca_{67}Mg_{19}Cu_{14}$	0.60	[48]
$Ca_{57}Mg_{19}Cu_{24}$	0.64	[48]
$Cu_{65}Hf_{35}$	0.62	[49]
$Cu_{49}Hf_{42}Al_9$	0.62	[50]
$Cu_{64}Zr_{36}$	0.64	[51]
$La_{55}Al_{25}Ni_{20}$	0.71	[32]
$La_{62}Al_{15.5}(Cu,Ni)_{22.3}$	0.58	[52]
$La_{50.2}Al_{20.5}(Cu,Ni)_{29.3}$	0.47	[52]
$Ni_{62}Nb_{38}$	0.60	[37]
$Ni_{61}Nb_{33}Zr_6$	0.49	[53]
$Pd_{40}Ni_{40}P_{20}$	0.67	[54]
$Pd_{40}Cu_{30}Ni_{10}P_{20}$	0.67	[18,55]
$Zr_{41.2}Ti_{13.8}Cu_{12.5}Ni_{10}Be_{22.5}$	0.624	[45]
$Zr_{45.38}Ti_{9.62}Cu_{8.75}Ni_{10}Be_{26.25}$	0.50	[44]

- The concept of  $T_{rg}$  was introduced for kinetic reasons with the need to avoid crystallization [46]. It is known (and we will discuss this in some detail in Section 3.4) that  $T_g$  is a very weak function of the solute content, i.e.,  $T_g$  varies much more slowly with solute concentration than the liquidus temperature,  $T_l$ . Consequently, the value of  $T_{rg}$  increases with increasing solute content, up to the eutectic composition, and therefore it becomes easier to avoid crystallization of the melt at the eutectic composition [13]. This reasoning seems to work well in simple binary alloy systems. But, in the case of multicomponent alloy systems such as the BMG compositions, the values of  $T_g$  and  $T_l$  vary significantly. Since the variation of viscosity with temperature is different for different alloy systems (and depends on whether a glass is strong or fragile),  $T_g$  alone may not provide information about the variation of viscosity with temperature and therefore, the  $T_{rg}$  criterion may not be valid in some systems.

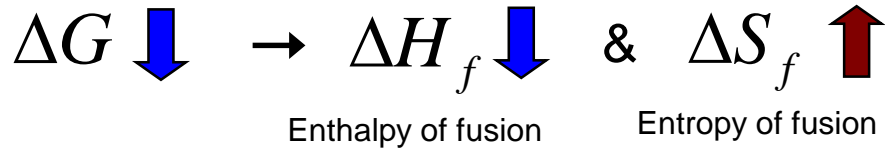
Easy glass formation at compositions corresponding to high  $T_{rg}$  can be easily realized in alloy systems that feature deep eutectic reactions in their phase diagrams, and this is further explained in Section 3.4.

### 3.4 Deep Eutectics (Thermodynamic aspect for glass formation)

- High GFA : low free energy  $\Delta G(T)$

for transformation of liquid to crystalline phase

$$\Delta G(T) = \Delta H_f - T\Delta S_f$$



$\Delta S_f \uparrow$   
Entropy of fusion

: proportional to the number of microscopic states

**Multi-component alloy systems** containing more than 3 elements  
*causes an increase in the degree of dense random packing*

$\Delta H_f \downarrow$   
Enthalpy of fusion

**Large negative enthalpy of mixing** among constituent elements

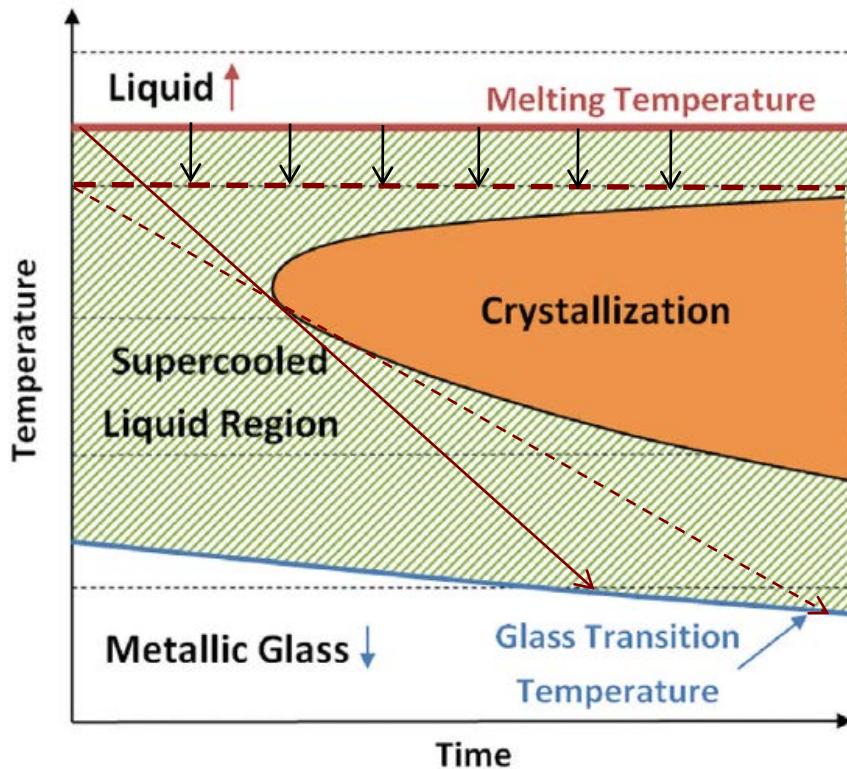
- \* The free energy at a constant temperature also decreases in the cases of low chemical potential caused by **low enthalpy** and **high reduced glass transition temperature** ( $=T_l/T_g$ ) and **high interface energy** between liquid and solid phase.

### 3.4 Deep Eutectics (Thermodynamic aspect for glass formation)

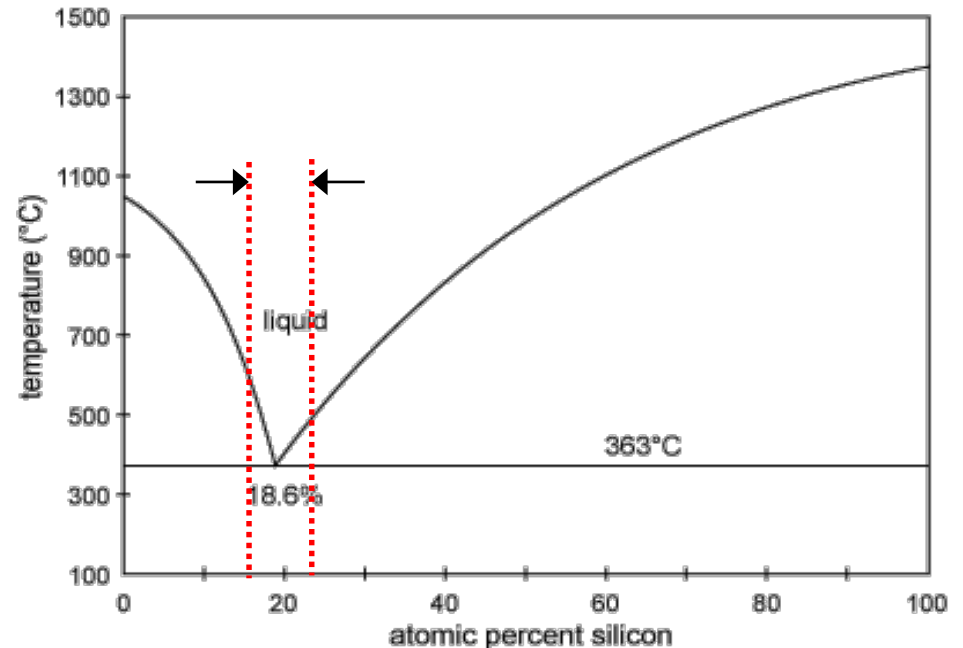
$\Delta H_f \downarrow \rightarrow$  deep eutectic condition: increase stability of stable liquid ( $= T_g/T_l \uparrow$ )

- decreasing melting point  $\rightarrow$  less supercooled at  $T_g \rightarrow \Delta G = G^{liq} - G^{cryst} \downarrow$

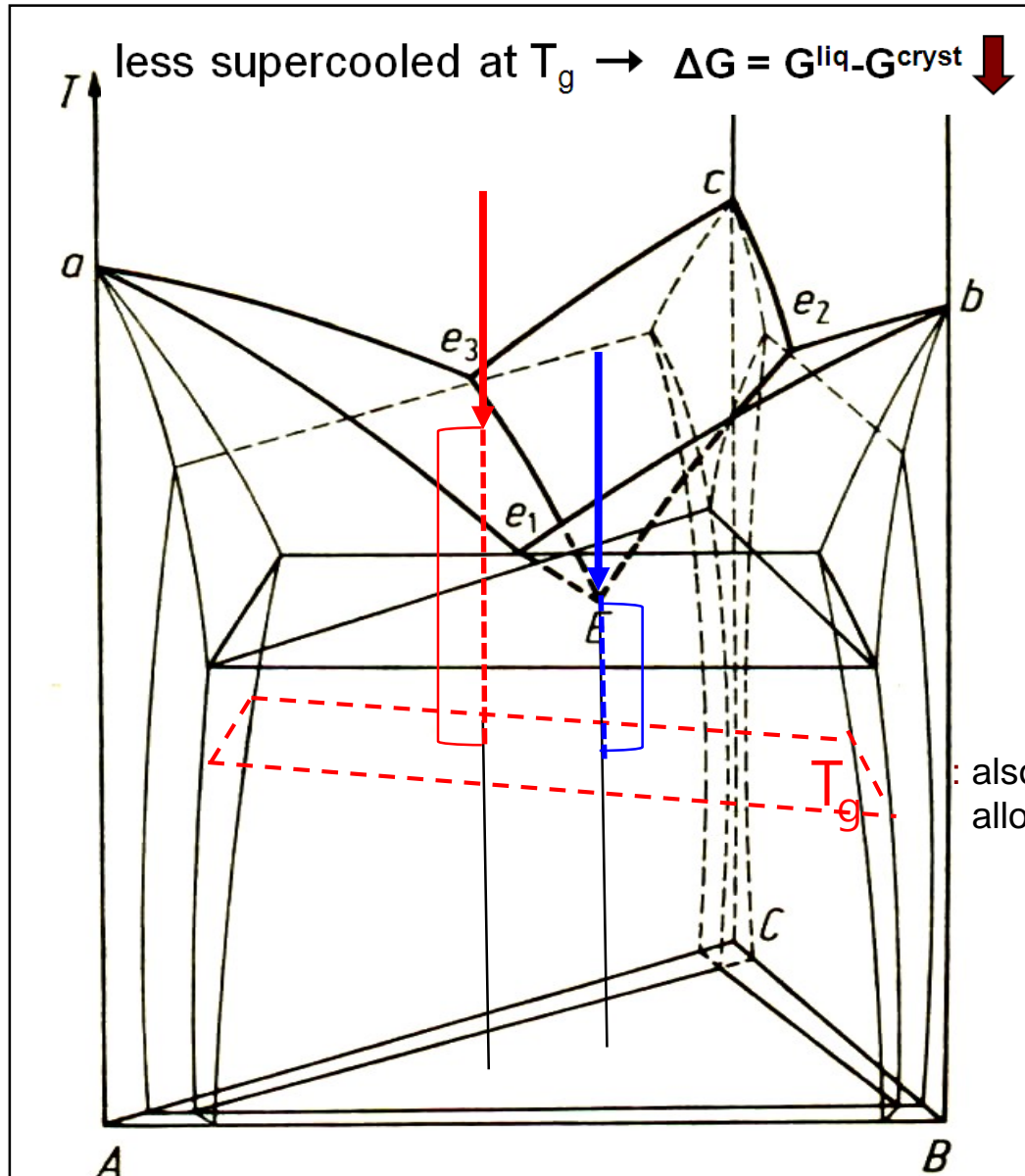
ex) metallic / inorganic system



Glass forming region:  
Compositions near the eutectic



# Multi-component eutectic alloys with strong negative heat of mixing



: also changes depending on alloy composition

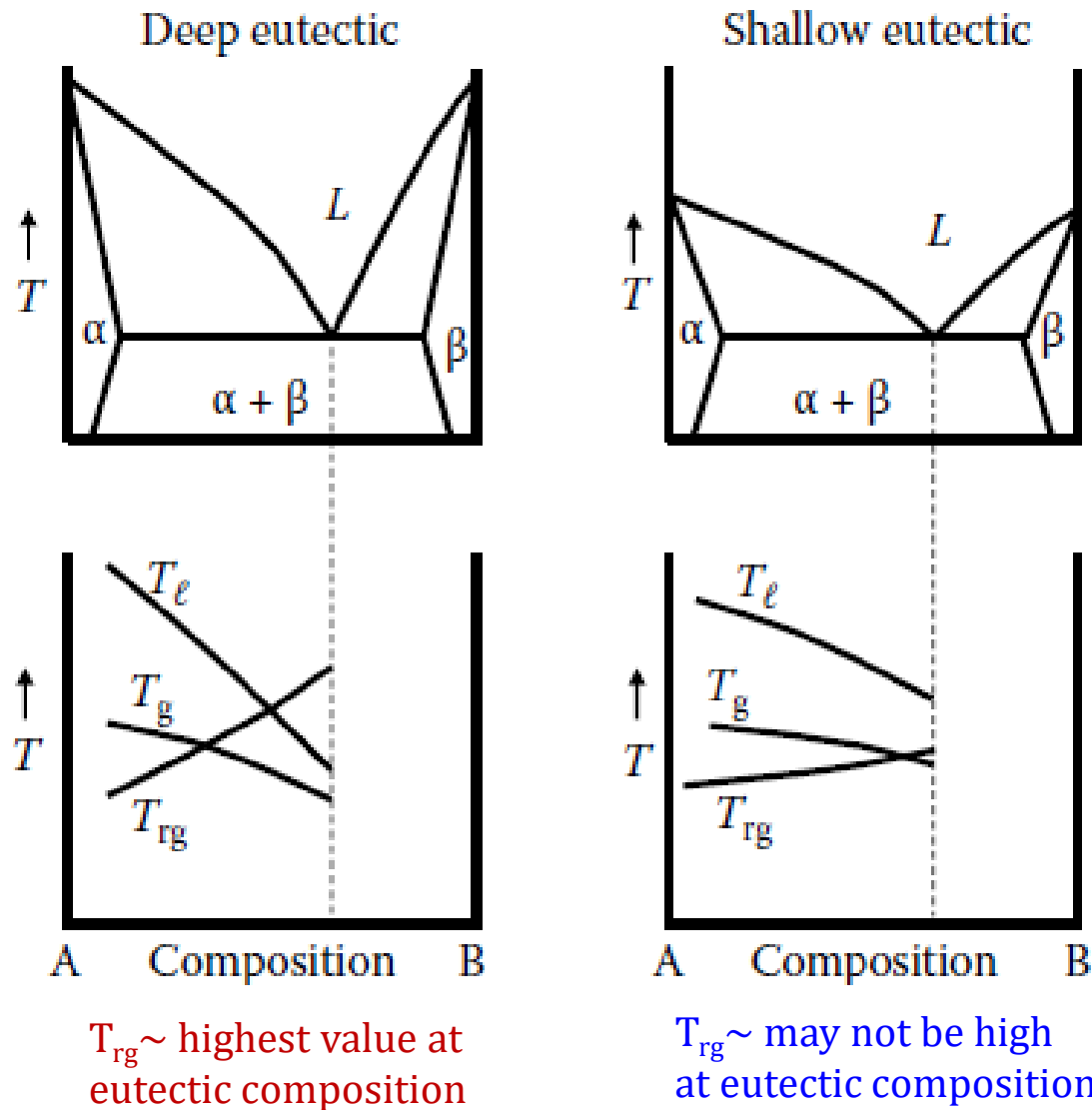


**FIGURE 3.3**

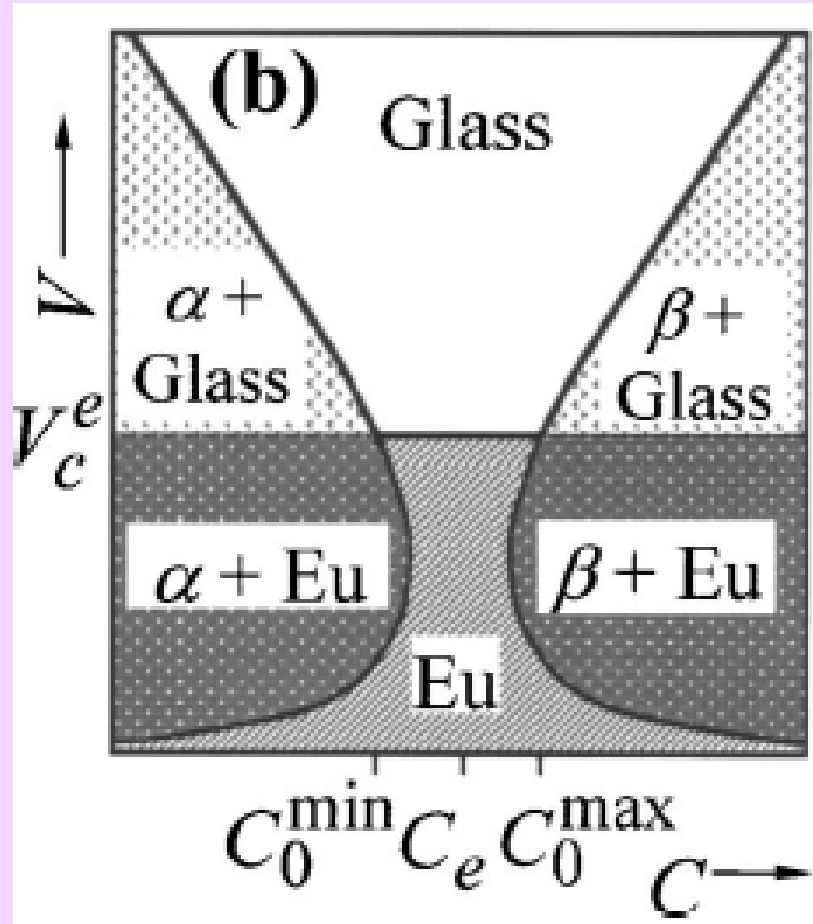
Schematic variation of the glass transition temperature,  $T_g$ , liquidus temperature,  $T_l$ , the reduced glass transition temperature,  $T_{rg}$ , in two different types of eutectic systems—deep eutectic and shallow eutectic.

Ribbons of about 20–50 μm in thickness were produced by melt-spinning techniques in a number of binary alloy systems near eutectic compositions and they were confirmed to be glassy. Some of the most investigated eutectic compositions are found in Fe–B, Pd–Si, Cu–Zr, Ni–Nb, Ni–Ta, etc., alloy systems [1,2]. There have been some reports in recent years of “bulk” (?) metallic glass synthesis in binary alloy systems such as Ca–Al [59], Cu–Hf [49], Cu–Zr [51], Ni–Nb [37], and Pd–Si [42]. But, the maximum diameters of these binary alloy glassy rods were only 1 or 2 mm, and even then, some of these alloy glasses contained nanocrystalline particles embedded in the glassy matrix [60]. This point will be further discussed in detail in later chapters. But, the

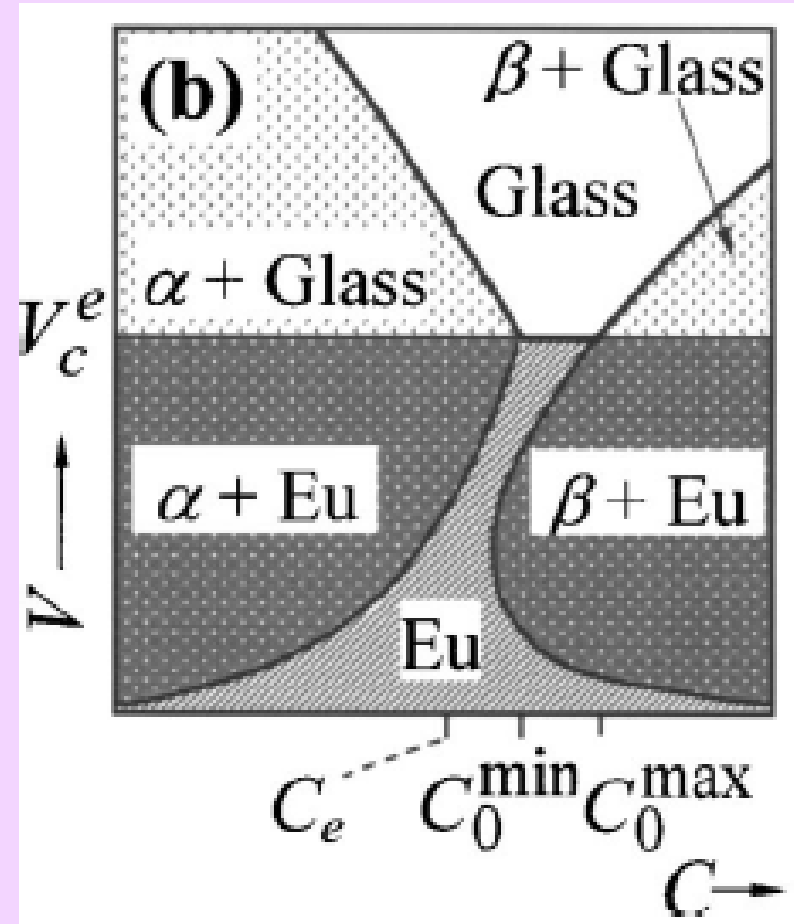
- important point here is that the “bulk” glassy phase is produced not at the eutectic composition, but, at off-eutectic compositions. Further, the highest GFA, i.e., the composition at which glass formation was the easiest or the maximum diameter of the BMG rod could be obtained, was located away from the eutectic composition. The best glass-forming compositions have been reported to be at 35 at.% Hf in Cu–Hf, 36 at.% Zr in Cu–Zr, 38 at.% Nb in Ni–Nb, and 19 at.% Si in Pd–Si alloy systems. But, the eutectic compositions in these alloy systems are at 33.0 and 38.6 at.% Hf in Cu–Hf, 38.2 at.% Zr in Cu–Zr, 40.5 at.% Nb in Ni–Nb, and 17.2 at.% Si in Pd–Si systems [61]. Similarly, it was reported that while a nearly fully glassy rod with 12 mm diameter could be obtained at an off-eutectic composition near  $\text{La}_{62}\text{Al}_{15.7}(\text{Cu},\text{Ni})_{22.3}$ , only a 1.5 mm diameter rod could be obtained in a fully glassy condition for the eutectic alloy of  $\text{La}_{66}\text{Al}_{14}(\text{Cu},\text{Ni})_{20}$  [52].

## Strategy for pinpointing the best glass-forming alloys

< Symmetric Eutectic >



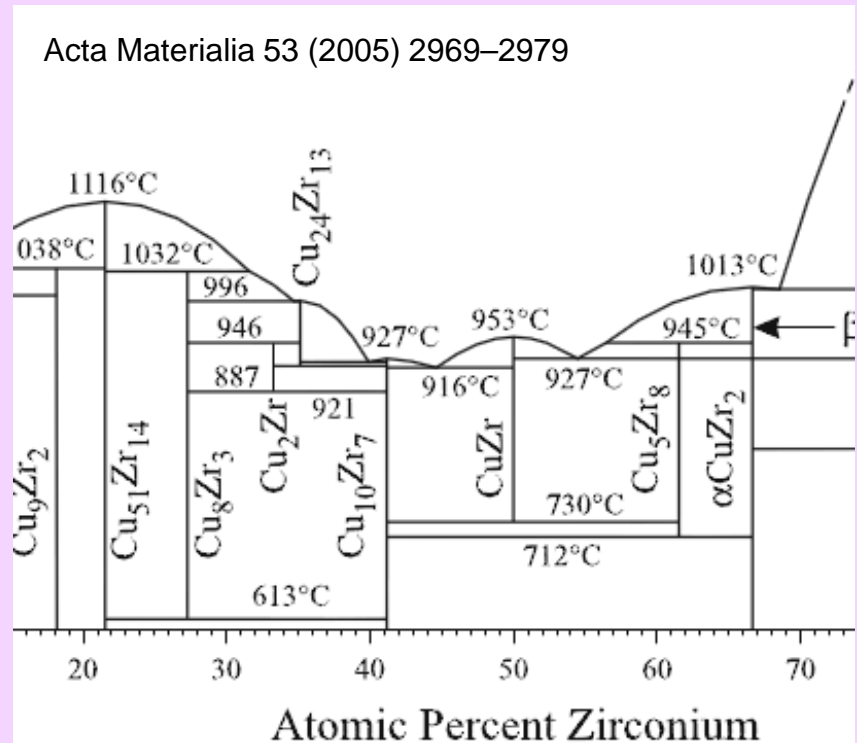
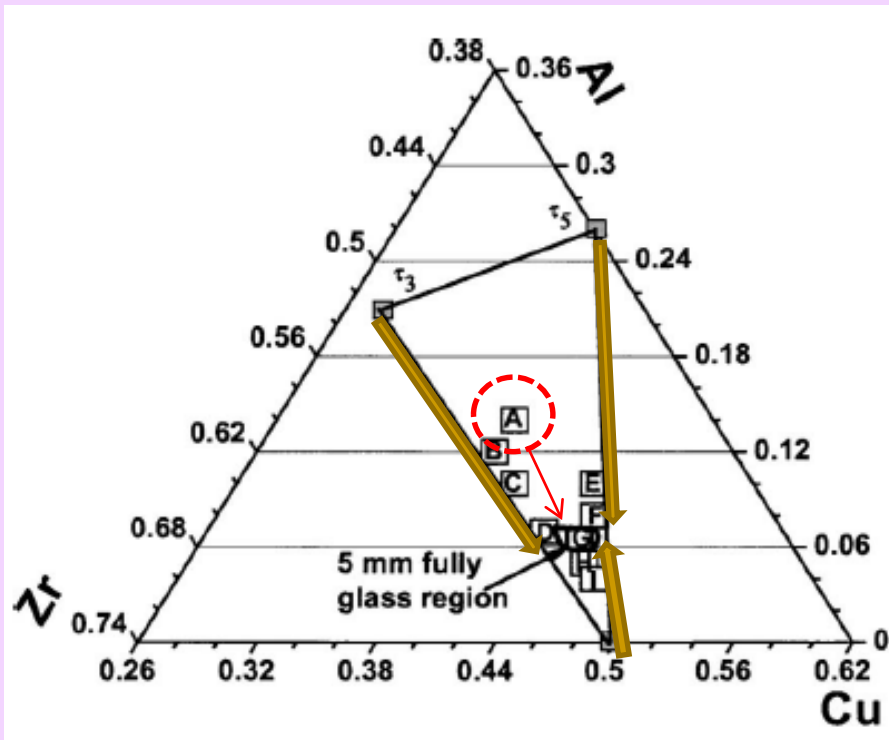
< Non-symmetric Eutectic >



► Glass region is located between composites with different 2<sup>nd</sup> phases.

➔ Useful to find the composition with maximum GFA

# Composites & Glass forming composition

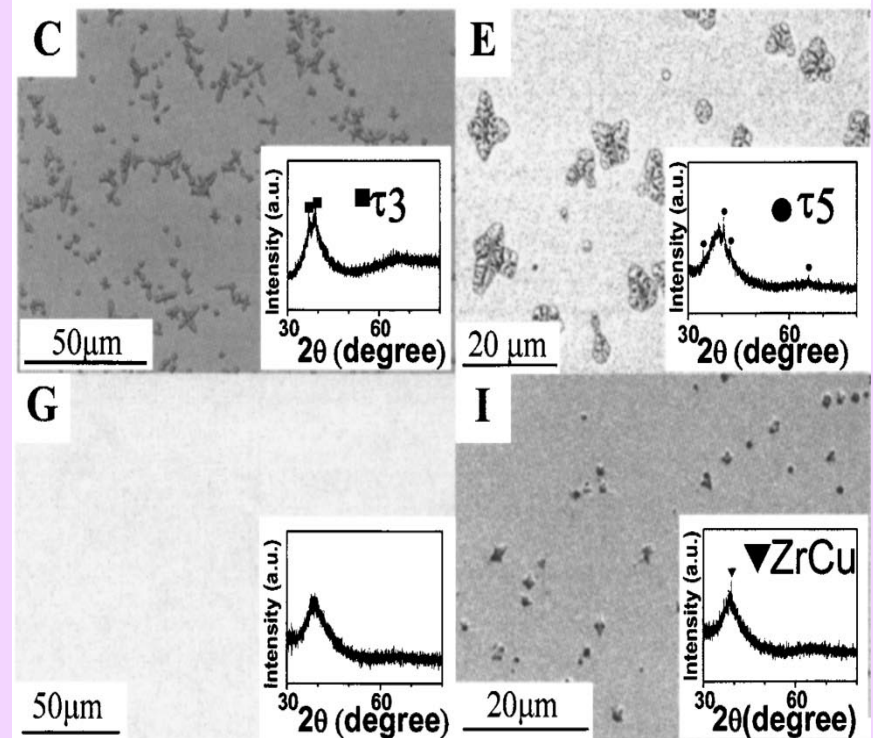
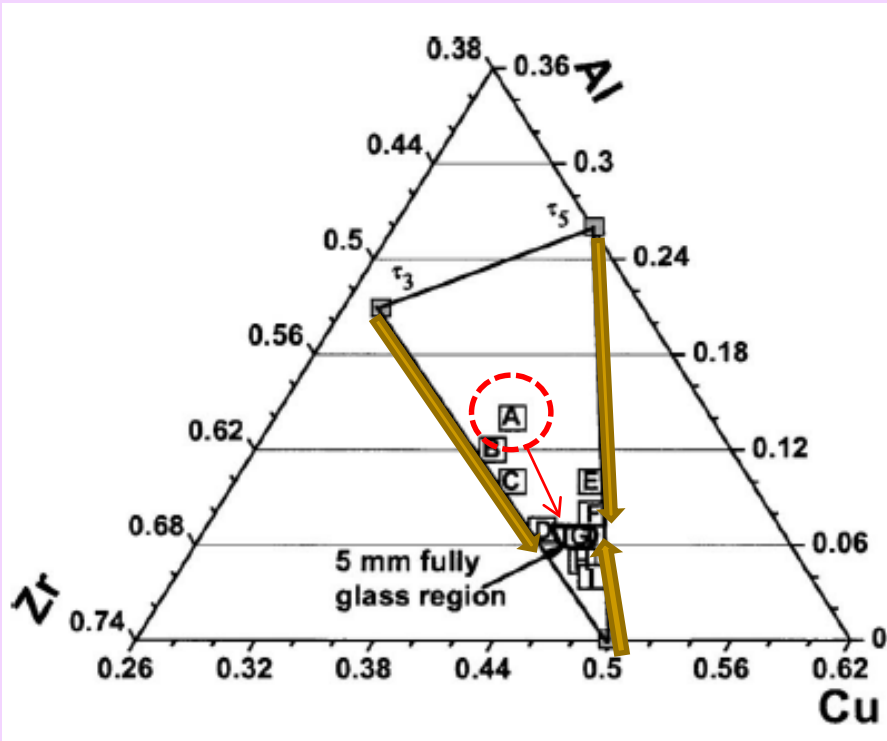


► Tie triangle among  $\text{ZrCu}$ ,  $\tau_3$ ,  $\tau_5 \rightarrow A = \text{“ternary eutectic composition”}$

1.  $A(\text{Zr}_{48}\text{Cu}_{38}\text{Al}_{14})$  : eutectic composition but glass and composite X

➔ In Cu-Zr alloy, the composition with high GFA is moved to near liquidus line with higher slope of Zr-rich composition.

# Composites & Glass forming composition



2. Three composition forming region (casted into 5 mm-diam copper mold)

Following arrows,  $\tau_3$ +glass (B,C,D),  $\tau_5$ +glass (E,F), ZrCu + glass (I,H) ~

➔ At point G, competing crystalline phase changes

➔ G = Formation of fully glass

### 3.5 Topological Model (Structural aspect for glass formation)

Metallic glasses produced by RSP methods in the form of thin ribbons have been traditionally classified into two groups, viz., metal–metalloid and metal–metal types. Structural models of the metal-metalloid-type metallic glasses have identified that the best composition to form a glass is one that contains about 80 at.% of the metal component and 20 at.% of the metalloid component. The actual glass composition ranges observed are 75–85 at.% of the metal and 15–25 at.% of the metalloid. As stated in Chapter 2, the 80 at.% of the metal can be either a single transition metal or a combination of transition metals or one or a combination of noble metals. Similarly, the 20 at.% of the metalloid content could be made up of just one component or a mixture of a number of components. In the case of metal-metal types, however, there is no such restriction on compositions. Metal-metal-type metallic glasses have been observed to form over a wide range of compositions, starting from as low as 9 at.% of solute. Some typical compositions in which metal-metal type glasses have been obtained are  $\text{Cu}_{25-72.5}\text{Zr}_{27.5-75}$ ,  $\text{Fe}_{89-91}\text{Zr}_{9-11}$ ,  $\text{Mg}_{68-75}\text{Zn}_{25-32}$ ,  $\text{Nb}_{55}\text{Ir}_{45}$ , and  $\text{Ni}_{58-67}\text{Zr}_{33-42}$  [65].

# \* Metallic glass : Randomly dense packed structure

## 1) Atomic size difference: TM – metalloid (M, ex) Boron)

- M is located at interior of the tetrahedron of four metal atoms ( $TM_4M$ )
- denser  by increasing resistivity of crystallization, GFA 
- Ex) Fe-B: tetrahedron with B on the center position
  - 1) interstitial site, B= simple atomic topology
  - 2) skeleton structure
  - 3) bonding nature: close to covalent bonding

Irrespective of the actual size of the voids and whether the above model is valid or not, it is of interest to note that the metal-metalloid-type binary phase diagrams exhibit deep eutectics at around a composition of 15–25 at.% metalloid. Some typical examples are Fe–B (17 at.% B), Au–Si (18.6 at.% Si), and Pd–Si (17.2 at.% Si). Therefore, the concepts of deep eutectics and structural models also seem to converge in obtaining glasses in the (transition or noble) metal-metalloid types.

### 3.5.2. Egami and Waseda Criterion

One of the possible ways by which a crystalline metallic material can become glassy is by the introduction of lattice strain. The lattice strain introduced disturbs the crystal lattice and once a critical strain is exceeded, the crystal becomes destabilized and becomes glassy. In fact, Egami takes pains to state that “In general, alloying makes glass formation easier, not because alloying stabilizes a glass, but because it destabilizes a crystal” [72, p. 576]. Using the atomic scale elasticity theory, Egami and Waseda [73] calculated the atomic level stresses in the solid solution (the solute atoms are assumed to occupy the substitutional lattice sites in the solid solution) and the glassy phase. They observed that in a glass, neither the local stress fluctuations nor the total strain energy vary much with solute concentration, when normalized with respect to the elastic moduli. But, in a solid solution, the strain energy was observed to increase continuously and linearly with solute content. Thus, beyond a critical solute concentration, the glassy alloy becomes energetically more favorable than the corresponding crystalline lattice. From the vast literature available on the formation of binary metallic glasses obtained by RSP methods, the authors noted that a minimum solute concentration was necessary in a binary alloy system to obtain the stable glassy phase by RSP methods.

2) min. solute content,  $C_B^*$ : empirical rule

By Egami & Waseda: in A-B binary system

$$C_B^{\min} \left| \frac{(v_B - v_A)}{v_A} \right| = C_B^{\min} \left| \left( \frac{r_B}{r_A} \right)^3 - 1 \right| \approx 0.1$$

$v$ : atomic volume  
 A: matrix, B: solute

minimum concentration of B for glass formation

→ Inversely proportional to atomic volume mismatch

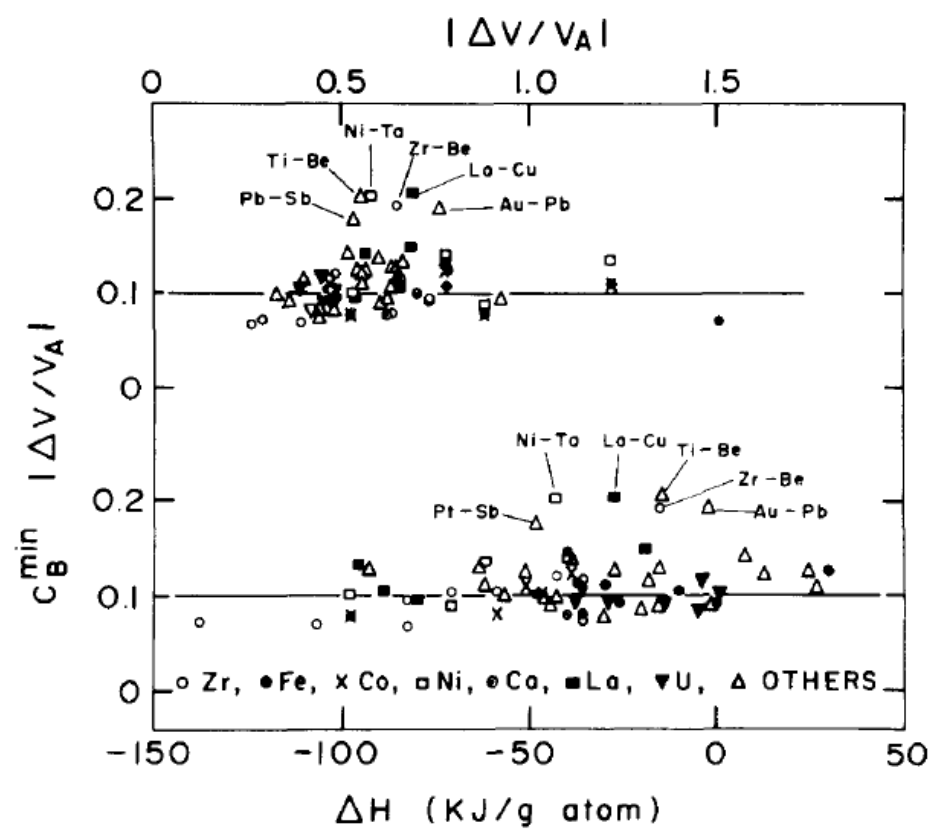
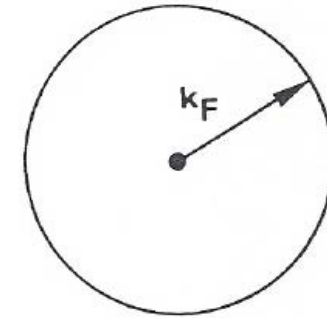
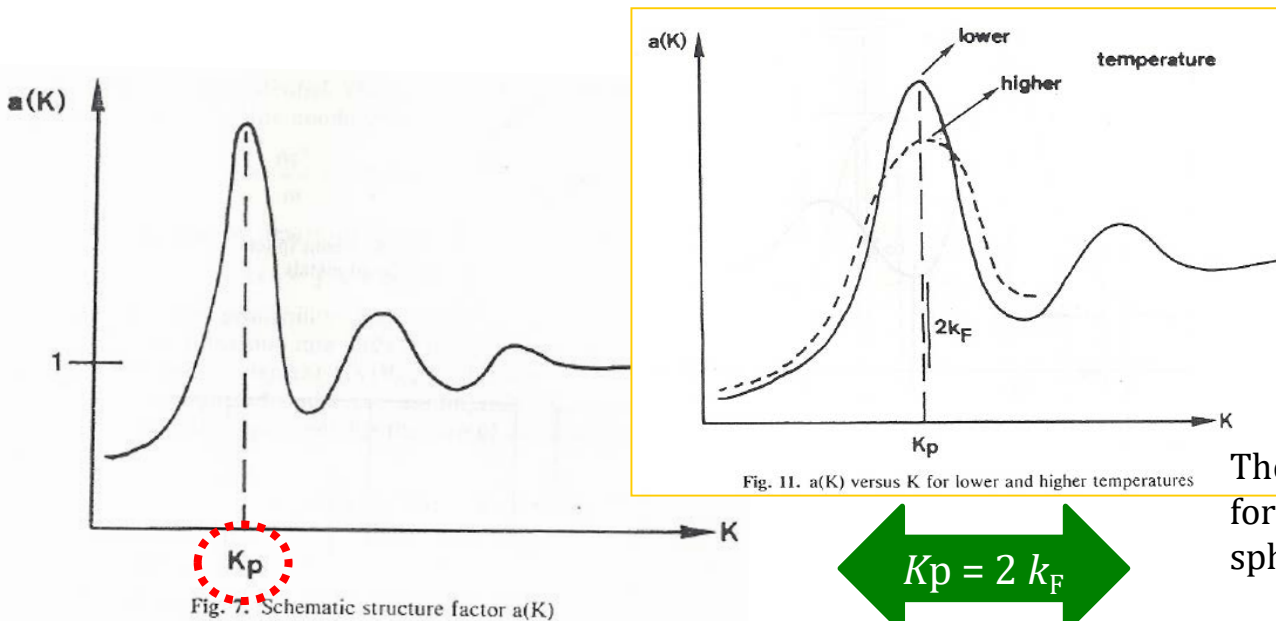


Fig. 1. Relation between  $|\lambda_0| = C_B^{\min} |\Delta v/v_A|$ , and  $|\Delta v/v_A|$  and  $\Delta H$ , for 66 binary systems which can be vitrified by liquid quenching.

### 3.5.3. Nagel and Tauc Criterion

Nagel and Tauc [74,75] proposed that a glass is most likely to form if its electronic energy lies in a local metastable minimum with respect to composition change. They showed that if the structure factor corresponding to the first strong peak of the diffuse scattering curve,  $K_p$ , satisfies the relationship  $K_p = 2 k_F$ , where  $k_F$  is the wave vector at the Fermi energy, then the electronic energy does indeed occupy a local minimum.



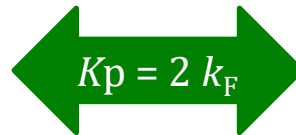
The conduction electrons are supposed to form a degenerate free-electron gas with a spherical **Fermi surface**.

$$2K_F = 2(3\pi^2 n)^{1/3} = 2 \left( \frac{3\pi^2}{eR_H} \right)^{1/3}$$

$a(K)$  Fourier transform of the pair correlation function  $g(r)$

$K_p$  Nearest neighbor distance of the liquid metal in  $K$ -space

: Diameter of Fermi surface



## 3.6 Bulk Metallic Glasses

Since 1989, intense research has been carried out in synthesizing and characterizing BMGs with a section thickness or diameter of a few millimeters to a few centimeters.

First, phase diagrams are not available for the multicomponent alloy systems. Therefore, we do not know where the eutectic compositions lie, and much less about deep eutectics.

Additionally, because the number of components is really large, determining the minimum solute content will be a formidable problem since the contribution of each component to the volumetric strain is going to be different depending on their atomic sizes.

Therefore, newer criteria have been proposed to explain glass formation in BMGs in view of the large number of components present.

## 3.7 Inoue Criteria – Empirical Rules

1. The alloy must contain at least three components. The formation of glass becomes easier with increasing number of components in the alloy system.

### a) Thermodynamic point of view

Since the value of  $\Delta S_f$  can be significantly increased by increasing the number of components in the alloy, it has been relatively easy to produce BMGs in multicomponent alloys. Since an increase in  $\Delta S_f$  also leads to an increase in the degree of the dense random packing of atoms, this results in a decrease in  $\Delta H_f$  and also an increase in the solid–liquid interfacial energy,  $\sigma$ . Both these factors contribute to a decrease in the free energy of the system.

### b) Kinetic point of view

Since the equation for homogeneous nucleation rate for the formation of crystalline nuclei from a supercooled melt (Equation 2.4) contains  $\eta$ ,  $\alpha$ , and  $\beta$ , control of these parameters can lead to a reduction in the nucleation rate. For example, a reduction in  $\Delta H_f$ , and an increase in  $\sigma$  and/or  $\Delta S_f$  can be achieved by an increase in  $\alpha$  and  $\beta$  values. This, in turn, will decrease the nucleation rate and consequently promote glass formation. An increase in the viscosity of the melt will also lead to a reduction in both nucleation and growth rates.

### 3.7 Inoue Criteria – Empirical Rules

2. A significant atomic size difference should exist among the constituent elements in the alloy. It is suggested that the atomic size differences should be above about 12% among the main constituent elements.

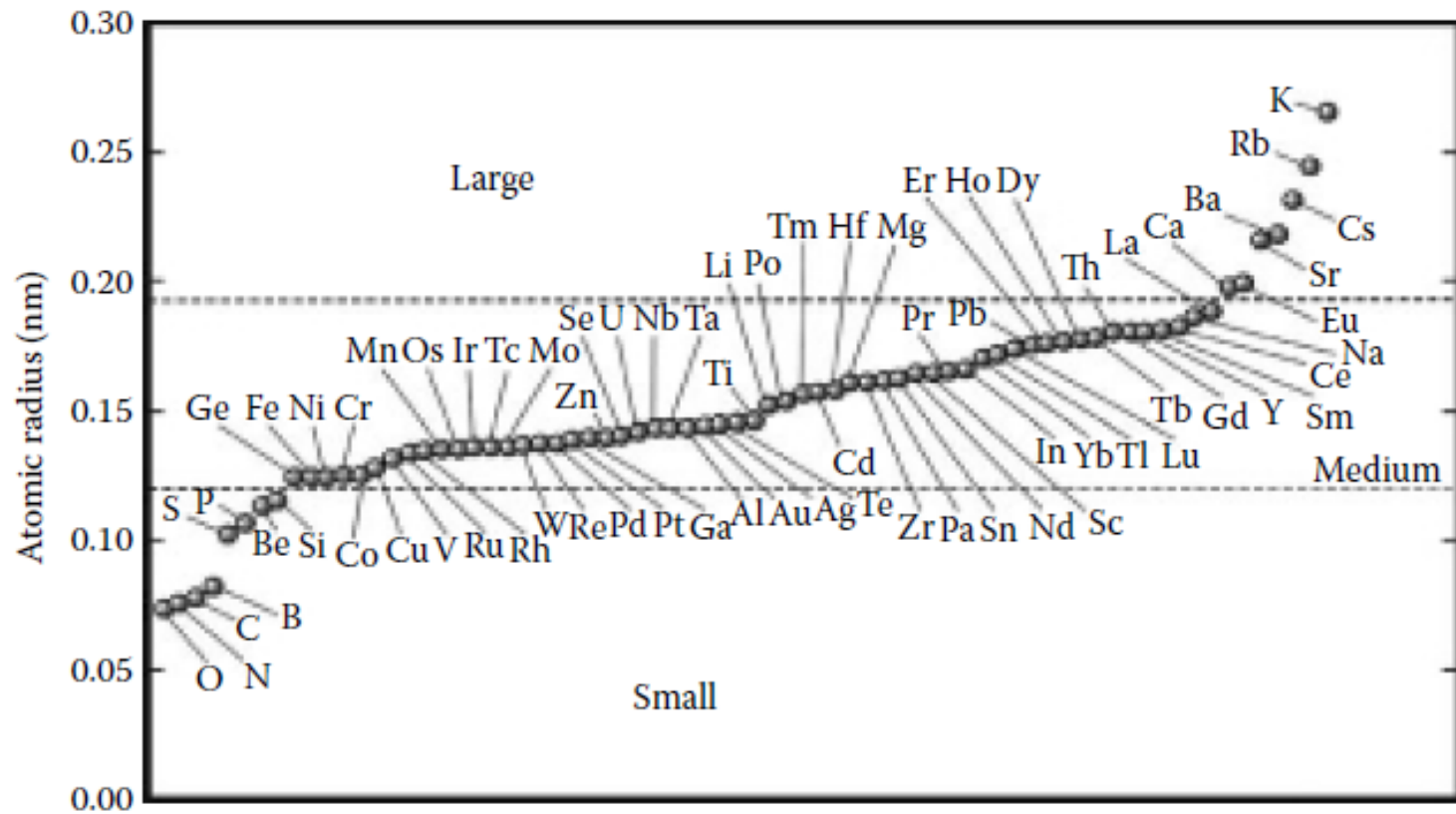
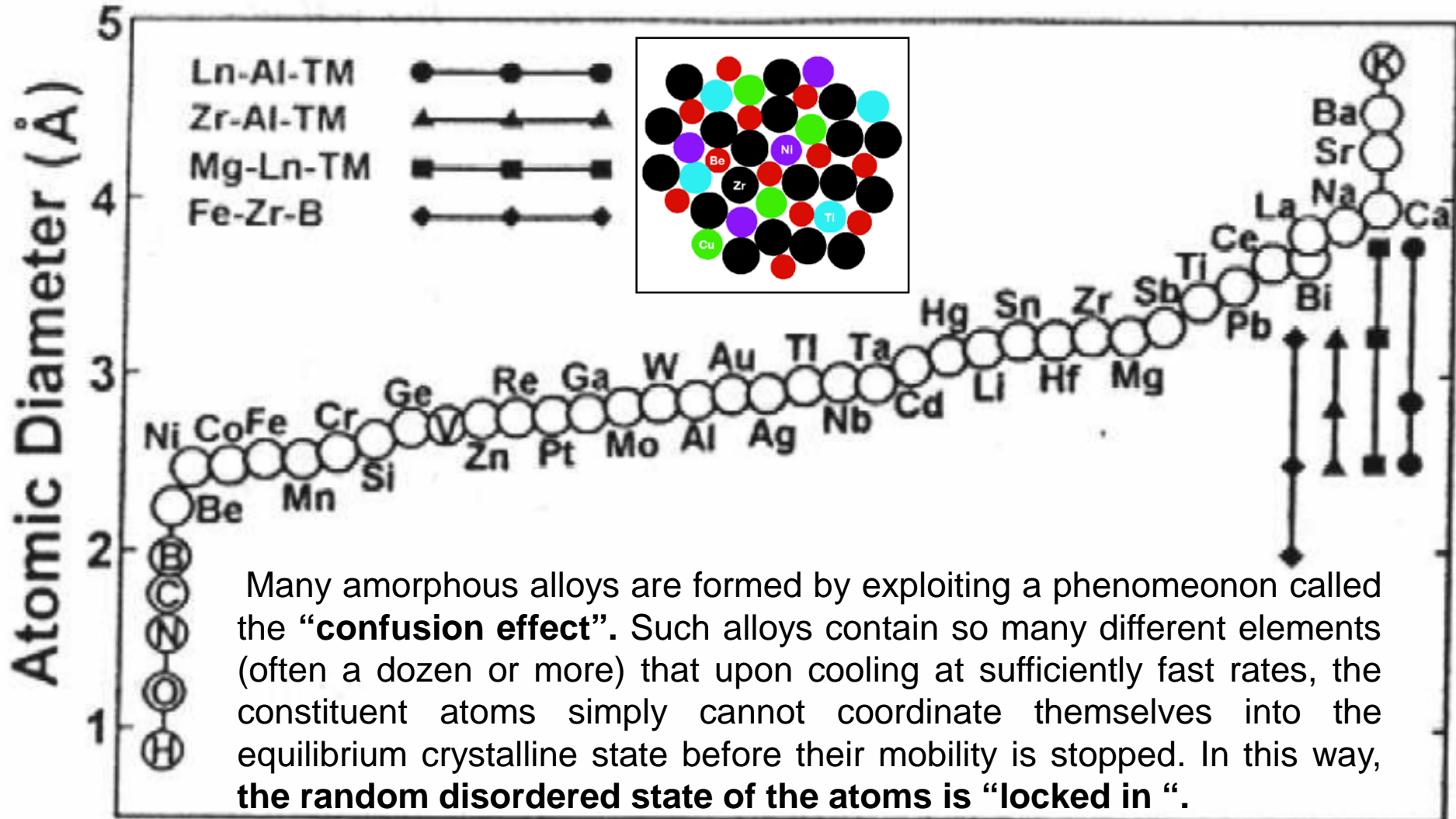


FIGURE 3.4

Atomic diameters of the elements that constitute bulk metallic glasses. These can be classified into three major groups of large, medium, and small sizes.

< significant difference in atomic size ratios >



## 3.7 Inoue Criteria – Empirical Rules

3. There should be negative heat of mixing among the (major) constituent elements in the alloy system.

The combination of the significant differences in atomic sizes between the constituent elements and the negative heat of mixing is expected to result in efficient packing of clusters (see Section 3.12.2) and consequently increase the density of random packing of atoms in the supercooled liquid state. This, in turn, leads to increased liquid–solid interfacial energy,  $\sigma$  and decreased atomic diffusivity, both contributing to enhanced glass formation.

Table 3.3

Nearest Neighbor Distances ( $r$ ) and Coordination Numbers ( $N$ ) of the Different Atomic Pairs in a Glassy  $Zr_{60}Al_{15}Ni_{25}$  Alloy Both in the As-Quenched and Crystallized States

Condition		$r_1$ (nm)	$N_{Zr-Ni}$	$r_2$ (nm)	$N_{Zr-Zr}$	$N_{Zr-Al}$
As-quenched	(a)	$0.267 \pm 0.002$	$2.3 \pm 0.2$	$0.317 \pm 0.002$	$10.3 \pm 0.7$	$-0.1 \pm 0.9$
	(b)	$0.267 \pm 0.002$	$2.1 \pm 0.2$	—	—	—
	(c)	$0.269 \pm 0.002$	$2.3 \pm 0.2$	—	—	—
Crystallized	(a)	$0.268 \pm 0.002$	$3.0 \pm 0.2$	$0.322 \pm 0.002$	$8.2 \pm 0.7$	$0.8 \pm 0.9$
	(b)	$0.267 \pm 0.002$	$3.0 \pm 0.2$	—	—	—
	(c)	$0.273 \pm 0.002$	$2.3 \pm 0.2$	—	—	—

Significant change in the coordination # of Zr-Al atomic pairs on crystallization

→ This suggests that there is necessity for long-range diffusion of Al atoms around Zr atoms during crystallization, which is difficult to achieve due to the presence of dense randomly packed clusters.

Source: Matsubara, E. et al., *Mater. Trans. JIM*, 33, 873, 1992. With permission.

Notes: Data from (a) ordinary radial distribution function (RDF), (b) conventional RDFs for Zr, and (c) conventional RDFs for Ni. “—” means that no values were given in the original publication.

The presence of dense randomly packed atomic configurations in the glassy state of BMGs can also be inferred from the small changes in the relative densities of the fully glassy and the corresponding fully crystalline alloys (see Table 6.1). It is noted that the densities of the glassy alloys are lower than those in the crystallized state. The difference between the fully glassy and fully crystalline alloys is typically about 0.5%, but is occasionally as high as 1% (see, for example, Ref. [81]). Further, the density difference between the structurally relaxed and fully glassy states is about 0.11%–0.15%. Thus, the small density differences between the glassy and crystallized conditions suggest that the glassy alloys contain dense randomly packed clusters in them.

# *Glass formation*

*Retention of liquid phase*

*Formation of crystalline phases*

*Thermodynamical point*

Small change in free E. (liq. → cryst.)

*Kinetic point*

Low nucleation and growth rates

*Structural point*

Highly packed random structure

## *Empirical rules*

- (1) multi-component alloy system
- (2) significant difference in atomic size ratios
- (3) negative heats of mixing
- (4) close to a eutectic composition
- (5) compositions far from a Laves phase region

- **Higher degree of dense random packed structure**
- *Suppression* of nucleation and growth of crystalline phase

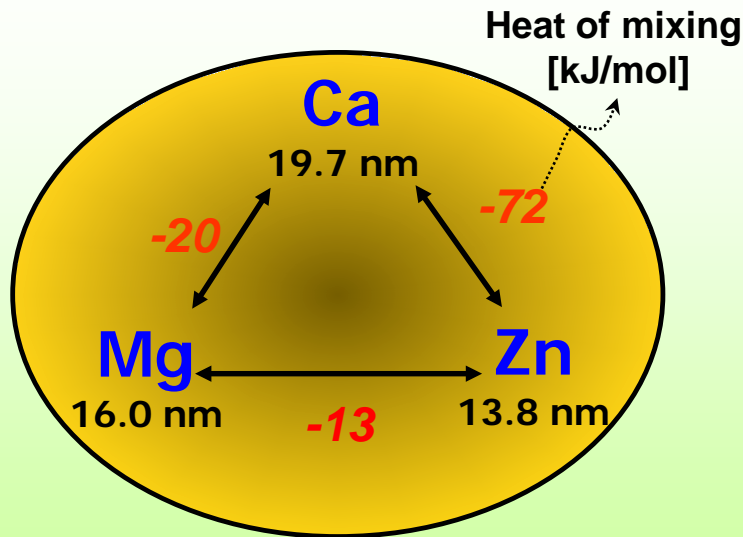


**High glass-forming ability (GFA)**

# Alloy design and new BMG development

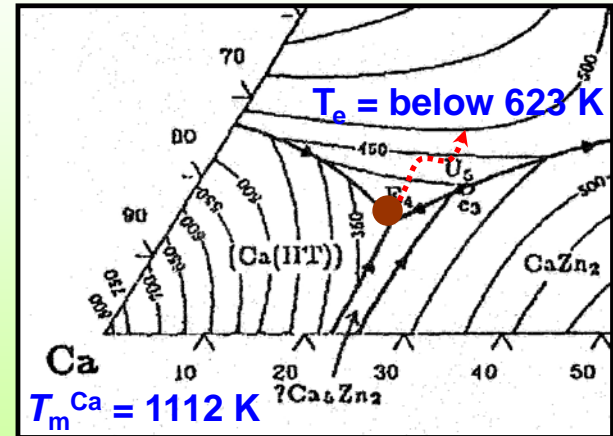
## Ca-Mg-Zn alloy system

- Dense packed structure



- Large difference in atomic size
- Large negative heat of mixing

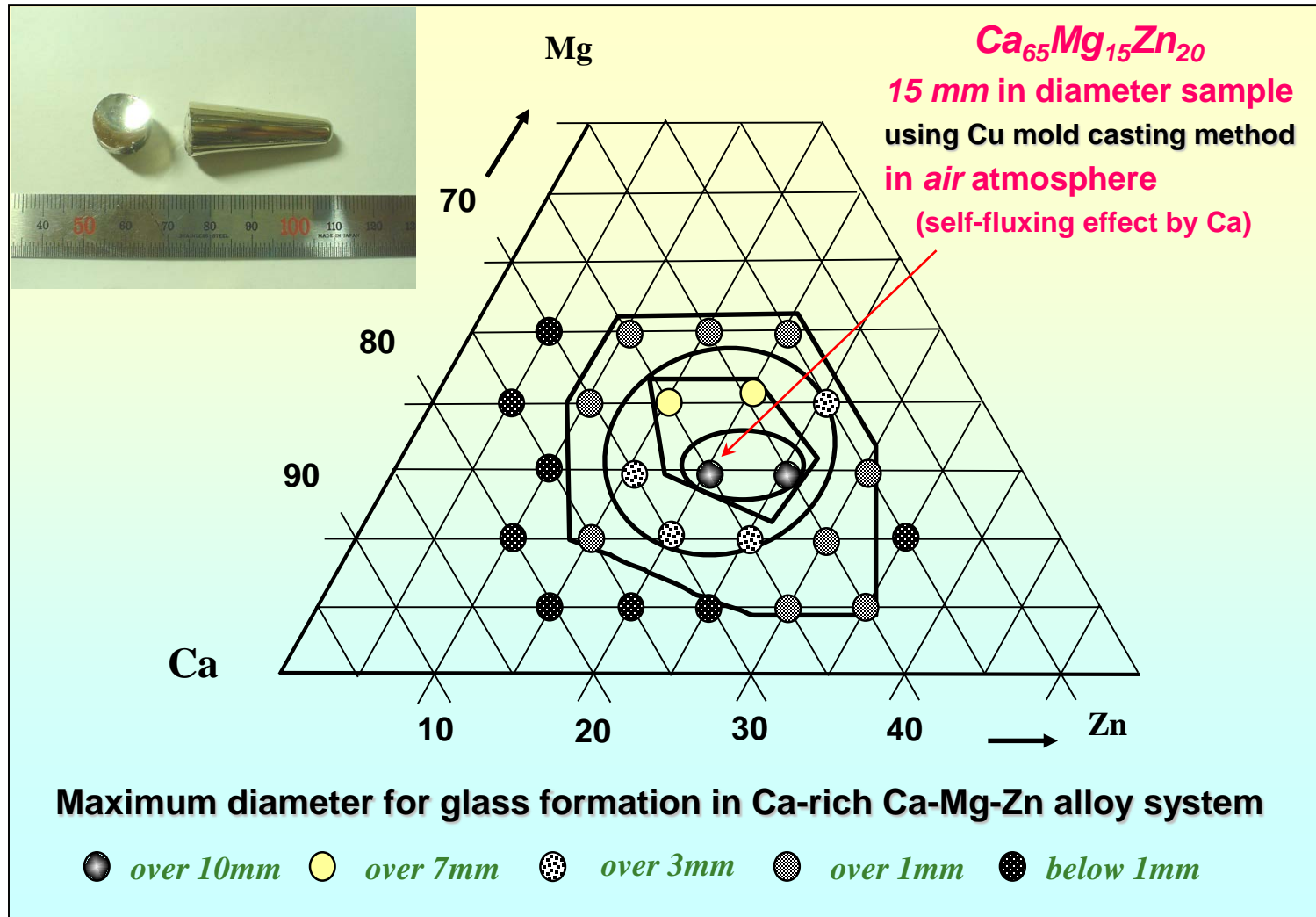
- Decrease of melting temp.



Deep eutectic condition

$$T_e / T_m^{\text{Ca}} = 0.560$$

# Ca-Mg-Zn alloy system



\* J. Mater. Res. 19, 685 (2004)

\* Mater. Sci. Forum 475-479, 3415 (2005)

## 3.8 Exceptions to the Above Criteria

### 3.8.1 Less Than Three Components in an Alloy System – Binary BMGs

One of the apparent exceptions to this empirical rule appears to be that BMGs have been produced in binary alloy systems such as Ca–Al [59], Cu–Hf [49], Cu–Zr [51], Ni–Nb [37], and Pd–Si [42].

Two important points:

- 1) The maximum diameter of the glassy rods obtained in these binary alloys is relatively small, i.e. a maximum of only about 2 mm.
- 2) The “glassy” rods of the binary BMG alloys often seem to contain some nanocrystalline phases. (?)

Even though glassy (BMG) alloys of 1 or 2 mm diameter are produced in binary alloy compositions., their GFA improves dramatically with the addition of a third component. This observation again proves that a minimum of three components is required to produce a BMG alloy with a reasonably large diameter.

Hattori et al. [90] had conducted very careful high-pressure experiments on elemental Zr and Ti using a newly developed in situ angle-dispersive XRD using a two-dimensional detector and x-ray transparent anvils. These authors noted that despite the disappearance of all the Bragg peaks in the one-dimensional energy-dispersive data, two-dimensional angle-dispersive data showed several intense Bragg spots even at the conditions where amorphization was reported in these two metals. This investigation clearly confirms that pure metals cannot be amorphized

### 3.8.2 Negative Heat of Mixing

Phase separation is generally expected to occur in alloy systems containing elements that exhibit a positive heat of mixing. This is indicated by the presence of a miscibility gap in the corresponding phase diagram. Therefore, if phase separation has occurred, one immediately concludes that the constituent elements have a positive heat of mixing

It has been suggested that it is theoretically possible to observe phase separation in alloy systems containing three or more elements, even though the heat of mixing is negative between any two elements in the alloy system. According to Meijering [94,95], a ternary alloy phase, consisting of components A, B, and C, can decompose into two phases with different compositions even when the enthalpy of mixing between any two components is negative. This is possible when the enthalpy of mixing,  $\Delta H$  for one of the three possible binary alloy systems is significantly more negative than the others. For example, it is possible that in a ternary alloy system A–B–C,  $\Delta H_{A-B}$  is much more negative than  $\Delta H_{B-C} \approx \Delta H_{A-C}$ . This argument suggests that a miscibility gap could be present in a ternary (or higher-order) BMG alloy system even when all the constituent elements have a negative enthalpy of mixing. In other words, phase separation is possible even in an alloy with a reasonably good GFA.

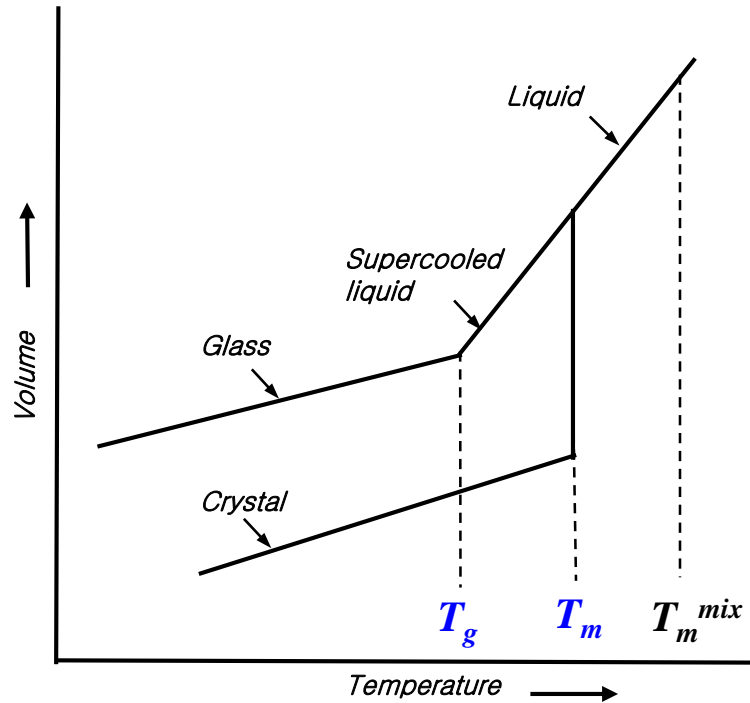
### 3.9 New Criteria: to develop better and more precise criteria to predict the GFA of alloy systems

All the new criteria that have been proposed in recent years to explain the high GFA of BMGs can be broadly grouped into the following categories:

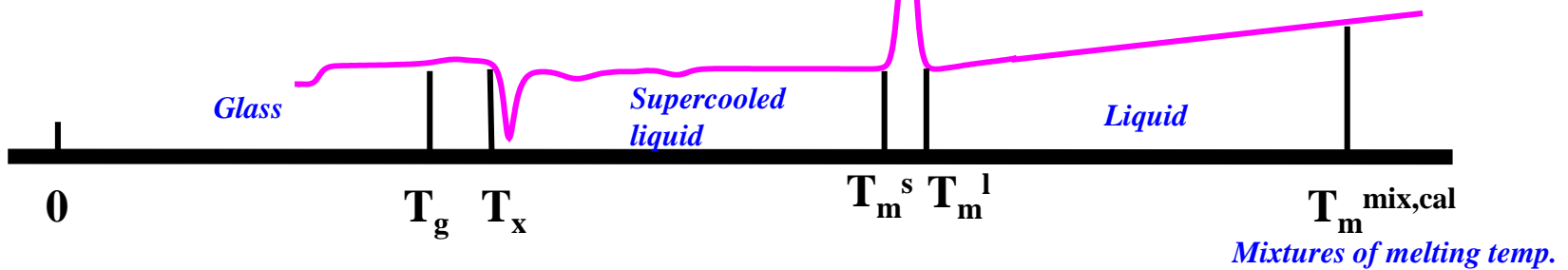
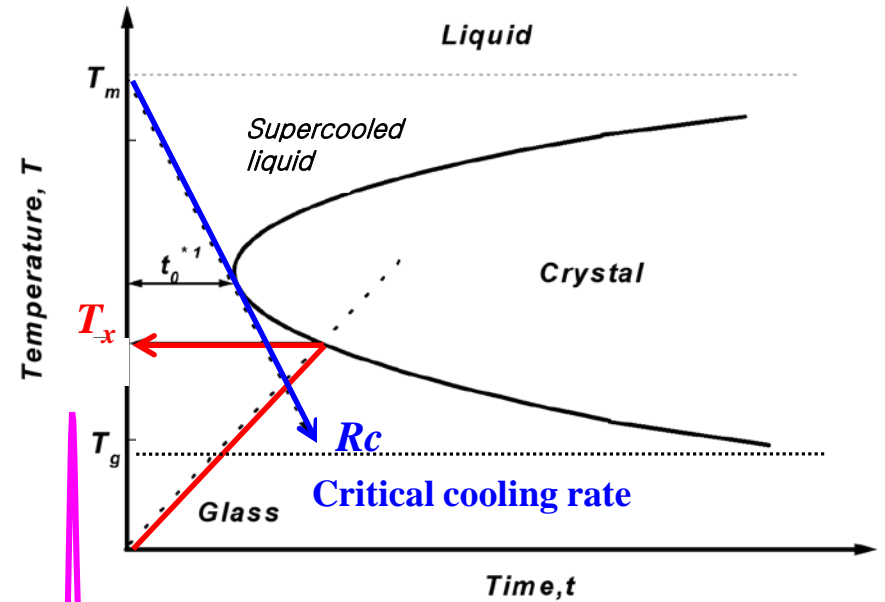
1. *Transformation temperatures of glasses.* In this group, the GFA is explained on the basis of the characteristic transformation temperatures of the glasses such as  $T_g$ ,  $T_x$ , and  $T_l$ , and the different combinations of these three parameters.
2. *Thermodynamic modeling.* Thermodynamic parameters such as heat of mixing are used in this group to predict the glass formation and evaluate GFA in a given alloy system.
3. *Structural and topological parameters.* In this group, consideration is given to the atomic sizes of the constituent elements, their electronegativity, electron-to-atom ratio, heat of mixing, etc. Majority of the work in this area has been due to Egami [107] and Miracle [108,109].
4. *Physical properties of alloys.* This group considers the physical properties of materials such as the viscosity of the melt, heat capacity, activation energies for glass formation and crystallization, bulk modulus, etc.
5. *Computational approaches.* These methods help in predicting the GFA of alloys from basic thermodynamic data [110,111], and without the necessity of actually conducting any experiments to synthesize the glass and determine the GFA.

### 3.10 Transformation Temperatures of Glasses

< V - T diagram >



< TTT diagram >



# Representative GFA Parameters

---

Based on thermal analysis ( $T_g$ ,  $T_x$  and  $T_l$ ): thermodynamic and kinetic aspects

$$T_{rg} = T_g / T_l$$

D. Turnbull et al., *Contemp. Phys.*, 10, 473 (1969)

$$K = (T_x - T_g) / (T_l - T_x)$$

A. Hruby et al., *Czech.J.Phys.*, B22, 1187 (1972)

$$\Delta T^* = (T_m^{mix} - T_l) / T_m^{mix}$$

I. W. Donald et al., *J. Non-Cryst. Solids*, 30, 77 (1978)

$$\Delta T_x = T_x - T_g$$

A. Inoue et al., *J. Non-Cryst. Solids*, 156-158, 473 (1993)

$$\gamma = T_x / (T_l + T_g)$$

Z.P. Lu and C. T. Liu, *Acta Materialia*, 50, 3501 (2002)

Based on thermodynamic and atomic configuration aspects

$$\sigma = \Delta T^* \times P'$$

E. S. Park et al., *Appl. Phys. Lett.*, 86, 061907 (2005)

$\Delta T^*$  : Relative decrease of melting temperature +  $P'$  : atomic size mismatch

: can be calculated simply using data on melting temp. and atomic size

# GFA Parameters on the basis of thermodynamic or kinetic aspects :

## 1) $\Delta T_x$ parameter = $T_x - T_g$

- quantitative measure of glass stability toward crystallization upon reheating the glass above  $T_g$ : stability of glass state
- cannot be considered as a direct measure for GFA

## 2) K parameter = $(T_x - T_g)/(T_l - T_x) = \Delta T_x / (T_l - T_x)$

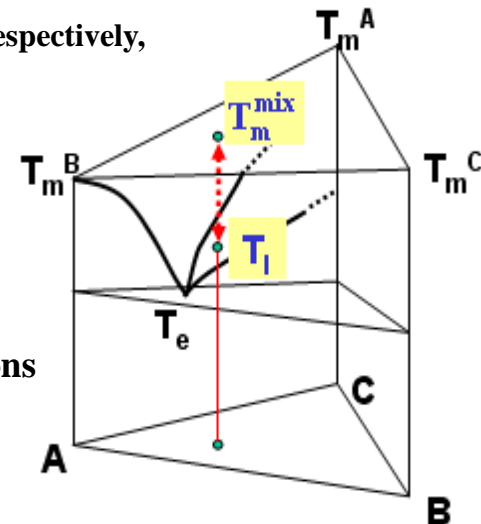
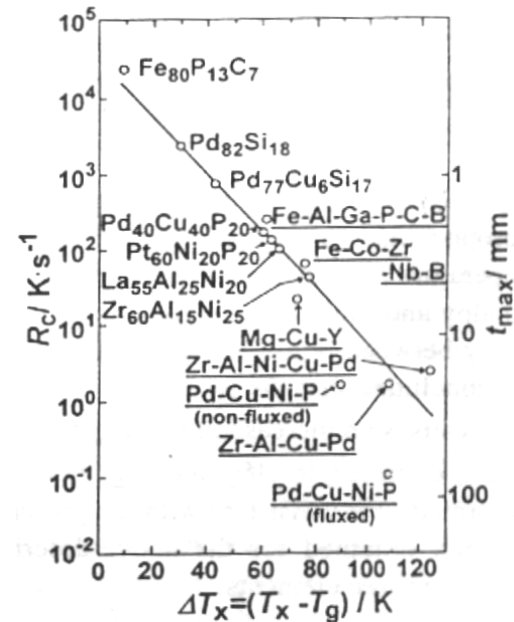
- based on thermal stability of glass on subsequent reheating
- includes the effect of  $T_l$ , but similar tendency to  $\Delta T_x$

## 3) $\Delta T^*$ parameter = $(T_m^{mix} - T_l) / T_m^{mix}$

$$T_m^{mix} = \sum_i^n n_i \cdot T_m^i \quad (\text{where } n_i \text{ and } T_m^i \text{ are the mole fraction and melting point, respectively, of the } i \text{ th component of an } n\text{-component alloy.})$$

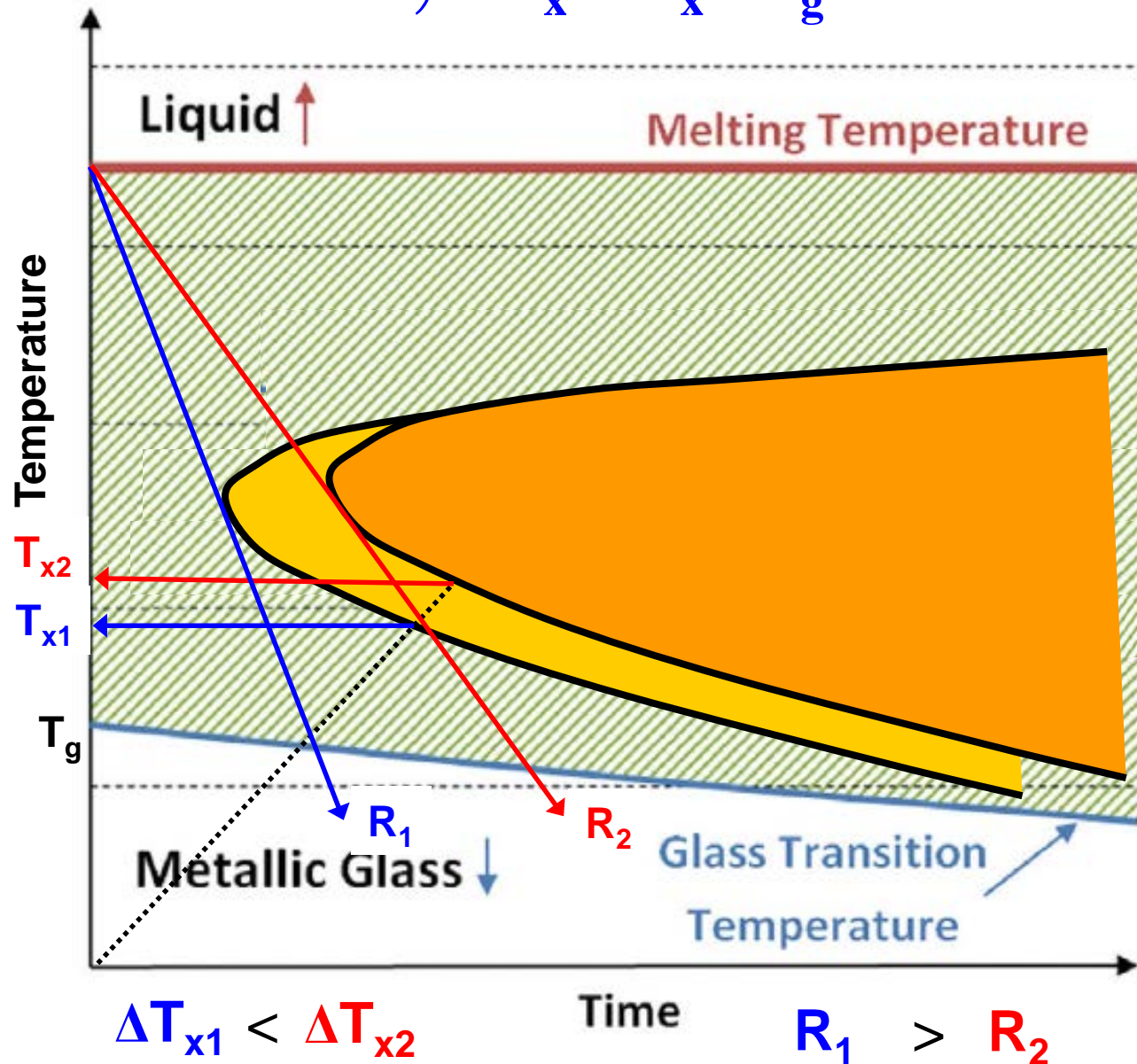
- evaluation of the stability of the liquid at equilibrium state
- alloy system with deep eutectic condition ~ good GFA
- for multi-component BMG systems: insufficient correlation with GFA

➔  $T_m^{mix}$  represents the fractional departure of  $T_m$  with variation of compositions and systems from the simple rule of mixtures melting temperature

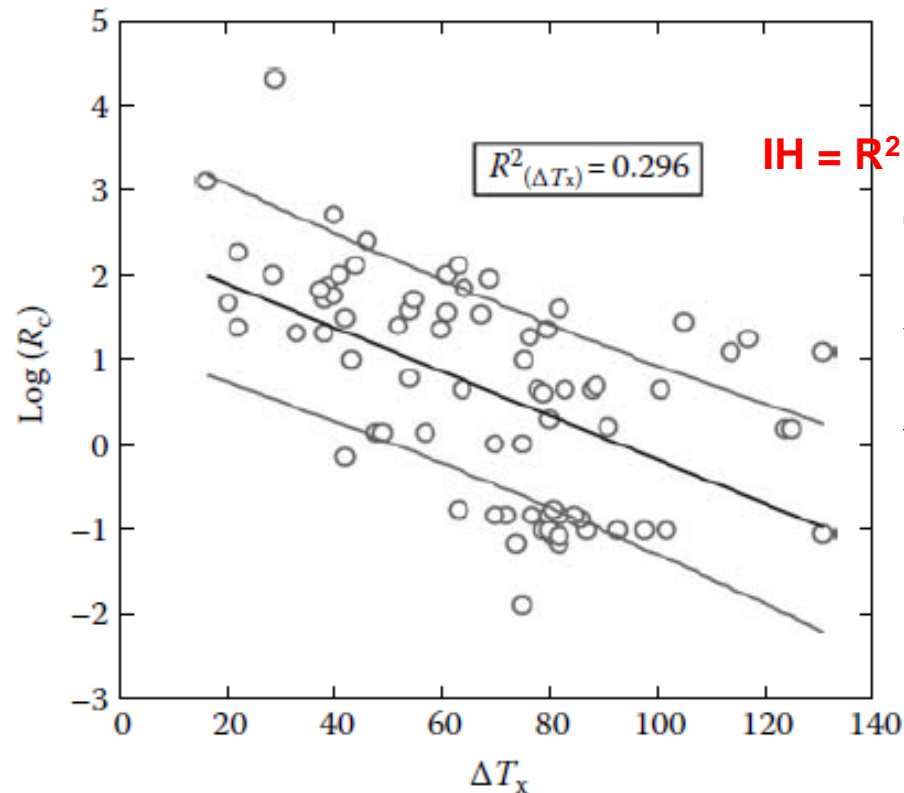


# Time Temperature Transformation diagram:

$$1) \Delta T_x = T_x - T_g$$



From the above discussion, it is clear that the description of the GFA of alloys using the  $\Delta T_x$  parameter as a criterion has not been found universally applicable in all situations and for all alloy systems. Some exceptions have been certainly noted. But, it should, however, be emphasized in this context that this was one of the most successful parameters in the early years of research on BMGs.



The  $R^2$  value can range from 0 to 1 and is an indicator of the reliability of the correlation. The higher  $R^2$  value, the more reliable the regression is.

**FIGURE 3.5**

Variation of the critical cooling rate,  $R_c$  with the width of the supercooled liquid region,  $\Delta T_x$  for a number of multicomponent bulk metallic glasses. Data for some of the binary and ternary metallic glasses reported earlier are also included for comparison.

# GFA Parameters on the basis of thermodynamic or kinetic aspects :

1)  $\Delta T_x$  parameter =  $T_x - T_g$

- quantitative measure of glass stability toward crystallization upon reheating the glass above  $T_g$ : stability of glass state
- cannot be considered as a direct measure for GFA

2) K parameter =  $(T_x - T_g)/(T_l - T_x) = \Delta T_x / (T_l - T_x)$

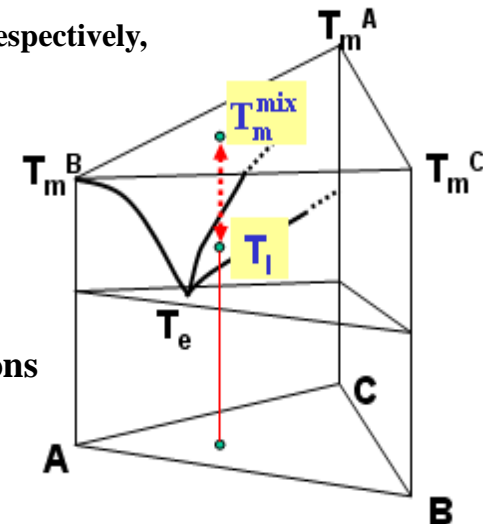
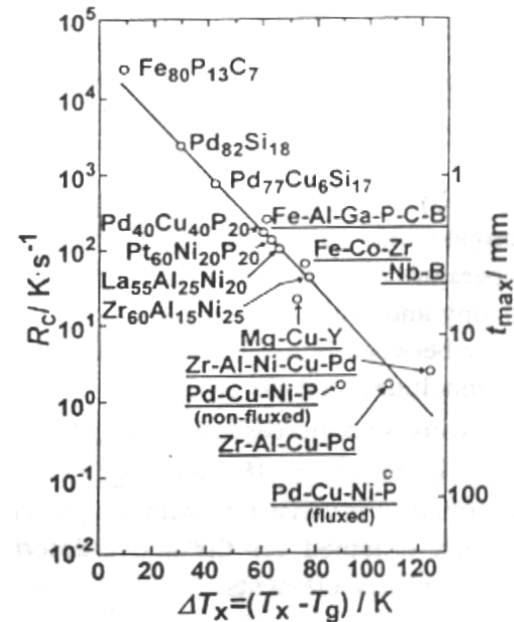
- based on thermal stability of glass on subsequent reheating
- includes the effect of  $T_l$ , but similar tendency to  $\Delta T_x$

3)  $\Delta T^*$  parameter =  $(T_m^{mix} - T_l) / T_m^{mix}$

$$T_m^{mix} = \sum_i^n n_i \cdot T_m^i \quad (\text{where } n_i \text{ and } T_m^i \text{ are the mole fraction and melting point, respectively, of the } i \text{ th component of an } n\text{-component alloy.})$$

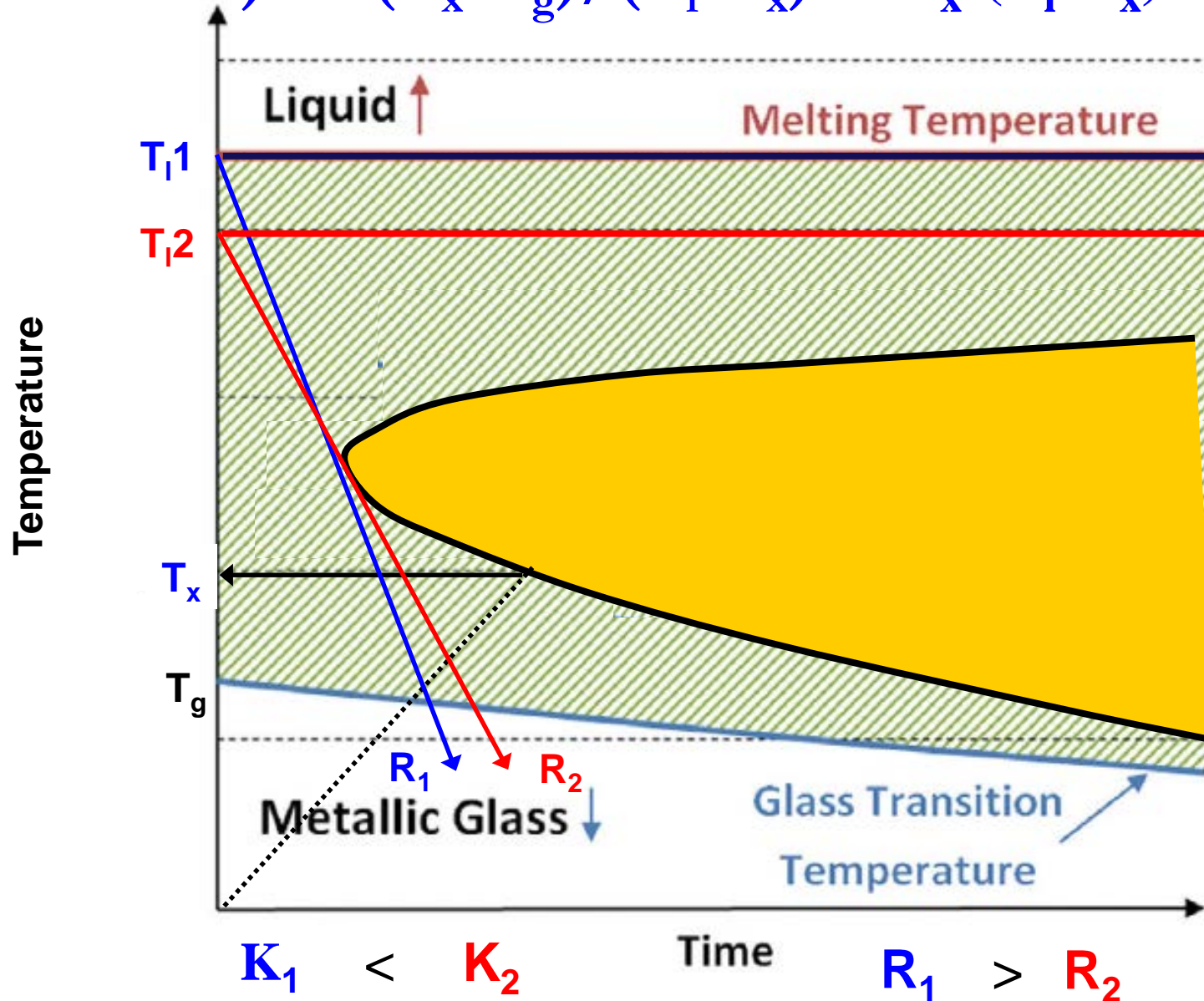
- evaluation of the stability of the liquid at equilibrium state
- alloy system with deep eutectic condition ~ good GFA
- for multi-component BMG systems: insufficient correlation with GFA

➔  $T_m^{mix}$  represents the fractional departure of  $T_m$  with variation of compositions and systems from the simple rule of mixtures melting temperature



Time Temperature Transformation diagram:

$$2) K = (T_x - T_g) / (T_1 - T_x) = \Delta T_x / (T_1 - T_x)$$



# GFA Parameters on the basis of thermodynamic or kinetic aspects :

## 1) $\Delta T_x$ parameter = $T_x - T_g$

- quantitative measure of glass stability toward crystallization upon reheating the glass above  $T_g$ : stability of glass state
- cannot be considered as a direct measure for GFA

## 2) K parameter = $(T_x - T_g)/(T_l - T_x) = \Delta T_x / (T_l - T_x)$

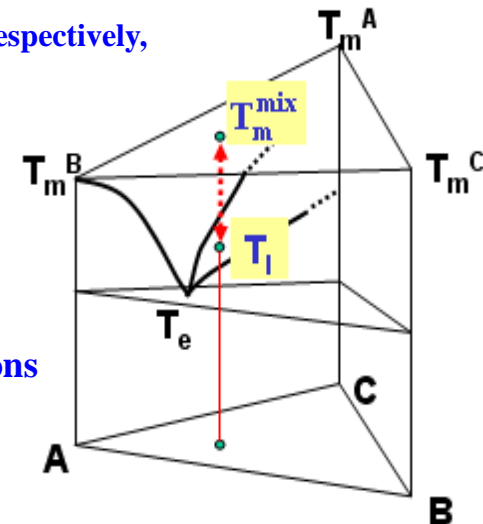
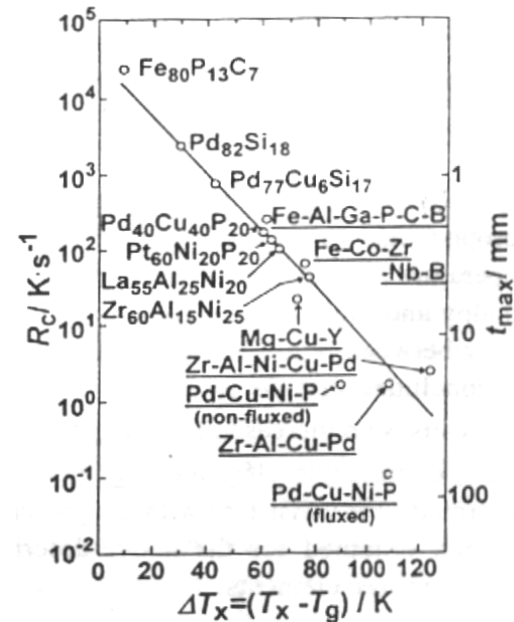
- based on thermal stability of glass on subsequent reheating
- includes the effect of  $T_l$ , but similar tendency to  $\Delta T_x$

## 3) $\Delta T^*$ parameter = $(T_m^{mix} - T_l) / T_m^{mix}$

$$T_m^{mix} = \sum_i^n n_i \cdot T_m^i \quad (\text{where } n_i \text{ and } T_m^i \text{ are the mole fraction and melting point, respectively, of the } i \text{ th component of an } n\text{-component alloy.})$$

- evaluation of the stability of the liquid at equilibrium state
- alloy system with deep eutectic condition ~ good GFA
- for multi-component BMG systems: insufficient correlation with GFA

➔  $T_m^{mix}$  represents the fractional departure of  $T_m$  with variation of compositions and systems from the simple rule of mixtures melting temperature



# ★ Relative decrease of melting temperature

: ratio of Temperature difference between liquidus temp.  $T_l$  and imaginary melting temp.  $T_m^{mix}$  to  $T_m^{mix}$

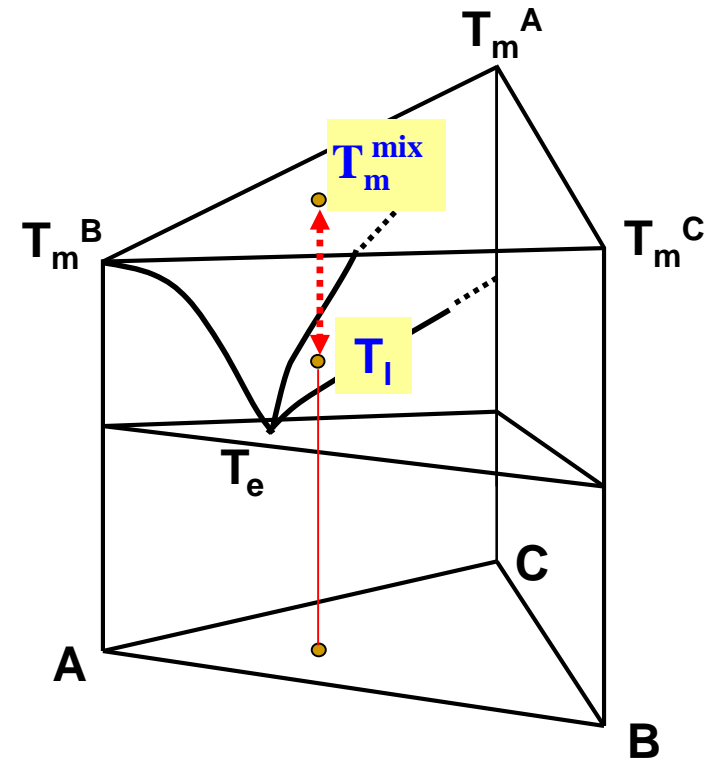
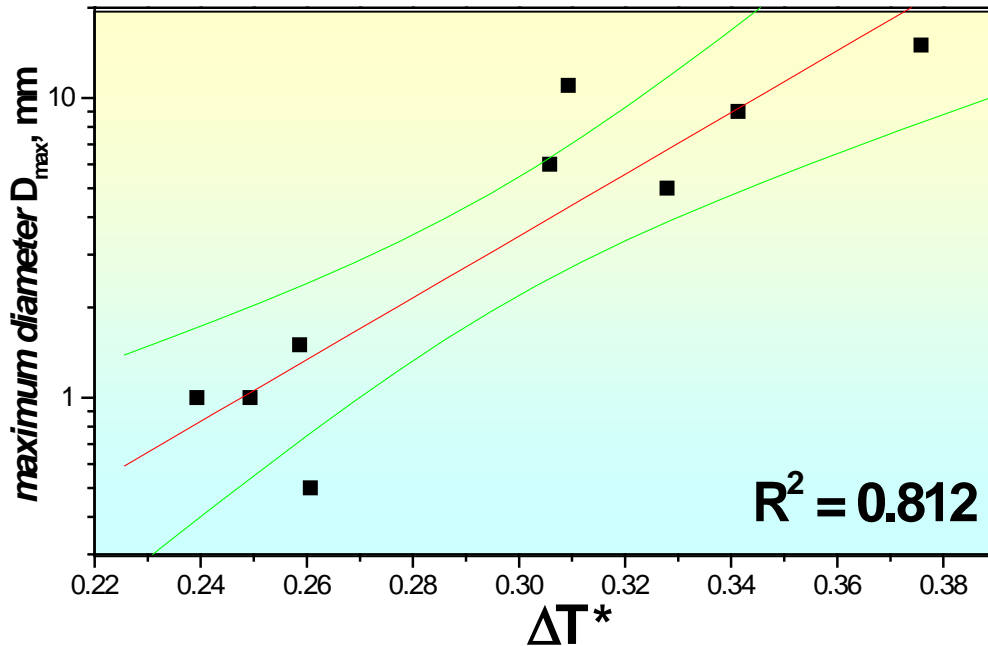
(where,  $T_m^{mix} = \sum x_i T_m^i$ ,  $x_i$  = molefraction,  $T_m^i$  = melting point)

$$\Delta T^* = \frac{T_m^{mix} - T_l}{T_m^{mix}}$$

by I.W. Donald et al. (*J. Non-Cryst. Solids*, 30, 77 (1978))

➡  $\Delta T^* \geq 0.2$  in most of glass forming alloys

*Ca-Mg-Zn alloy system*



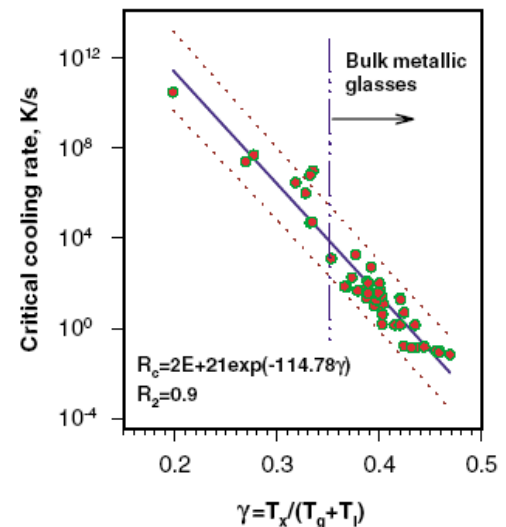
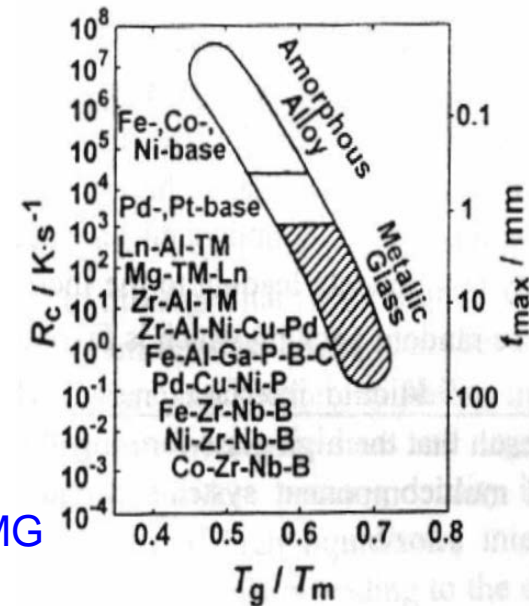
# GFA Parameters on the basis of thermodynamic or kinetic aspects :

## 4) $T_{rg}$ parameter = $T_g/T_l$

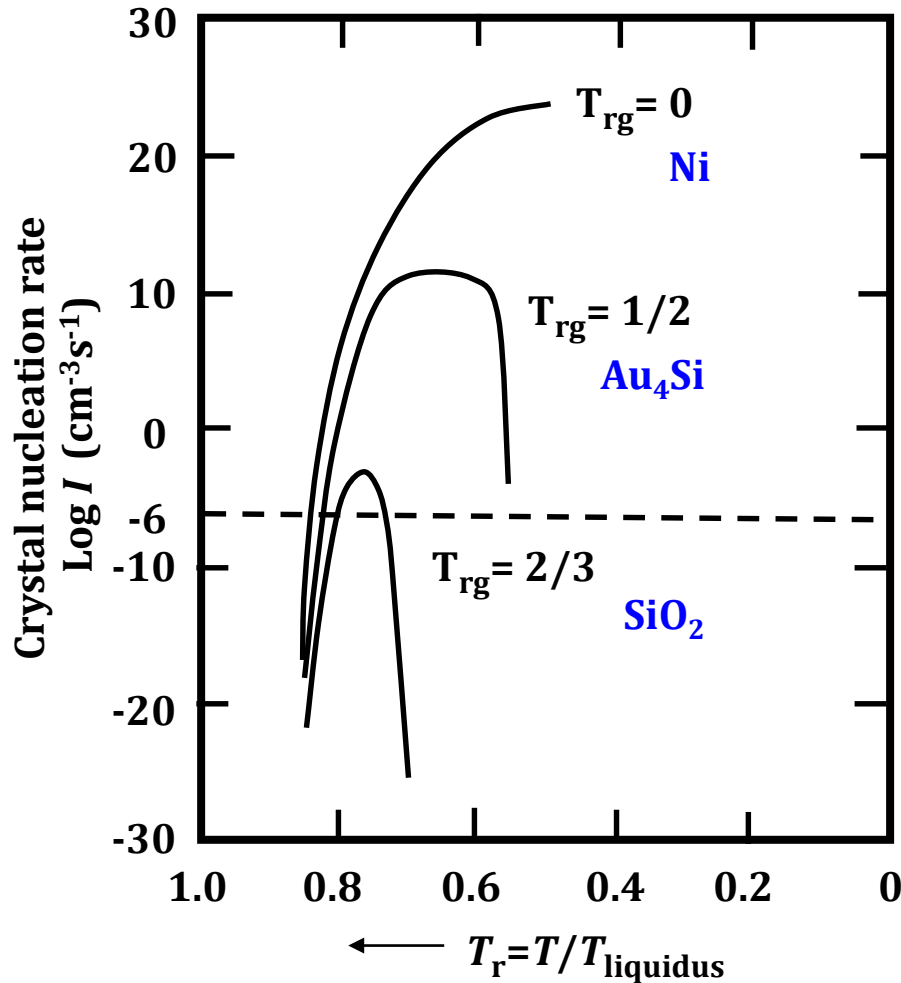
- kinetic approach to avoid crystallization before glass formation
- Viscosity at  $T_g$  being constant, the higher the ratio  $T_g/T_l$ , the higher will be the viscosity at the nose of the CCT curves, and hence the smaller  $R_c$
- $T_l \downarrow$  and  $T_g \uparrow \rightarrow$  lower nucleation and growth rate  $\rightarrow$  GFA  $\uparrow$ 
  - significant difference between  $T_l$  and  $T_g$  in multi-component BMG
  - insufficient information on temperature-viscosity relationship
  - insufficient correlation with GFA

## 5) $\gamma$ parameter = $T_x / (T_l + T_g)$

- thermodynamic and kinetic view points - relatively reliable parameter
- stability of equilibrium and metastable liquids:  $T_l$  and  $T_g$
- resistance to crystallization:  $T_x$



$T_{rg}$  parameter =  $T_g/T_l \sim \eta$  : the higher  $T_{rg}$ , the higher  $\eta$ , the lower  $R_c$   
 : ability to avoid crystallization during cooling



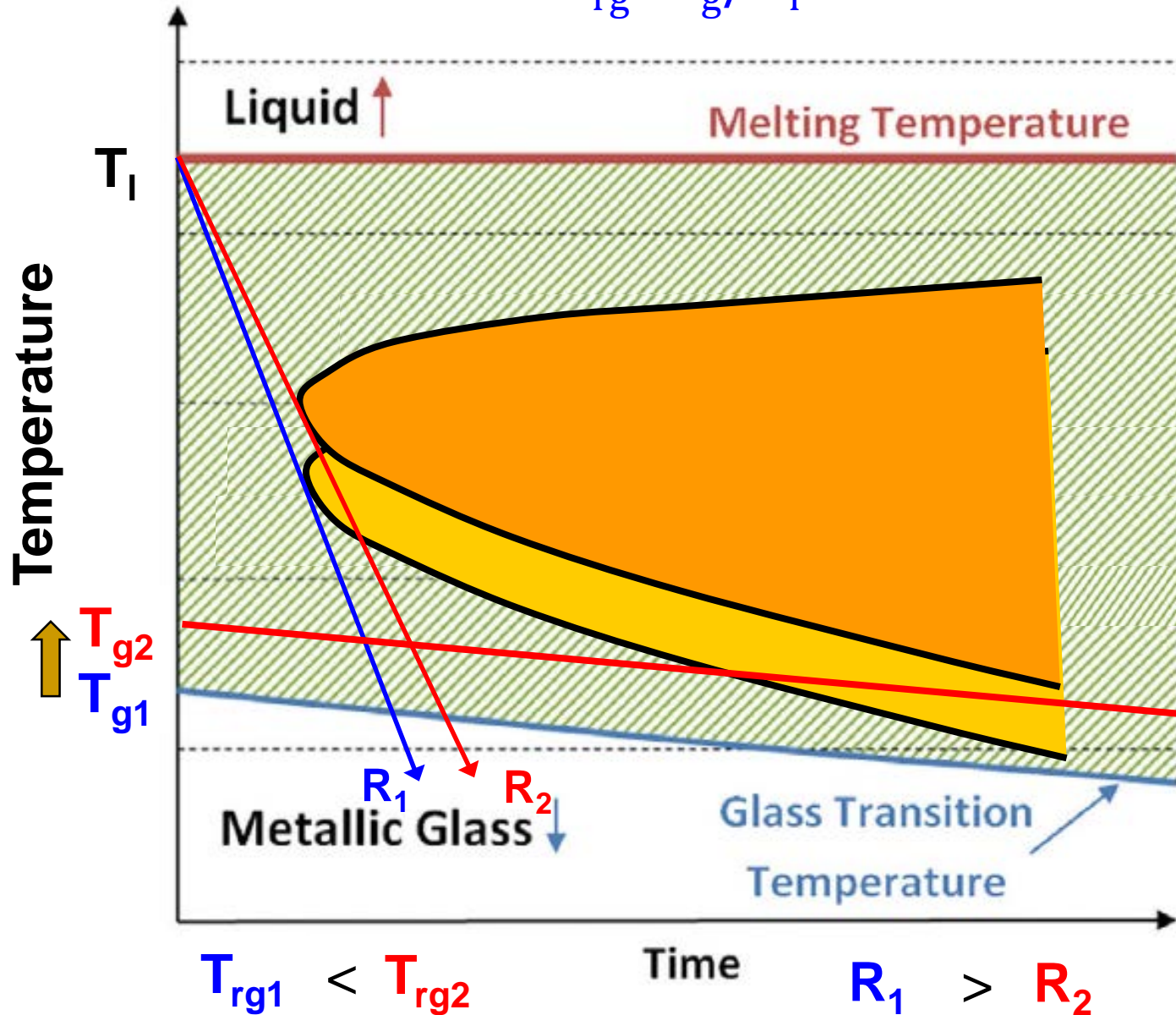
$$T_{rgNi} < T_{rgAu4Si} < T_{rgSiO2}$$

$$R_{Ni} > R_{Au4Si} > R_{SiO2}$$

Turnbull, 1959 ff.

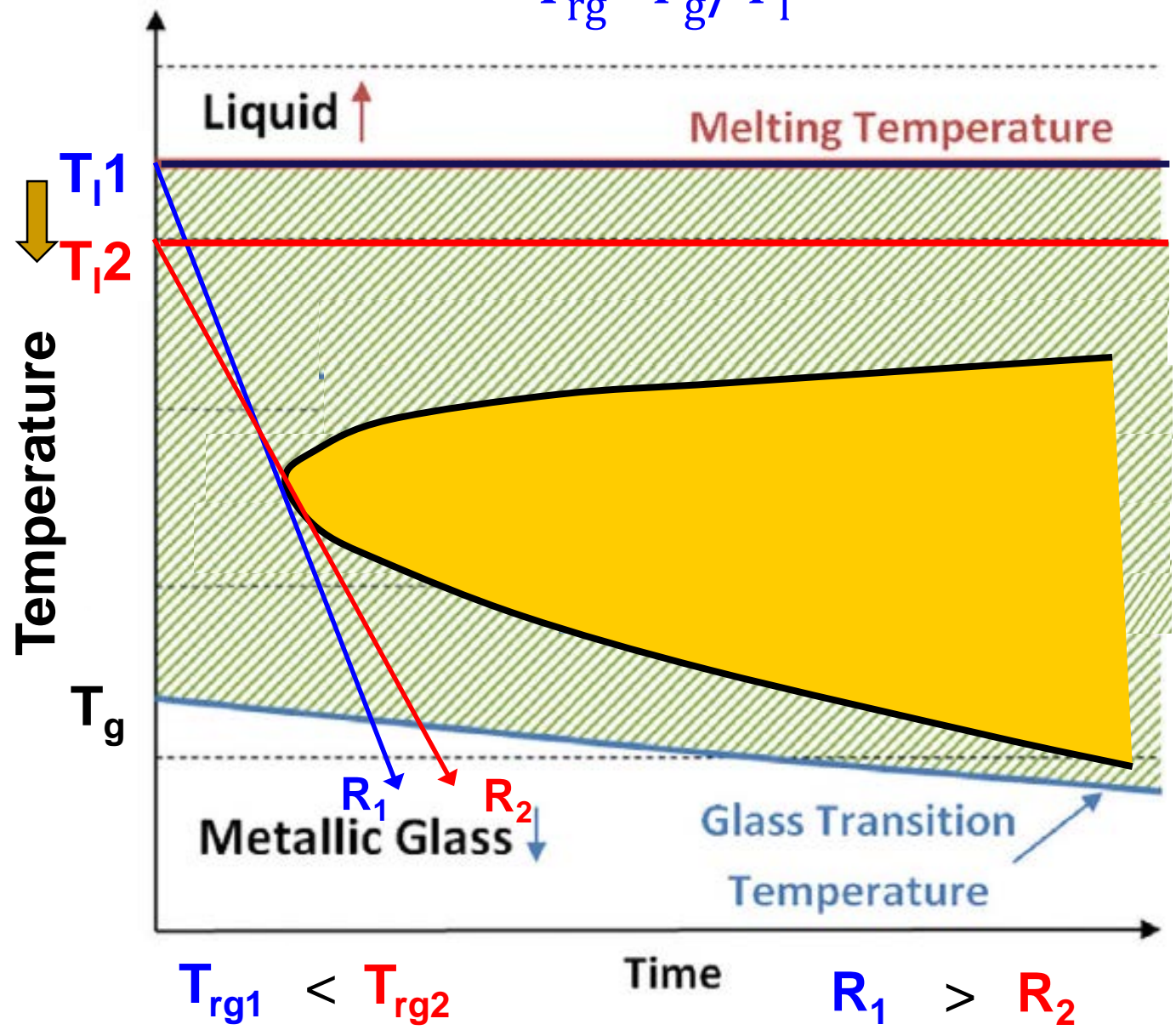
# Time Temperature Transformation diagram:

$$T_{rg} = T_g / T_l$$



# Time Temperature Transformation diagram:

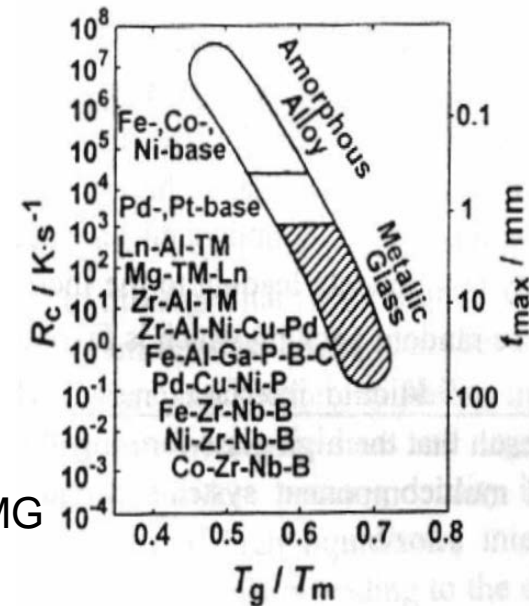
$$T_{rg} = T_g / T_l$$



# GFA Parameters on the basis of thermodynamic or kinetic aspects :

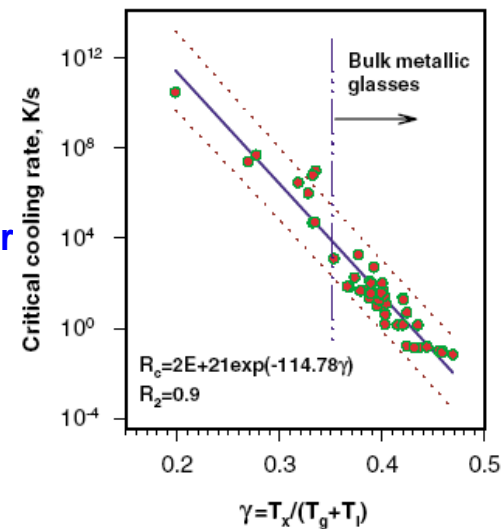
## 4) $T_{rg}$ parameter = $T_g/T_l$

- kinetic approach to avoid crystallization before glass formation
- Viscosity at  $T_g$  being constant, the higher the ratio  $T_g/T_l$ , the higher will be the viscosity at the nose of the CCT curves, and hence the smaller  $R_c$
- $T_l \downarrow$  and  $T_g \uparrow$   $\blacktriangleright$  lower nucleation and growth rate  $\blacktriangleright$  GFA  $\uparrow$ 
  - significant difference between  $T_l$  and  $T_g$  in multi-component BMG
  - insufficient information on temperature-viscosity relationship
  - insufficient correlation with GFA



## 5) $\gamma$ parameter = $T_x / (T_l + T_g)$

- thermodynamic and kinetic view points - **relatively reliable parameter**
- stability of equilibrium and metastable liquids:  $T_l$  and  $T_g$
- resistance to crystallization:  $T_x$



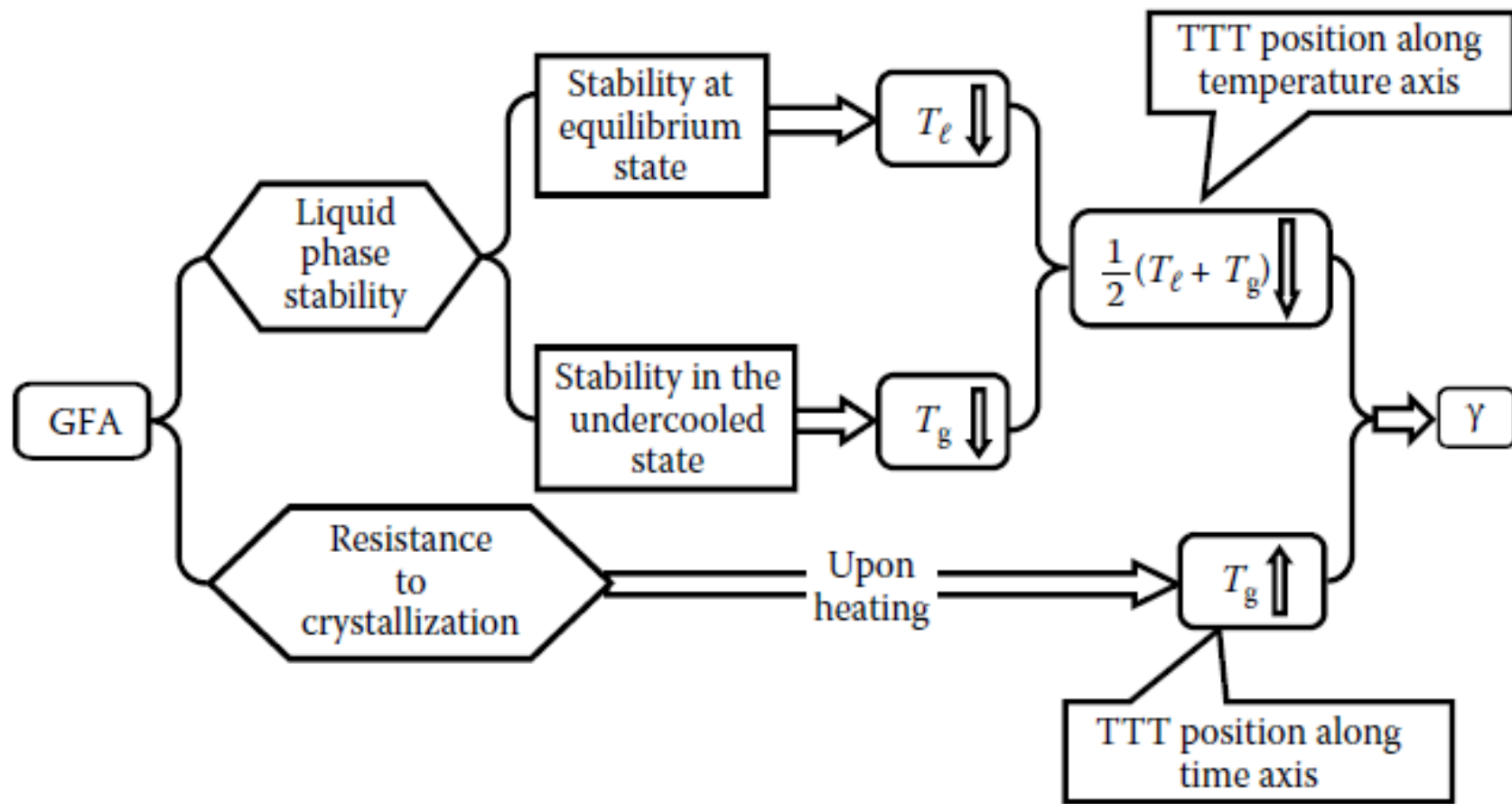
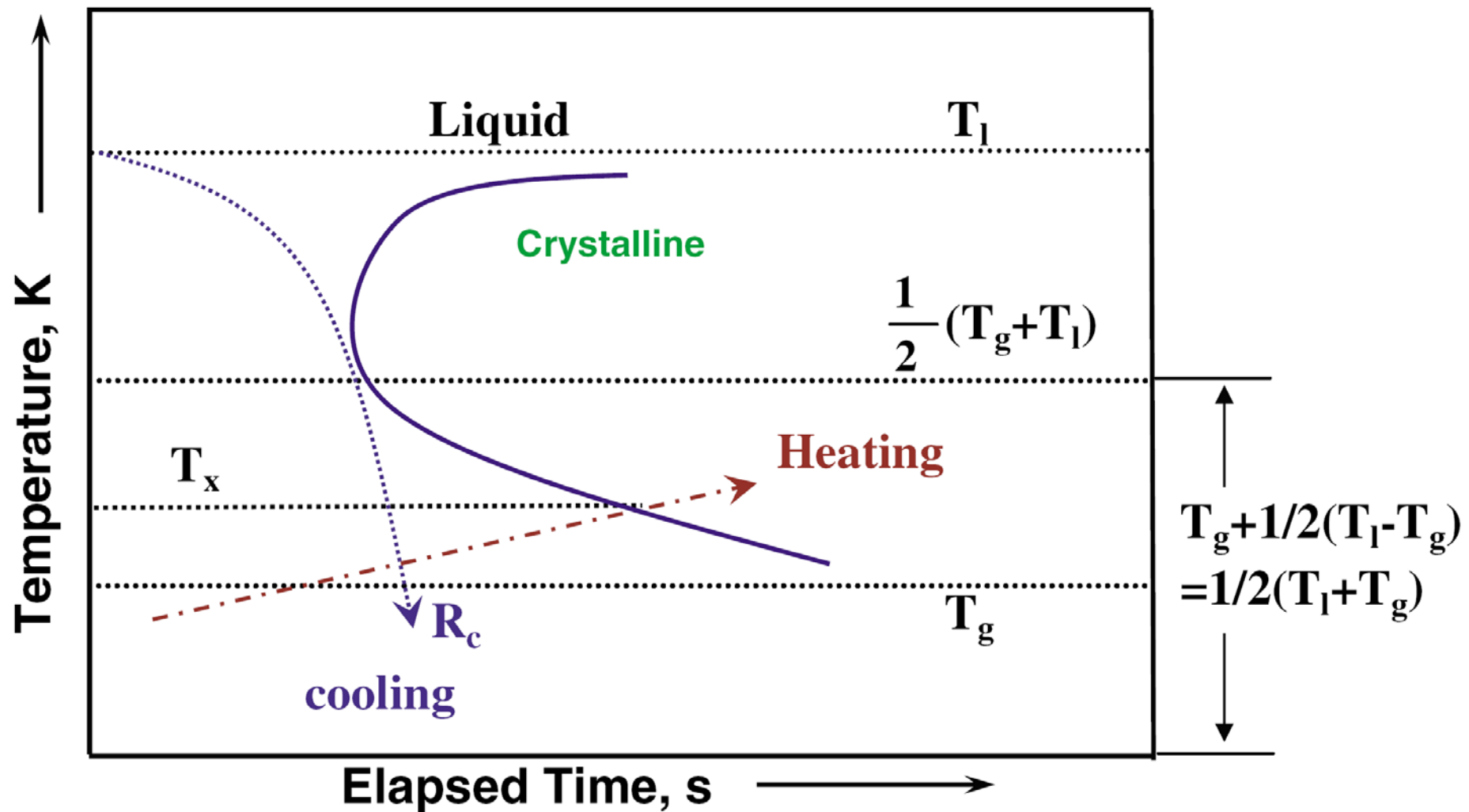


FIGURE 3.8

Schematic to illustrate the different factors involved in deriving the  $\gamma$  parameter to explain the GFA of alloys. (Reprinted from Lu, Z.P. and Liu, C.T., *Intermetallics*, 12, 1035, 2004. With permission.)

$$\gamma \propto T_x \left[ \frac{1}{2(T_g + T_1)} \right] \propto \frac{T_x}{T_g + T_1}$$



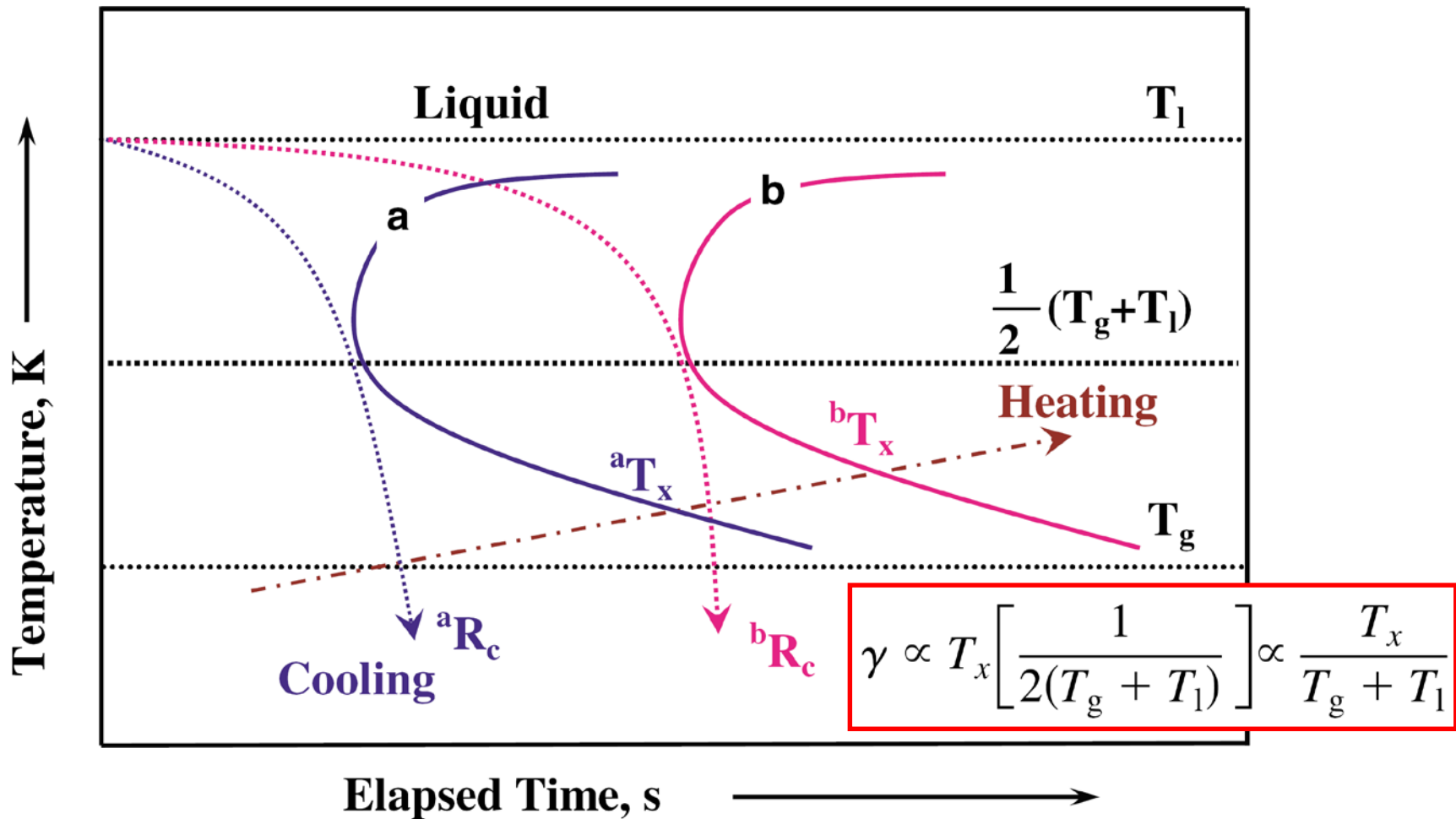


FIG. 2 (color online). Schematic TTT curves showing the effect of  $T_x$  measured upon continuous heating for different liquids with similar  $T_1$  and  $T_g$ ; liquid  $b$  with higher onset crystallization temperature  ${}^bT_x$  ( ${}^aT_x < {}^bT_x$ ) shows a lower critical cooling rate  ${}^bR_c$  ( ${}^bR_c < {}^aR_c$ ).

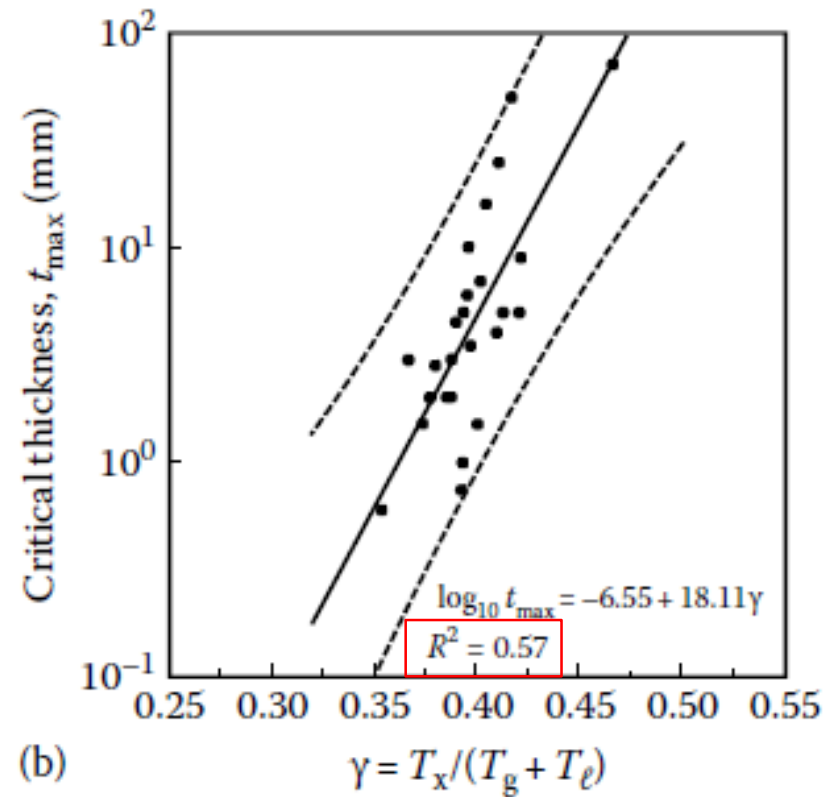
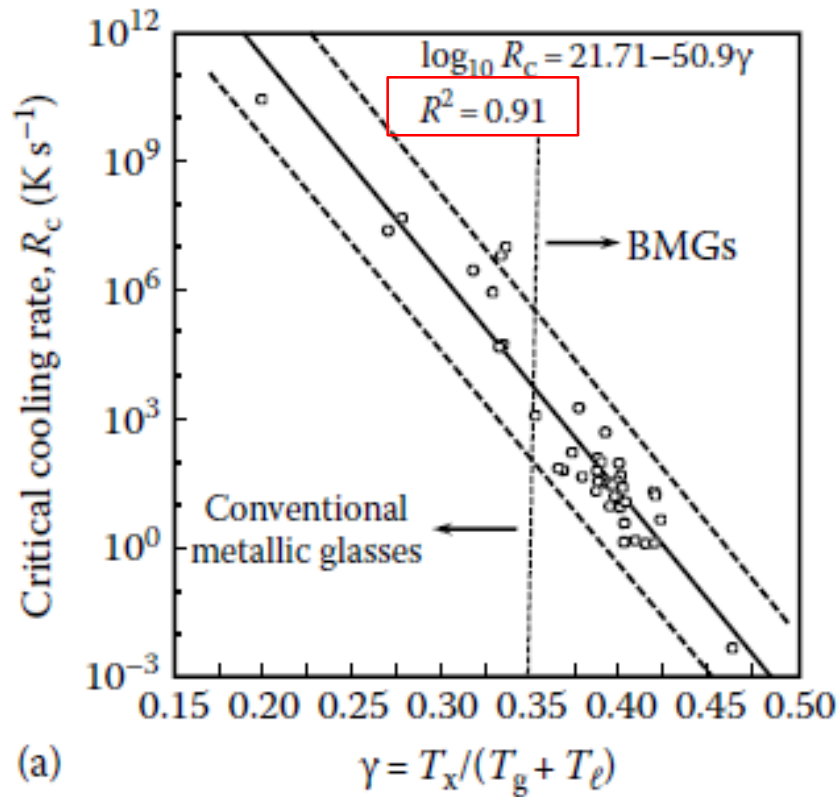
$$\log_{10} R_c = (21.71 \pm 1.97) - (50.90 \pm 0.71)\gamma \quad \log_{10} t_{\max} = (-6.55 \pm 1.07) + (18.11 \pm 0.70)\gamma$$

$$R_c = R_0 \exp\left[\left(-\frac{\ln R_0}{\gamma_0}\right)\gamma\right]$$

$$t_{\max} = t_0 \exp\left[\left(-\frac{\ln t_0}{\gamma_1}\right)\gamma\right]$$

$$R_c = 5.1 \times 10^{21} \exp(-117.2\gamma)$$

$$t_{\max} = 2.80 \times 10^{-7} \exp(41.7\gamma)$$



Wide scatter for the  $t_{\max}$  correlation

FIGURE 3.9

(a) Correlation between the critical cooling rate ( $R_c$ ) and the  $\gamma$  parameter for BMGs. (b) Correlation between the maximum section thickness ( $t_{\max}$ ) and the  $\gamma$  parameter for BMGs. (Reprinted from Lu, Z.P. and Liu, C.T., *Acta Mater.*, 50, 3501, 2002. With permission.)

# GFA Parameters *on the basis of thermodynamic or kinetic aspects*

GFA parameters	Expression	Year established
$T_{rg}$	$T_g / T_l$	1969 D.Turnbull,Contemp.Phys.10(1969) 473
$K$	$(T_x - T_g) / (T_l - T_x)$	1972 A.Hruby, Czech. J.Phys. B 22 (1972) 1187
$\Delta T^*$	$(T_m^{mix} - T_l) / T_m^{mix}$	1978 I.W.Donald, J.Non-Cryst.Solids 30 (1978) 77
$\Delta T_x$	$T_x - T_g$	1993 A.Inoue, J.Non-Cryst.Solids 156-158(1993)473
$\gamma$	$T_x / (T_l + T_g)$	2002 Z.P.Lu, C.T.Liu, Acta Mater. 50 (2002) 3501
$\delta$	$T_x / (T_l - T_g)$	2005 Q.J.Chen,Chinest Phys.Lett.22 (2005) 1736
$\alpha$	$T_x / T_l$	2005 K.Mondal, J.Non-Cryst.Solids 351(2005) 1366
$\beta$	$T_x / T_g + T_g / T_l$	2005 K.Mondal, J.Non-Cryst.Solids 351(2005) 1366
$\varphi$	$(T_g / T_l)(T_x - T_g / T_g)^a$	2007 G.J.Fan,J.Non-Cryst. Solids 353 (2007) 102
$\gamma_m$	$(2T_x - T_g) / T_l$	2007 X.H.Du,J.Appl.phys.101 (2007) 086108
$\beta$	$(T_g / T_l - T_g)(T_g / T_l - T_g)$	2008 Z.Z.Yuan, J. Alloys Compd.459 (2008)
$\xi$	$\Delta T_x / T_x + T_g / T_l$	2008 X.H.Du,Chinese Phys.B 17(2008) 249